Mena11a-isoform specific regulation of actin cytoskeleton organization and cell behavior

By

Chandrani Mondal

B.S in Molecular and Cellular Biology
Johns Hopkins University, 2008
M.S. in Molecular and Cellular Biology
Johns Hopkins University, 2009

SUBMITTED TO THE DEPARTMENT OF BIOLOGY IN PARTIAL FULFILLMENT OF THE REQUIREMENTS FOR THE DEGREE OF

DOCTOR OF PHILOSOPHY IN BIOLOGY
AT THE
MASSACHUSETTS INSTITUTE OF TECHNOLOGY

FEBRUARY 2016

Signature of Author: Signature redacted
Department of Biology
January 22, 2016

Certified by: Signature redacted
Frank B. Gertler
Professor of Biology
Thesis Supervisor

Accepted by: Signature redacted
Michael Hemann
Associate Professor of Biology
Co-Chair, Biology Graduate Committee

Mena11a-isoform specific regulation of actin cytoskeleton organization and cell behavior

By

Chandrani Mondal

Submitted to the Department of Biology on January 22, 2016 in Partial Fulfillment of the Requirements for the Degree of Doctor of Philosophy in Biology

ABSTRACT

Ena/VASP proteins are a conserved family of actin regulatory proteins that modulate cell motility and morphology by altering actin dynamics. Mena, an Ena/VASP protein, is alternatively spliced, producing protein isoforms with distinct functions. Here, we characterize the expression, function, and regulation of the Mena11a splice isoform at the molecular and cellular level. We find that Mena11a is enriched in epithelia and muscle in both embryonic and adult tissues.

Recent evidence demonstrates Mena upregulation in breast cancer; Mena promotes cell motility, invasiveness, and metastasis in a growth factor dependent manner. We demonstrate that Mena11a depletion in epithelial-like breast cancer cells disrupts cell-cell junctions and increases cell motility. Mena11a dampens growth factor-mediated membrane protrusion and attenuates G-actin incorporation to barbed ends of actin filaments. In addition, Mena11a alters the actin cytoskeleton and decreases Arp2/3 recruitment to the leading edge of lamellipodia.

Mass spectrometry analysis demonstrates that Mena11a is phosphorylated. The expression of a nonphosphorylatable mutant of Mena11a does not retain the ability of Mena11a to dampen membrane protrusion, decrease G-actin incorporation at barbed ends, and reduce Arp2/3 recruitment at the lamellipodial edge; thus, our results suggest that phosphorylation of Mena11a is coupled to its activity.

Thesis Supervisor: Frank B. Gertler
Title: Professor of Biology

ACKNOWLEDGMENTS

First, I would like to thank Frank Gertler for being my thesis advisor and supporting me through my scientific career during the past few years. Frank has helped me to think critically about experiments and become better and more precise at articulating my ideas and thoughts. I would also like to thank my committee members, Jackie Lees and Doug Lauffenburger, for their key insights into my project, ability to keep me on track towards graduation, and very helpful advice, as well as Forest White, for being my outside committee member.

In addition, I would like to thank Michele Balsamo, the scientist with whom I have worked most closely with in the Gertler lab. As soon as I rotated in the lab, Michele immediately took me under his wing and showed me the ropes, from troubleshooting experiments to eventually writing a paper together. Our collaboration has been one of the highlights of graduate school, and Michele has been a great mentor and friend to me, even from across the seas. I am at the finish line today because of his continued help and encouragement, and I am very grateful for that.

I would also like to thank the Gertler lab members, especially Guillaume Carmona, Shannon Hughes, Marina Vidaki, and Russell McConnell for their scientific insight. We have had many great discussions, and they were always willing to help me out and answer the many hundreds of questions I've had over the years. Thank you to Daisy Riquelme for being a good friend and fellow graduate student in the lab. We've been through it all together, and have had some great laughs in between.

Graduate school at MIT has its many challenges, but I am so lucky to have made some lifelong friends along the way. Thank you to Frank Solomon for always believing in me, and to Mike Hemann, for his support and friendship over the years. Katie, Jim, Ann, Sara, Kaitlin, Simina, Pete, Dahlia, Julia, Jenny (and so many more fantastic folks) - you have been there for me day in and day out, through thick and thin. I am so lucky to have such a wonderful set of friends in my life. We always found a way to seize the moment and have fun together, which I am so grateful for.

My family is my life and heart. Mom and Dad, your unconditional love and unwavering support has meant the world to me. You should teach a master class in parenting (and life, in general), because there are no parents better than you. You are pillars of strength and examples to live by. You are both the most generous, kind-hearted, courageous people I know, and you never, ever give up, no matter the circumstances. I am honored and privileged to be your child, and can't thank you enough for everything you have done for us.

And to the most important person in my life, my best friend, Indrani - this PhD thesis is dedicated to you. There are not enough words for me to describe how amazingly blessed I am to have you as a sister. You have been my mentor and guide since I can remember. I followed you, because you lead so well. Never have I met a more intelligent, fierce, fearless, just, loyal, compassionate, strong, analytical, determined,

dedicated, multifaceted individual. You have always believed in me and pushed me to greater heights, far outside my comfort zone, because you truly thought I had the ability to do it. Thank you for being there for me, no matter what. To you I am forever grateful.

TABLE OF CONTENTS

Chapter 1: Introduction

TABLE OF CONTENTS

1.1 Actin cytoskeleton regulation of cell motility

Cell movement is required in key physiological processes in metazoans, including morphogenesis during gastrulation (1), neurulation (2), wound repair after injury (3), and immune surveillance (4). In a disease context, motile and invasive cancer cells can disseminate and form metastases, contributing to cancer progression (5). Cell motility involves the dynamic reorganization of the actin cytoskeleton, which is orchestrated by signaling pathways, mechanical cues, and actin regulatory proteins coordinated in a spatial and temporal manner (6). For a wide spectrum of cells, the cell motility cycle for "crawling" cell migration is initiated when a cell is morphologically polarized, thus having an asymmetry. The cell can establish polarity by various mechanisms, including the integration of signals from an external gradient or a uniform cue, mechanical confinement, or in a spontaneous manner due to internal fluctuations (6, 7). The polarized cell, in response to a diverse set of guidance cues and signaling (8), can form protrusive structures at the leading edge of the cell, or cell front in part due to the force generated by active remodeling of the actin architecture through its biochemical interactions with accessory proteins (9). One type of protrusive structure best characterized in mesenchymal-type cell motility *in vitro* is a flat, veil-like membranous extension called a lamellipodium that attaches to the substratum through the interaction of adhesion receptors with the cytoskeleton, forming adhesive focal contacts. Focal contacts are able to generate the traction and force necessary for translocation of the cell body (10). At the rear of the cell, myosin-II generated contractile forces release cell-substratum contacts to enable forward movement (Figure 1.1) (6).

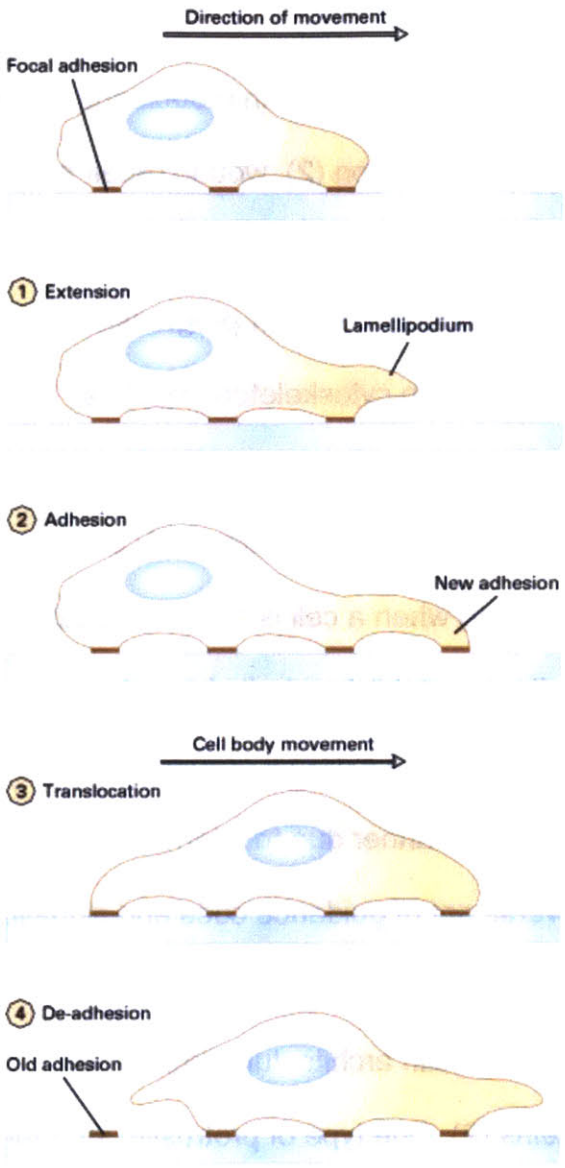

Figure 1.1: Steps of "crawling" cell motility. Adapted from Molecular Cell Biology, 4th edition.

In addition to cell motility, the constant assembly, disassembly, and remodeling of the actin network contributes to the regulation of a wide range of processes, including cell morphology (11), cell-cell (12) and cell-matrix adhesions (13), intracellular movement of pathogenic bacteria (14), cell division (15), endocytosis (16), and vesicular transport (17) in non-muscle cells, and multiple functions in muscle cells (18, 19).

1.2 Actin dynamics

Actin, a 42 kDa globular protein, has several isoforms in vertebrates; the alpha-actins are found in muscle cells, and both beta- and gamma-actin are found in non-muscle cells. Under physiological conditions, actin monomers can polymerize spontaneously into double-helical polymers. The initial step of polymerization, termed nucleation, requires actin monomers to form a trimeric structure and is rate-limiting (20). Once stable nuclei are formed, actin filaments can elongate rapidly, assembling polar filaments that have subunits oriented in the same "head-to-tail" direction. Myosin S1 heads bound to actin filaments first demonstrated the intrinsic polarity of actin filaments with a distinct arrowhead pattern; this resulted in one end of the filament being called the "barbed" end, and the other, the "pointed end."

Polymerization and depolymerization of ATP-actin or ADP-actin occurs at both the barbed and pointed ends of the actin filament, and the rate of actin assembly at either end is directly dependent on the concentration of free actin monomers in solution. After monomeric actin assembles into filaments, bound ATP in the F-actin polymer is hydrolyzed irreversibly, followed by the relatively slow dissociation of the gamma-phosphate. At steady-state, ATP hydrolysis is necessary for treadmilling, a phenomenon that maintains a net assembly of subunits at the barbed end that is equal to the net disassembly of subunits from the pointed end (21), governing actin turnover. In the absence of actin regulatory proteins at physiological, steady-state conditions, treadmilling occurs extremely slowly. This slow dissociation at the pointed end limits growth at the barbed end to a rate that is nearly 100-200 times slower than what is

found in cells (22), suggesting the absolute requirement of additional proteins to regulate this complex process (21).

Although there is a large repertoire of actin binding proteins *in vivo* that have diverse functions, including regulating the actin monomer pool, initiating nucleation and polymerization, controlling filament length, bundling and crosslinking actin filaments, severing filaments, and promoting actin turnover (21, 23), *in vitro* reconstitution assay experiments have demonstrated a core set of proteins, in addition to actin, that are required for the motility of intracellular bacterial pathogens, such as *Listeria monocytogenes* (24) (Figure 1.2). The minimum necessary proteins that allow for *Listeria* motility are actin, activated-Arp2/3, cofilin/ADF, and capping protein. Additional general actin regulatory proteins, including profilins, formins, and Ena/VASP, have key functions in regulating *Listeria* movement at speeds comparable to those in living cells (25–28).

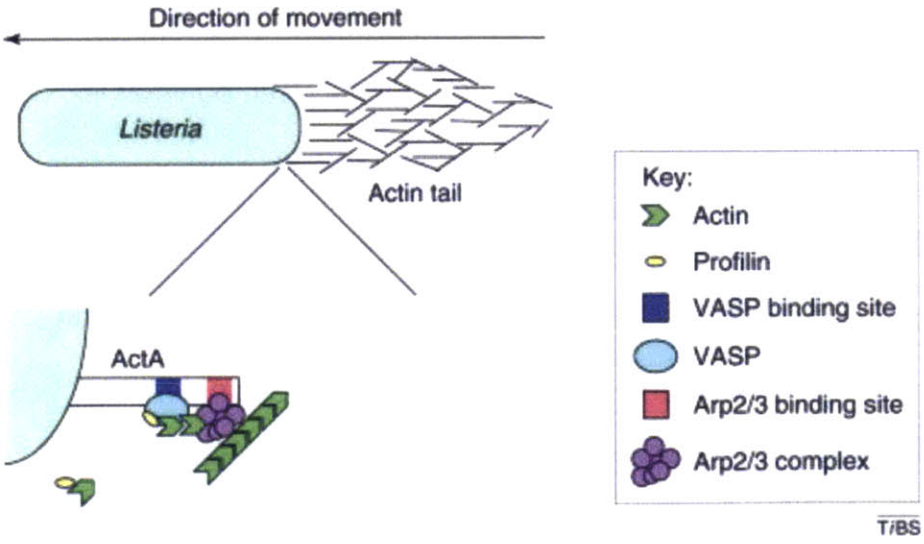

Figure 1.2: *Listeria monocytogenes* movement in host cell. Adapted from (29). *Listeria* hijacks the host cell's actin cytoskeletal machinery to propel itself through the cell. The *Listeria* surface ActA protein has an N-terminal domain that can bind Arp2/3 and actin monomers, a central pro-rich domain that binds Ena/VASP proteins, which can recruit profilin-G-actin, and a C-terminal domain that acts as a membrane anchor.

1.3 Actin regulatory proteins

1.3.1 Arp2/3

In order to nucleate actin rapidly, the cell must utilize actin-nucleating proteins, which can stabilize small actin oligomers. Actin nucleating proteins are activated downstream of intracellular signaling cascades, which are triggered by various external cues (21). One such nucleator, Arp2/3, was first discovered in *Acanthomoeba* and is comprised of seven tightly associated subunits (30). When activated by nucleation promoting factors (NPFs) (31), Arp2/3 nucleates new actin filaments that branch off existing "mother filaments" (32). In the *Listeria* model system, Arp2/3 was shown to be required for *Listeria* motility (26), and it was later determined that the *Listeria* bacterium contains the surface protein ActA, which interacts directly with Arp2/3 and acts as a nucleation promoting factor (33).

Structural evidence, FRET, and cryo-EM data have demonstrated a process by which Arp2/3 nucleates branched actin (34). Initially, Arp2/3 is in an open, inactive conformation, and is then able to bind the acidic region of the VCA/WA domain (V motif binds actin monomers, and the CA region binds Arp2/3) of a class I NPF, which confers a conformational change, bringing the two actin-related Arp2 and Arp3 subunits close together and allowing the Arp2/3 complex to bind to a pre-existing mother filament. The Arp2 and Arp3 subunits are positioned at the pointed end of the new daughter filament, which is oriented at a ~70 degree angle to the mother filament, and the V motif of the VCA domain is able to present ATP-actin monomers to the complex, allowing nucleation to occur (34).

1.3.2 Capping Protein

Capping proteins (CP) can bind to the barbed ends of filaments, terminating filament growth (35) by inhibiting the association and dissociation of actin monomers. CP is a heterodimer that binds with high affinity to the barbed end of the actin filament at a 1:1 stoichiometry *in vitro* (36). There are multiple regulators of CP, including elongation factors, like formins, that compete with CP for binding the barbed end of the filament, steric regulators, which directly bind to CP and block its interaction with the barbed end, and allosteric regulators, which can bind the CP through a capping protein interaction (CPI) motif, thus weakening its association with the barbed end (36). In the *Listeria* model system, CP has been suggested to promote Arp2/3-mediated nucleation through the "monomer-gating" model, in which CP caps barbed ends of actin filaments near the bacterium surface, allowing for additional monomeric-actin to be available for Arp2/3 nucleation, thus increasing *Listeria* motility (37).

1.3.3 ADF/cofilin family

The ADF/cofilin family, or AC family of actin binding proteins, is able to bind and sever actin filaments, generating free barbed ends. In addition, they contribute greatly to the process of actin turnover (22). In Arp2/3-mediated branched actin filaments, AC proteins bind aging filaments that have hydrolyzed ATP, promoting phosphate dissociation, severing of ADP-actin filaments, and subsequent debranching, due to low affinity of Arp2/3 for ADP-actin (38). In the *Listeria* model system, *Xenopus* AC protein was demonstrated to bind to ADP-F-actin and depolymerize actin filaments effectively (39). The newly depolymerized ADP-actin monomer remains bound to AC until profilin competes with AC (21). AC then acts as a nucleotide exchange factor, promoting

release of ADP from the actin monomer for ATP (40), thus replenishing the pool of actin monomer for continued dynamic actin remodeling in the cell.

1.3.4 Profilin

Pools of polymerization-competent actin monomers must be maintained at high concentrations in the cytosol of cells to allow for rapid actin polymerization. Profilin, an actin binding protein, binds ATP-actin monomers with high affinity in a 1:1 stoichiometric complex (41). The function of profilin in the cell is complex and extends beyond acting as a buffer for actin monomers: profilin-actin can bind free barbed ends of actin filaments and promotes elongation, inhibits binding of profilin-actin to the pointed end of filaments, inhibits spontaneous actin nucleation, and binds to other signaling proteins through proline-rich sequences (21, 42), suggesting an additional mechanism for maintaining a reserve of actin monomer. Profilin and thymosin-β4, another actin binding protein, compete to bind actin monomers, and thus the interplay of these two proteins allow for the cell to sequester actin-monomers to keep on reserve (41). Even though profilin-actin maintains a pool of polymerization-competent monomers readily available for barbed end filament elongation, both profilin-actin and thymosin-β4-actin inhibit spontaneous actin nucleation.

1.3.5 Formins

Formins are another family of proteins that nucleate actin filaments. Formin proteins are homodimers that interact directly with actin monomers via the formin-homology 2 (FH2) domain. The FH2-donut shaped dimer can form a stable complex with two actin monomers, and supports the elongation of unbranched filaments. The formin dimer remains persistently associated with the elongating barbed end of the

filament, and can increase the rate of filament elongation greater than the rate of diffusion-limited subunit addition through interactions of its FH1 domain with profilin-actin (32, 43). Processive capping, during which the formin dimer remains associated with the elongating barbed end of a filament, protects the filament from the addition of capping protein.

1.3.6 Ena/VASP

Another set of actin regulatory proteins that compete with CP for binding the barbed ends of actin filaments are Ena/VASP (enabled/vasodilator-stimulated phosphoprotein) proteins (36). Ena/VASP proteins form obligate tetramers that increase the rate at which actin monomers are added to barbed ends of actin filaments in the presence of CP, thus supporting the elongation of unbranched filaments (44–48), amongst other functions. Ena/VASP, although dispensible for *Listeria* motility, binds directly to the central pro-rich region of the bacterial ActA protein (Figure 1.2) and enhances F-actin tail formation and elongation, increasing bacterial velocity and directional persistence (49, 50).

1.4 Ena VASP family

The Ena/VASP family of conserved proteins has been implicated in regulating actin dynamics in many different organisms and in a wide variety of contexts, including axon guidance, T-cell activation, epithelial and endothelial morphogenesis, fibroblast migration, intracellular pathogenic bacterial movement, and cancer cell motility. Ena/VASP proteins localize to areas of actin remodeling, such as the edge of lamellipodial protrusions, tips of filopodia, at cell-cell adhesions, and at focal adhesions with the extracellular matrix (51).

Drosophila Enabled, one of first proteins identified in this family, was discovered in a genetic screen for dominant suppressors of *Drosophila*-Abl (D-Abl) mutants (52). Subsequent work demonstrated that *Drosophila* Enabled was a substrate for D-Abl kinase, and both proteins were enriched in axons of the embryonic nervous system (53). *Ena* mutant embryos had axonal architecture defects (53); later studies showed that both the *C.elegans* ortholog, UNC-34, and *Drosophila* Enabled function downstream of axon guidance receptor signaling (51, 54, 55).

Screening of a mouse brain cDNA library led to the discovery of mammalian Ena (Mena) (56). Sequence alignment of Mena yielded two similar sequences: a human EST, which was used to isolate a mouse cDNA termed Ena/VASP-like (EVL), and VASP (56). VASP was initially identified in human platelets as a substrate of cGMP/cAMP-dependent kinases (57, 58), and although VASP-deficient mice are viable and fertile, with a subtle phenotype, these studies demonstrate that VASP plays a role in inhibiting platelet activation and aggregation (59, 60).

In addition to the invertebrate orthologs *Drosophila* Enabled and *C.elegans* UNC-34, and the vertebrate paralogs Mena, VASP, and EVL, another ortholog was discovered in the non-metazoan *Dictystelium Discoideum,* known as DdVasp, which was demonstrated to regulate actin dynamics involved in filopodial formation and chemotaxis (61).

1.4.1 Domain structure and binding partners

Mena, VASP, and EVL have a similar domain structure: all three vertebrate paralogs contain an Ena/VASP-like homology domain 1 (EVH1), a central proline-rich region, and an Ena/VASP-like homology domain 2 (EVH2) (Figure 1.3) (56). The EVH1

domain interacts primarily with proteins containing a poly-proline consensus motif: (F/W/Y/L)PPPPX(D/E)(D/E)(D/E)Φ where X=any amino acid, Φ=hydrophobic amino acid (51, 56), abbreviated as F/LPPPP in Figure 1.3. Proteins that contain at least one F/LPPPP motif and interact directly with the EVH1 domain of Ena/VASP proteins include ActA on the surface of the bacterial pathogen *Listeria* (62), the focal adhesion proteins vinculin and zyxin (63, 64), and Lamellipodin (Lpd), which localizes to the edge of lamellipodia (65), amongst several others.

Interactions with the EVH1 domain regulate subcellular localization of Ena/VASP proteins and recruitment to signaling complexes (51). ActA contains FPPPP motifs that allow it to bind to the EVH1 domain of Ena/VASP, and this interaction targets Ena/VASP proteins to the *Listeria* surface, and is necessary for *Listeria* virulence and motility (62). Both zyxin (64) and vinculin (56, 63) are able to target Ena/VASP proteins to focal adhesions through EVH1-mediated interactions. Lamellipodin and Riam, proteins in the MRL family, both contain multiple putative EVH1 binding sites (65, 66). Lamellipodin is able to bind PI(3,4)P2 and Ras via its PH and RA domains, respectively, and can recruit Ena/VASP proteins to the leading edge membrane with its six FPPPP motifs (65). Interestingly, recent work has demonstrated that Lpd can directly bind F-actin at the leading edge and tether VASP at the barbed ends (67). Robo, another EVH1 binding protein, interacts with *Drosophila* Enabled to regulate axon guidance (55). Tes, a Mena-specific binding partner, can bind to the same region of EVH1 as proteins with FPPPP repeats; Tes interacts directly with the Mena EVH1 domain via a LIM3 domain, and is able to displace Mena from focal adhesions and the leading edge (68).

The central proline-rich region of Ena/VASP proteins can interact with –SH3 and –WW domain containing proteins, and with profilin (56, 69, 70). This region preferentially binds profilin-actin over profilin (71); the recruitment of profilin-actin by Ena/VASP proteins can enhance the motility of *Listeria* (25, 49), and is demonstrated to increase actin polymerization in the presence of CP *in vitro* (45), but is dispensable for whole cell motility (72).

The EVH2 domain has three conserved regions: a G-actin monomer binding region (GAB), an F-actin binding region (FAB), and a coiled-coil motif (CC) that has been demonstrated to mediate tetramerization (56, 73) (Figure 1.3). In fibroblasts, the EVH2 domain alone can localize to lamellipodia, but not focal adhesions, and functions like full-length Mena in random motility assays (72). The EVH2 domain is able to protect barbed ends from CP (45), and is the minimal domain necessary to form filopodia (74).

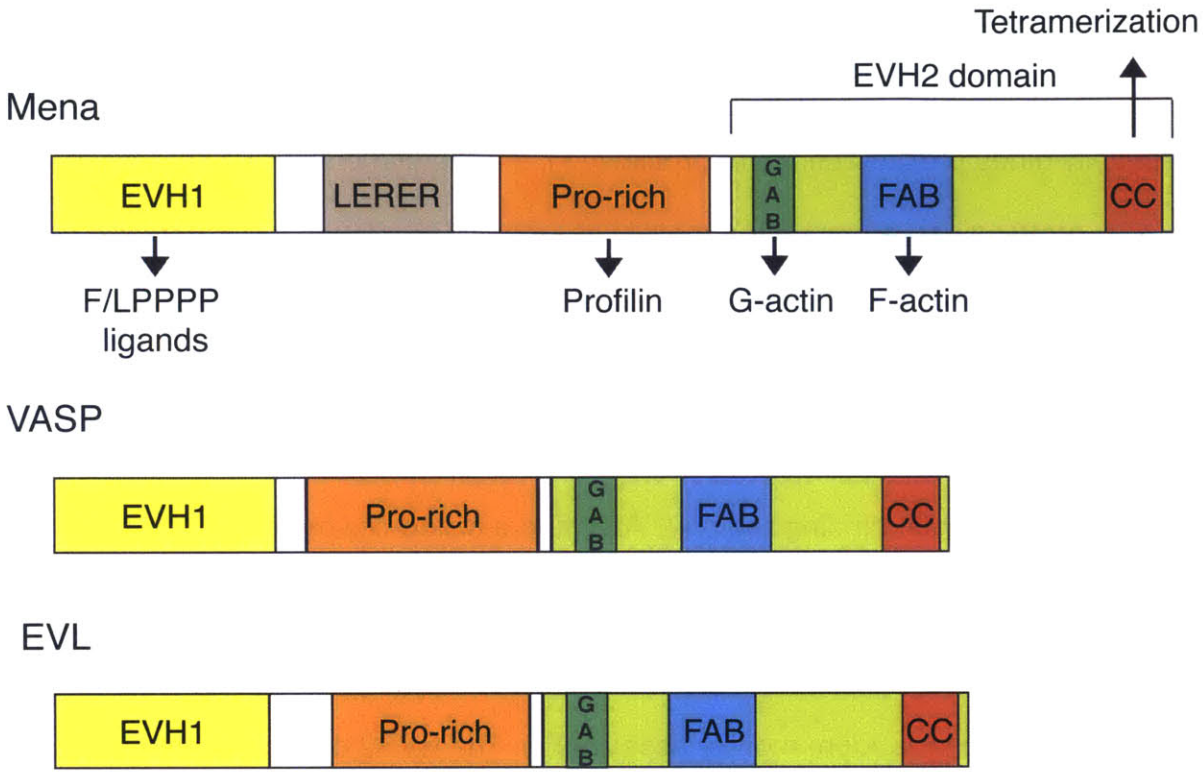

Figure 1.3: Domain structure of Ena/VASP proteins. Proteins share an EVH1 domain, a pro-rich central region, and an EVH2 domain that mediates interaction with F- and G-actin, and contains a coiled-coil that mediates tetramerization.

1.4.2 Function in protrusive structures

1.4.2.1 Lamellipodia

The ability of a cell to form a lamellipodial protrusion at the leading edge is initiated by sensing external cues, followed by signal integration which results in active remodeling of the actin network by proteins that mediate actin nucleation, branching, elongation, and disassembly (51). Cells can respond to multiple external cues and signals, including soluble (e.g. growth factors) and insoluble cues (e.g. extracellular matrix), resulting in lamellipodial formation (75). One well-characterized example of

signaling that drives actin protrusion is through the receptor tyrosine kinase EGFR; upon stimulation of EGFR by EGF, several pathways are turned on. One key pathway activates PI3K downstream of EGFR, which induces formation of the phospholipid PI(3,4,5)P3, which can directly activate the WAVE complex through the small G-protein Rac. The SCAR/WAVE proteins are Arp2/3 regulators that are recruited to the leading edge of the cell in order to activate Arp2/3. An additional pathway that activates WAVE downstream of EGFR includes the conversion of PI(3,4,5)P3 to PI(3,4)P2 via SHIP2, a 5' inositol phosphatase; subsequently, PI(3,4)P2 can recruit Lamellipodin, a protein that can interact directly with the WAVE complex via the ABI protein. Lamellipodin is also an effector of small G-proteins, such as Ras and Rac, which are also activated downstream of EGFR. Together, Lamellipodin and the SCAR/WAVE complex are demonstrated to control lamellipodial dynamics, and the speed and direction of cell migration (76). Additional control of WAVE complex activation and recruitment to the leading edge include phosphorylation by Abl kinase, interactions with proteins involved in trafficking, and alternate signaling pathways (77).

In order for the WAVE complex to activate Arp2/3-mediated nucleation, the Arp2/3 complex needs to associate with a free barbed end of a pre-existing mother filament; these can be generated by cofilin-severing, de novo, or by other mechanisms (77). Once branched actin has been nucleated, proteins such as Ena/VASP are necessary to control filament elongation, which ultimately determines cell directionality, persistence, and speed (44). Other proteins that regulate and promote the elongation of barbed ends at lamellipodia include formins, such as mDia2 (78), and the Diaphanous-related formin FMNL2 (79), and CARMIL, a protein that can bind directly to CP and

reduce its affinity to bind barbed ends of actin filaments (80). As actin filaments coordinately branch and elongate to form a dendritic array at the leading edge, there is simultaneous pointed-end disassembly, debranching, and destabilization at the rear of the lamellipodia (81). Cortactin interacts with Arp2/3-containing branches and stabilizes these filaments (82); in contrast, GMFß (83) and cofilin can both promote debranching (38), and Coronin 1B destabilizes filaments, induces Arp2/3 dissociation, and drives filament turnover (82, 84). Interestingly, all three of these proteins promote cell migration, reinforcing the notion that proper coordination of actin assembly at the front of the cell and disassembly at the rear are necessary for efficient cell migration (82, 83, 85).

The subcellular localization and function of Ena/VASP proteins in regulating lamellipodial protrusion has been analyzed in Ena/VASP-deficient mouse embryonic fibroblasts, as well as overexpression studies; all three vertebrate Ena/VASP proteins localize to lamellipodial protrusions (72, 86, 87). The direct interaction between the EVH2 domain and growing actin filaments is required to target Ena/VASP proteins to the lamellipodia, while the EVH1 domain is able to refine this subcellular targeting through its interactions with FPPPP ligands (44, 72). Interactions with proteins such as Lamellipodin can restrict Ena/VASP proteins to the tips of lamellipodia (44, 65).

Ena/VASP-deficient fibroblasts are able to form short, highly branched filaments, and exhibit lamellipodia that protrude slowly but persistently. Fibroblasts expressing Ena/VASP proteins form long, sparsely branched filaments and exhibit lamellipodia with rapid protrusion and withdrawal. The resulting effect on cell motility is that Ena/VASP-deficient fibroblasts had a greater net cell translocation, and those with excess

Ena/VASP protein inhibited net cell translocation, compared to control cells (Figure 1.4, adapted from (88)) (46, 86).

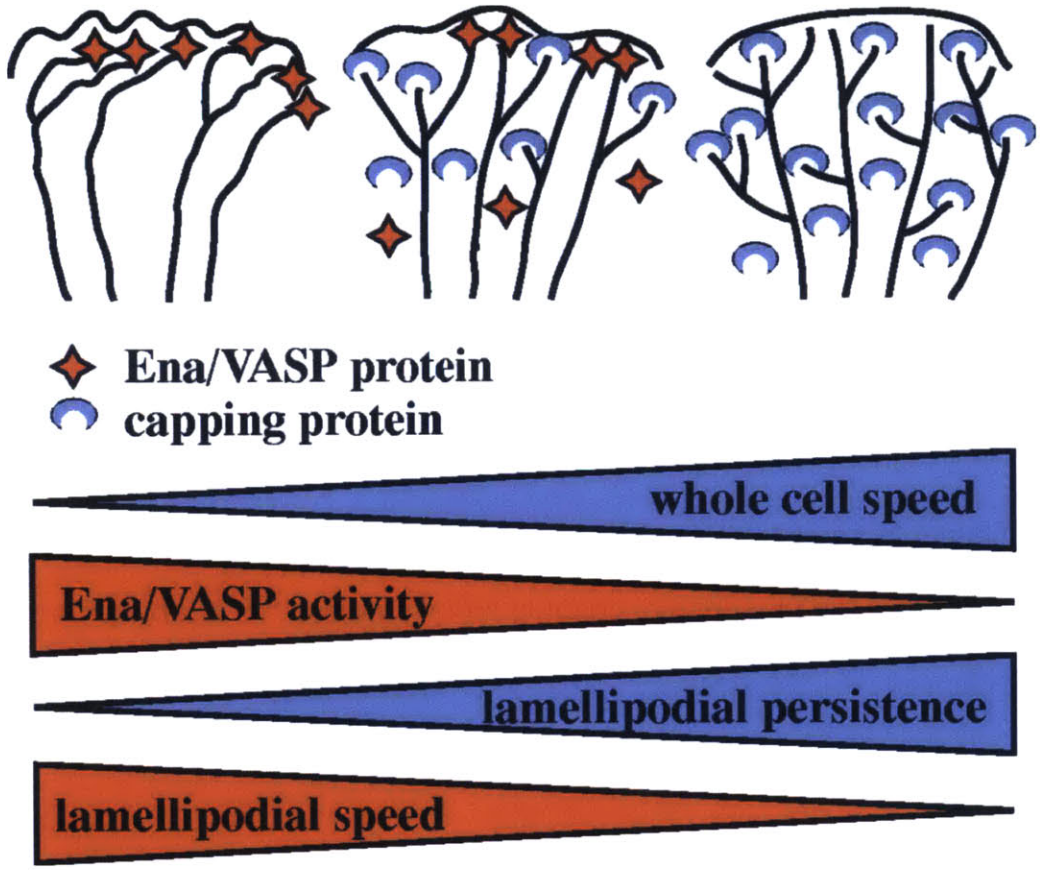

Figure 1.4: Ena/VASP effects on lamellipodial persistence, speed, and whole cell motility. (Adapted from (88)). Ena/VASP activity at the leading edge antagonizes capping protein, leading to increased lamellipodial speed but decreased lamellipodial persistence and whole cell motility.

The specific features of Ena/VASP, in particular, Mena, that affect lamellipodial protrusion and overall cell migration were further examined using a series of mutants in the Ena/VASP-deficient fibroblasts (72). The results indicated that the FAB region of the EVH2 domain and the first, conserved PKA/PKG site on Mena (S236) between the EVH1 and EVH2 domain are required to regulate random motility (72); interestingly, the

pro-rich region of Mena that interacts with profilin-G-actin is not necessary for the negative regulation of whole cell motility (72).

Based on this work, a molecular model, or "anti-capping" model, was proposed to explain how Ena/VASP regulate lamellipodial protrusion. The "anti-capping" model presumes that filament elongation by Ena/VASP proteins, resulting in long, sparsely branched filaments, is unable to overcome the forces produced by membrane tension, leading to the increased velocity but decreased persistence of individual lamellipodial protrusions, thus resulting in decreased whole cell migration (44, 46, 88) (Figure 1.4, adapted from (88)). Briefly, Ena/VASP tetramers are able to associate with the barbed ends of actin filaments, recruit profilin-G-actin monomers and load the monomers onto the barbed ends (71) in the presence of capping protein (Figure 1.5, adapted from (44)).

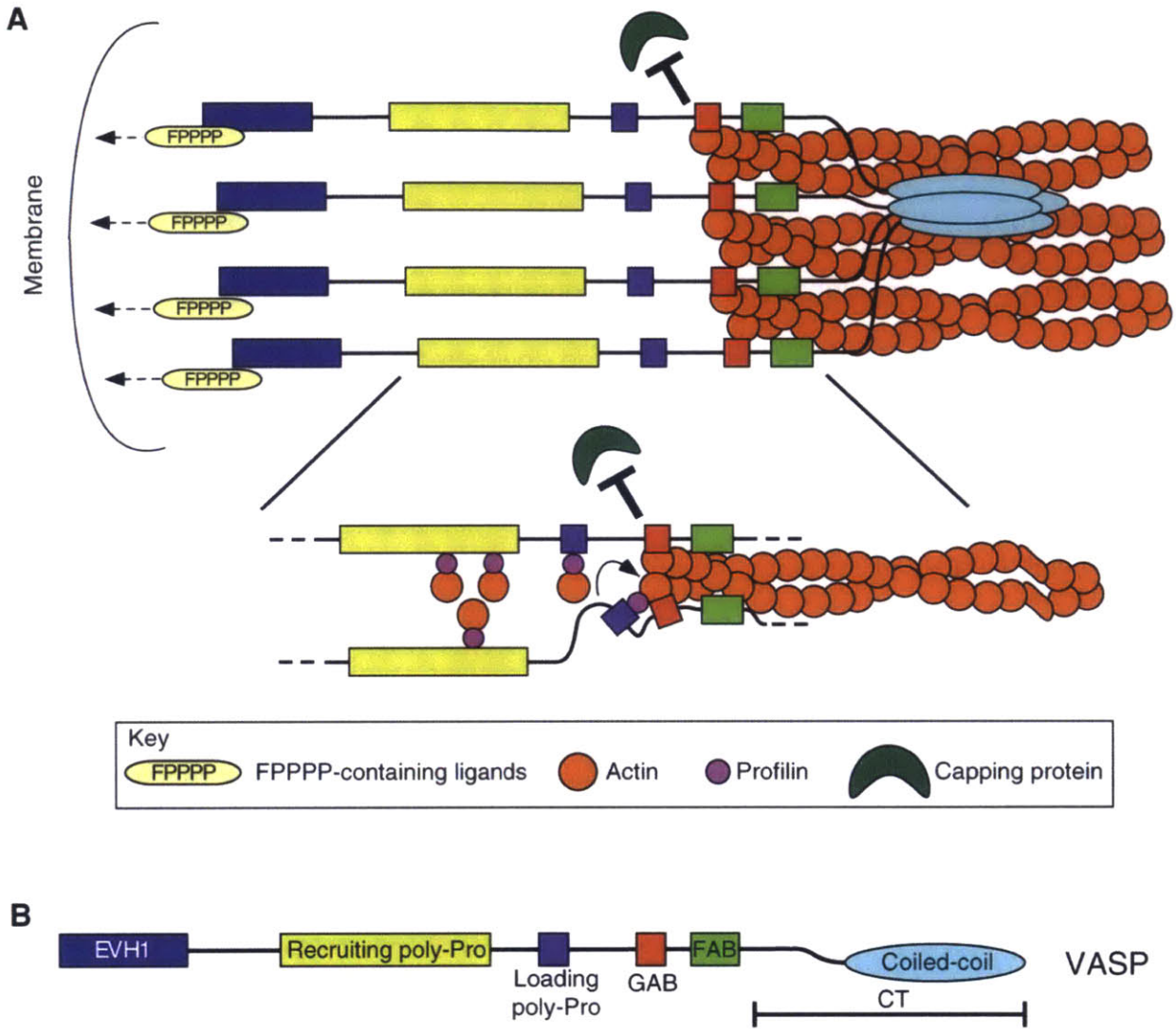

Figure 1.5: "Anti-capping" model of Ena/VASP regulation of actin filament elongation (Adapted from (44)). (A) VASP tetramer interacting with the barbed end of an actin filament, elongating the filament in the presence of CP. (B) Mechanism by which Ena/VASP proteins provide profilin-G-actin monomers to barbed ends of actin filaments.

1.4.2.2 Filopodia

Filopodia are actin-based protrusive structures that integrate extracellular stimuli into intracellular signaling, resulting in the regulation of multiple cellular processes (89), such as neurite initiation (90), axon outgrowth and guidance (91), and cell-cell (92) and

cell-matrix adhesion (93). Structurally, as demonstrated by EM, filopodia are tightly bundled, parallel actin filaments that extend beyond the cell edge (94). There are two prevailing models of filopodium initiation: the "convergent elongation" model and the "de novo" model (89).

In the "convergent elongation" model, filopodia arise from Arp2/3-mediated branched lamellipodial filaments that are formed downstream of Cdc42 signaling. Cdc42 (a small G protein) activates the WASP family of proteins, which are positive regulators of Arp2/3. The barbed ends of these branched lamellipodial filaments are decorated with Ena/VASP proteins, potentially acting as markers for filopodial initiation (89). In this model, Ena/VASP proteins associate with the barbed ends, cluster them, and promote polymerization of filaments by antagonizing CP. These filaments are bundled and further stabilized by fascin, an actin-crosslinking protein (89), resulting in a filopodia anchored to a lamellipodial network.

Another potential mechanism of filopodia initiation and subsequent formation is through the "de novo" model. This model suggests that filopodia arise from de novo nucleation of actin, followed by Diaphanous related formin Dia2-mediated filopodial formation. Dia2 promotes polymerization and elongation of actin filaments and protects barbed ends from CP; other formins can promote filopodia formation as well (89).

Ena/VASP proteins promote the formation and maintenance of filopodia, and multiple studies have demonstrated that Ena/VASP can increase the number of filopodia formed, filopodial length, and the rate of filopodial extension (95, 96). Ena/VASP proteins stably localize to tips of filopodia (74, 97); EVH1-mediated interactions (65) bring Ena/VASP proteins to the membrane, and the EVH2 domain can

stabilize Ena/VASP interactions at the tip with actin (74). Ena/VASP can bind processively to barbed ends of actin filaments and increase the rate of polymerization (48), protect barbed ends from CP (45, 46), and cluster barbed ends of actin filaments together (74).

Recent work has shown that Ena/VASP can modulate the function of other proteins that drive or regulate filopodia in coordination with the formin-family Diaphanous/mDia2 F-actin nucleation/elongation factors (97, 98) and the multifunctional Eps8 and IRSp53 proteins (99, 100), suggesting alternate mechanisms of filopodium initiation and formation are in play in a context-dependent manner. In both *Drosophila* and respective mammalian orthologs, Ena/VASP can regulate Dia/mDia2-mediated filopodial dynamics, and Ena/VASP and Dia/mDia2 are demonstrated to have different effects on filopodia structure and function; for example, Dia/mDia2 form significantly longer filopodia when compared to those resulting from Ena/VASP (97, 98). IRSp53 association with the capping protein Eps8 inhibits actin assembly at the plasma membrane; active Cdc42 is able to relieve this inhibition by promoting IRSp53-mediated clustering of VASP and allowing for processive filament elongation and filopodial formation (99, 100)

Ena/VASP proteins can regulate filopodial function in multiple cell types, including fibroblasts (74) and neurons (96). *In vivo,* Ena/VASP play a key role in the initiation of neurites, which are the precursors to axon and dendrite formation in neuronal development. Cortical neurons lacking Ena/VASP proteins have a defect in neuritogenesis due to a failure in bundling actin filaments and filopodia formation (101).

1.4.2.3 Growth cones

During development, neurons must be guided to reach their proper targets. The growth cone is a dynamic, "fan-shaped" structure at the end of axons composed of lamellipodia and filopodia that constantly protrude and retract in response to signaling downstream of guidance receptors. The cytoskeletal-mediated events during axonal outgrowth can be delineated into three main steps: a protrusive response towards a positive guidance cue, which is coordinated by tip-complex proteins (i.e. actin nucleating and actin binding proteins), subsequent interaction and polarized growth of microtubules (MT) along bundled actin filaments (coupled with shuttling of organelles and vesicles), resulting in directional axonal outgrowth, and final retraction through disassembly of both actin and MT filaments (102, 103).

Ena/VASP proteins function downstream of guidance receptor signaling; *Drosphila* Ena and *C. elegans* UNC-34 directly interact with the repulsive guidance receptors Robo and SAX-3, respectively, resulting in repulsive axon guidance (54, 55). Interestingly, Robo contains EVH1 binding sites, allowing Ena to bind directly to the CC2 cytoplasmic motif of Robo (55). The *C. elegans* UNC-34 ortholog also functions downstream of UNC-40/DCC and UNC-5, which are netrin guidance receptors (103). The vertebrate Ena/VASP proteins increase the number of filopodia formed and elongation of filopodia in neurons downstream of netrin-1, a ligand of the guidance receptor DCC (96), suggesting Ena/VASP proteins may have a role in regulating growth cone filopodial dynamics.

1.4.2.4 Cell-cell adhesions

Cell-cell adhesions provide mechanical support and barrier function to tissues and maintain apico-basal polarity. Vertebrate epithelia have specialized apical junctions, including tight junctions (TJ) and adherens junctions (AJ) (104). Tight junctions, which are more apical than adherens junctions, act as a paracellular barrier and regulate the intercellular movement of solutes and macromolecules. Architecturally, they consist of homo- and hetero-oligomers of cell adhesion molecules (i.e claudins and occludins), which recruit PDZ-motif containing scaffolding proteins (e.g. ZO-1) that interact with actin binding proteins and the actin cytoskeleton (105).

Adherens junctions, in particular, the zonula adherens (ZA) are formed from homophilic interactions between the ectodomains of cadherins, which are Ca2+-dependent cell adhesion molecules. Initially, cells make filopodia-like projections to contact neighboring cells, forming nascent adherens junctions. Although the extracellular interaction between cadherins is weak, this is further strengthened by interactions between the cytoplasmic tails of cadherins and beta-catenin/p120 catenin, which connect to the actin cytoskeleton through dynamic interactions with alpha-catenin and other actin binding proteins, such as zyxin, vinculin, and Ena/VASP (106). Linkage with the actin cytoskeleton can anchor and cluster adherens junctions, forming stable puncta or mature adherens junctions, thus strengthening the adhesion. Cadherin clusters are signaling hubs; homophilic E-cadherins can signal through the Rho family of small G- proteins, which regulate actin dynamics, as well as PI3K (107). The junctional cytoskeleton is dynamic; Arp2/3 nucleates and mediates actin assembly, and

can interact with non-muscle myosin II to generate tension, which can influence tissue organization. Adjacent mature adherens junctions form a zipper-like structure and cytoskeletal rearrangements form actin cables that help opposing membranes seal into epithelial sheets (106).

The Ena/VASP actin regulatory proteins localize and contribute to cell-cell adhesions in both invertebrates and vertebrates. The Ena/VASP ortholog in *C.elegans*, UNC-34 contributes to cadherin-based junctions in epidermal-sheet sealing (108), and *Drosophila Enabled* regulates the spatial organization of F-actin at cell-cell junctions of follicular epithelium during oogenesis (109) and plays a key role in epithelial morphogenetic processes such as dorsal closure (110). In vertebrates, Ena/VASP, as well as their EVH1 binding ligands, zyxin and vinculin, localize to cell-cell junctions (111, 92). Ena/VASP have roles in tension-regulated actin dynamics at epithelial zonula adherens (112), and also maintain endothelial cell junctions *in vivo*; Ena/VASP deficient mice have severe endothelial barrier defects (113).

1.4.2.5 Cell-matrix adhesions

Cells make nascent adhesions, transient focal complexes, and focal adhesions with the extracellular matrix (ECM); the composition of these adhesions is continuously changing as the adhesion matures and turns over (114). Integrins are heterodimeric adhesion receptors that coordinate bidirectional signaling between the intracellular actin cytoskeleton and the ECM (115). Integrin-based adhesions are highly complex, with over ~150 proteins making up the integrin adhesome (116). During cell migration, initial nascent adhesions and focal complexes form at the edge of protrusions, and these can

mature into more stable focal adhesions, which contain clusters of activated integrins. The extracellular domain of integrins bind ECM, and the cytoplasmic domain recruits signaling proteins, such as FAK, structural proteins, such as talin, and actin regulatory proteins, such as vinculin, zyxin, and Ena/VASP, amongst the many other proteins that compose the integrin adhesome (116). Eventually, the focal adhesions turnover, which is FAK and Src-tyrosine kinase regulated in protrusions (117).

Ena/VASP proteins localize to focal adhesions and interact with multiple focal adhesion proteins, including zyxin and vinculin (51). The function of Ena/VASP at cell-matrix adhesions remains an area of active study. VASP regulates activation of the αIIbβ3 integrin (60), and recent work demonstrated that the "LERER" region of Mena interacts directly with the cytoplasmic tail of α5 integrin and contributes to many α5β1 functions, including cell spreading, cell motility on fibronectin, phosphorylation of focal adhesion kinase (FAK) and paxillin, and bidirectional signaling (118). RIAM and Lamellipodin, which are both Ena/VASP binding proteins (65, 66), drive talin mediated inside-out activation of integrins (119, 120).

1.5 Differences among Ena/VASP proteins

Mena, VASP, and EVL are not created equally; two or more of the paralogs share similar characteristics, and other characteristics are unique to Mena (Figure 1.6). Mena, but not VASP and EVL, contains a 5-residue LERER motif that is repeated between the EVH1 domain and proline-rich region (called the "LERER repeat") (56, 121). The "LERER" repeat has been shown to interact directly with the cytoplasmic tail of α5 integrin (118). The α5:Mena interaction contributes to key α5β1-mediated functions, including cell motility on fibronectin and bidirectional signaling (118).

Mena and EVL are alternatively spliced; VASP is not. Mena has multiple alternate exons, including the INV exon between the EVH1 and LERER region (56), the v6 isoform which excludes an exon between the LERER repeat region and the central pro-rich region (122), and the 11a exon, another small exon included in the EVH2 domain between the FAB and the CC region (123) (Figure 1.6), amongst others. EVL protein, like Mena, has a small exon included in the EVH2 domain between the FAB and CC region, termed EVL-I (69) that is regulated by phosphorylation. Alternative splicing of Mena results in distinct isoforms with separate functions; the Mena isoform, $Mena^{INV}$ confers invasive phenotypes to cancer cells, whereas Mena11a does not (121, 123–126).

Ena/VASP proteins are post-translationally modified by phosphorylation; all three vertebrate paralogs are substrates for the cGMP/cAMP-dependent kinases PKA and PKG (56, 69, 127) (Figure 1.6). VASP contains three Ser/Thr phosphorylation sites that are PKA/PKG substrates (S157, S239, and T278 in human VASP); Mena contains two (S236, S376 in murine Mena), and Evl contains one (S160 in human EVL). The phosphorylation site upstream of the pro-rich region is conserved in all three vertebrates (S157 in human VASP, S236 in murine Mena, S160 in human EVL, Figure 1.6), and causes an electrophoretic mobility bandshift (56, 57, 69). In VASP, phosphorylation of the S157 site can inhibit binding to αII-spectrin at endothelial cell-cell contacts (128), and enhance VASP subcellular localization to the leading edge and focal adhesions in endothelial cells (129). Phosphorylation of the same conserved site in Mena S236 affects random fibroblast motility, but has no effect on subcellular targeting (72), and

phosphorylation of the conserved site in Evl S160 disrupts Evl binding to the SH3 domain containing proteins nSrc and Abl and regulates its interaction with F-actin (69).

The PKA/PKG-mediated phosphorylation site S239 in VASP has recently been demonstrated to be upregulated in Ras-transformed cells to promote apical extrusion (130), and also regulates smooth muscle cell contraction and invasion in response to nitric oxide (131). Both S239 and T278 phosphorylation in VASP impairs F-actin accumulation *in vitro* (45, 129). In Mena, the additional PKA/PKG-mediated phosphorylation site S376 has no apparent function in random fibroblast motility (72), but pseudo-phosphorylation of this site does affect F-actin accumulation *in vitro* (129).

Recent work has demonstrated that S157, and an additional site, S322 on VASP can be phosphorylated by PKD1, resulting in the relocalization of VASP from focal contacts to the leading edge (132), and T278 and S322 on VASP can be phosphorylated by AMPK, primarily affecting interaction with F-actin (133, 134). EVL-I is also phosphorylated by PKD in the 21 amino acid insertion in the EVH2 domain at S345 (murine). Phosphorylated Evl-I is enriched at cell-cell junctions, and impairment of S345 phosphorylation increases lamellipodial ruffling (135).

Mena has two additional Ser/Thr phosphorylation sites that are currently being investigated: S125, which is upstream of the INV inclusion (Riquelme, communication), and S3 in the 21 amino acid 11a inclusion (Mondal, unpublished data, Figure 1.6). Although primarily Ser/Thr phosphorylated, it has been shown that the neural variant of Mena (which includes the + exon between the LERER region and pro-rich region) is a substrate for tyrosine phosphorylation, and one study demonstrates that Abi1 promotes Mena tyrosine phosphorylation at Y296 by c-Abl kinase (136). Interestingly, *Drosophila*

Enabled, a substrate of D-Abl, is tyrosine and serine phosphorylated (53), but the function of this phosphorylation is still not clear (137, 138).

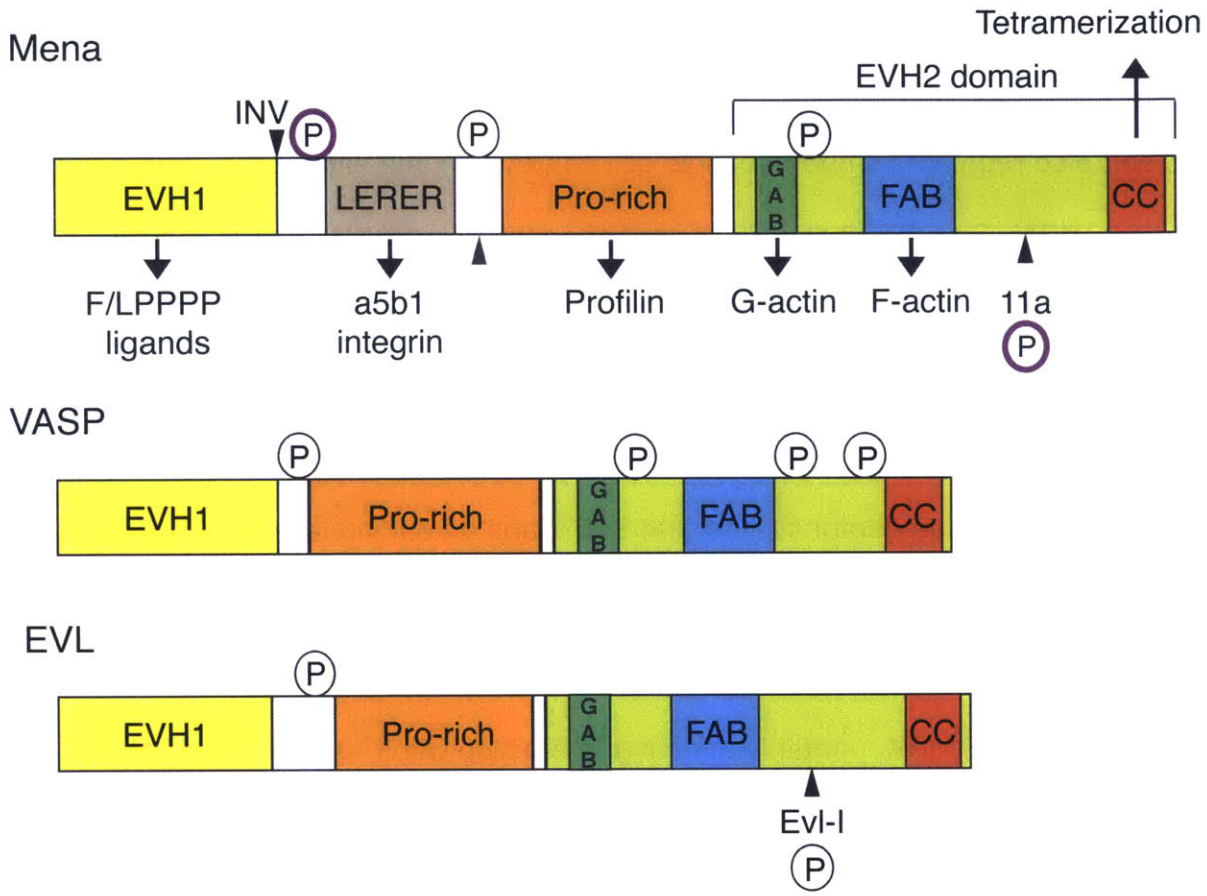

Figure 1.6. Domain structure of vertebrate Ena/VASP proteins highlighting differences. Encircled P = sites of Ser/Thr phosphorylation. Encircled P highlighted in purple = unpublished Ser/Thr phosphorylation sites. Carrots indicate sites of alternate exon inclusion.

1.6 Ena/VASP proteins in human disease

The alteration of Ena/VASP protein expression can result in human disease; VASP is evidenced to play a role in thrombosis, arteriosclerosis, and nephritis (139), and both Mena and VASP are implicated in cardiac abnormalities (139–141). All three Ena/VASP proteins are expressed in many cancer types (142–144) and play key roles in regulating breast cancer progression (142, 143, 145). Interestingly, during breast tumor

progression, Mena is alternatively spliced to produce multiple protein isoforms; Mena and its isoforms, Mena^{INV} and Mena11a, have distinct roles in tumor cell motility and invasion (142), and the functionality of each isoform continues to be an active area of study.

1.6.1 Mena isoforms in cancer

1.6.1.1 Mena

Mena is upregulated in multiple human epithelial tumors, including breast, pancreas, colon, and cervix (146–150), and in invasive mammary carcinoma cells collected *in vivo* using chemoattractant-containing needles (151, 152). To study the effects of Mena *in vivo,* mice containing the polyoma middle-T transgene (MMTV-PyMT) were crossed to Mena deficient mice. In this model, which recapitulates human pathology (153), Mena deficiency delays tumor progression and reduces invasion, intravasation, and metastatic spread of carcinoma cells, but has no effect on tumor growth (154). In breast cancer patients, metastatic risk is correlated with the density of tripartite anatomical structures that contain an endothelial cell, a macrophage, and a carcinoma cell expressing Mena (TMEM, tumor microenvironment of metastasis) within tumors (155, 156).

In vitro, MTLn3 rat mammary carcinoma cells overexpressing Mena have been demonstrated to exhibit lamellipodial protrusion in response to low EGF concentrations when compared to control cells, promote invasion in a 3D collagen matrix, and increase the stability and degradation of invadopodia, which are specialized actin-rich protrusion structures (121). When highly invasive carcinoma cells are cultured on dense ECM,

they form membrane protrusions, or invadopodia, in response to EGF that can degrade the matrix beneath (157). Mechanistically, Mena has recently been demonstrated to regulate receptor tyrosine kinase signaling in average primary tumor cells; activated EGFR recruits complexes that contain Mena and PTP1B, a tyrosine phosphatase, in a SHIP2-dependent manner, resulting in the attenuation of receptor tyrosine kinase signaling (158).

1.6.1.2 Mena^{INV}

In vivo, invasive migratory mammary carcinoma cells spontaneously express Mena^{INV}; the "INV" exon is alternatively included between the EVH1 domain and LERER repeat region (Figure 1.6). Mena^{INV} expressing cells can invade or chemotax in response to approximately 25-50 fold less EGF than cells expressing equivalent levels of Mena lacking the INV inclusion (121); Mena^{INV} potentiates actin polymerization at the leading edge, invadopodium stabilization, extracellular matrix degradation, and *in vivo* migration and intravasation, increasing cells' invasive and metastatic capability (121, 124, 125). In invasive tumor cells expressing high levels of Mena^{INV}, recruitment of PTP1B to EGFR is disrupted, resulting in decreased receptor dephosphorylation, sensitized response to EGF and other growth factors, increased resistance to tyrosine kinase inhibitors, and differential tyrosine phosphorylation of EGFR and a subset of its downstream signaling targets compared to control cells (158).

1.6.1.3 Mena11a

Mena11a was first cloned from the human SBT breast cancer cell line (123), and includes a 21 amino acid sequence between the FAB and CC of the EVH2 domain of Mena (Figure 1.6). Mena11a is expressed in epithelial-like breast cancer cell lines, and

long-term treatment with EGF in these cell lines resulted in phosphorylation of the isoform, as demonstrated by 2D-gel electrophoresis (123). Expression of Mena11a at the protein level was also determined in non-neoplastic pancreatic cell lines with high E-cadherin levels; Mena11a was also constitutively phosphorylated in these cell lines, suggesting additional levels of regulation of this isoform (126).

The Mena11a isoform is expressed primarily in epithelial carcinoma cell lines in part by the activity of epithelial-specific splicing factors, such as the ESRP family (159). Depletion of ESRP1 and ESRP2 in a human prostatic epithelial cell line, PNT2, resulted in decreased 11a inclusion (159). Further analysis demonstrated Mena11a as part of an ESRP-regulated "splicing-signature," and found that the 11a exon was included in epithelial cancer cells, but excluded in mesenchymal cancer cells at the mRNA level (160). In human mammary epithelial cells that have undergone epithelial-to-mesenchymal transition (EMT) through Twist expression (HMLE-Twist), Mena11a protein levels are reduced. Expression of ESRP1 in HMLE-Twist cells was sufficient for the re-expression of Mena11a protein (161). In addition, the RbFox family of splicing factors have been demonstrated to regulate 11a inclusion (162–164). Mena11a exclusion from mesenchymal cells (123, 126) is regulated by drivers of EMT, as well as additional splicing pathways (161–163, 165). Downregulation of CLK2, a kinase that phosphorylates SR proteins, results in the decrease of RbFox2 expression and 11a inclusion in the MCF7 human epithelial-like breast cancer cell line, suggesting that the effects of Clk2 on 11a inclusion may occur in an RbFox2-mediated manner (165).

In MTLn3 rat mammary adenocarcinoma cells, overexpression of the Mena11a isoform resulted in decreased EGF-elicited 3-dimensional (3D) invasion in collagen

matrix both *in vitro* and *in vivo.* Xenograft studies demonstrated that MTLn3 cells overexpressing Mena11a were able to form primary mammary tumors but unable to metastasize to the lungs efficiently (125). Mena11a expression was examined in clinical samples; multiplexed quantitative immunofluorescence (MQIF) of tissue microarrays was used to measure protein expression of all Mena isoforms (with a pan-Mena antibody (166)) and Mena11a (with an isoform-specific antibody (126)) in three independent breast cancer patient cohorts (167, 168). Protein expression levels of Mena or Mena11a alone were not associated with overall survival; however, high values of MenaCalc (hereafter MenaCalc^{PR}), a metric measuring the difference between all Mena isoforms and Mena11a protein levels, were associated with decreased overall survival (167, 168).

Mena11a is demonstrated to play a role in cancer progression; however, the molecular and cellular function of Mena11a protein has not yet been investigated. In this work, we examine the expression and spatial distribution of Mena11a in normal tissues, the molecular and cellular function of Mena11a protein in multiple contexts, and determine the regulation of Mena11a function.

1.7 References

1. McMahon A, Supatto W, Fraser SE, Stathopoulos A (2008) Dynamic Analyses of Drosophila Gastrulation Provide Insights into Collective Cell Migration. *Sci* 322 (5907):1546–1550.
2. Theveneau E, Mayor R (2012) Neural crest migration: interplay between chemorepellents, chemoattractants, contact inhibition, epithelial-mesenchymal transition, and collective cell migration. *Wiley Interdiscip Rev Dev Biol* 1(3):435–445.
3. Friedl P, Gilmour D (2009) Collective cell migration in morphogenesis, regeneration and cancer. *Nat Rev Mol Cell Biol* 10(7):445–457.
4. Friedl P, Weigelin B (2008) Interstitial leukocyte migration and immune function. *Nat Immunol* 9(9):960–969.
5. Friedl P, Wolf K (2003) Tumour-cell invasion and migration: diversity and escape mechanisms. *Nat Rev Cancer* 3(5):362–374.
6. Lauffenburger DA, Horwitz A (1996) Cell migration: a physically integrated molecular process. *Cell* 84(3):359–69.
7. Sarris M, Sixt M (2015) Navigating in tissue mazes: chemoattractant interpretation in complex environments. *Curr Opin Cell Biol* 36:93–102.
8. Haeger A, Wolf K, Zegers MM, Friedl P (2015) Collective cell migration: guidance principles and hierarchies. *Trends Cell Biol* 25(9):556–566.
9. Blanchoin L, Boujemaa-Paterski R, Sykes C, Plastino J (2014) Actin dynamics, architecture, and mechanics in cell motility. *Physiol Rev* 94(1):235–263.
10. Huttenlocher A (1995) Adhesion in cell migration. *Curr Opin Cell Biol* 7(5):697–706.
11. Clark AG, Wartlick O, Salbreux G, Paluch EK (2014) Stresses at the cell surface during animal cell morphogenesis. *Curr Biol* 24(10):R484–94.
12. Nelson WJ (2008) Regulation of cell–cell adhesion by the cadherin–catenin complex. *Biochem Soc Trans* 36(2):149–155.
13. Case LB, Waterman CM (2015) Integration of actin dynamics and cell adhesion by a three-dimensional, mechanosensitive molecular clutch. *Nat Cell Biol* 17(8):955–963.
14. Dramsi S, Cossart P (1998) INTRACELLULAR PATHOGENS AND THE ACTIN CYTOSKELETON. *Annu Rev Cell Dev Biol* 14(1):137–166.

15. Heng Y-W, Koh C-G (2010) Actin cytoskeleton dynamics and the cell division cycle. *Int J Biochem Cell Biol* 42(10):1622–1633.

16. Engqvist-Goldstein ÅEY, Drubin DG (2003) Actin Assembly and Endocytosis: From Yeast to Mammals. *Annu Rev Cell Dev Biol* 19(1):287–332.

17. Stamnes M (2002) Regulating the actin cytoskeleton during vesicular transport. *Curr Opin Cell Biol* 14(4):428–433.

18. Gunst SJ, Zhang W (2008) Actin cytoskeletal dynamics in smooth muscle: a new paradigm for the regulation of smooth muscle contraction. *Am J Physiol Cell Physiol* 295(3):C576–87.

19. Batters C, Veigel C, Homsher E, Sellers JR (2014) To understand muscle you must take it apart. *Front Physiol* 5:90.

20. Pollard TD, Cooper JA (2009) Actin, a Central Player in Cell Shape and Movement. *Sci* 326 (5957):1208–1212.

21. Pollard TD, Borisy GG (2003) Cellular motility driven by assembly and disassembly of actin filaments. *Cell* 112(4):453–465.

22. Bamburg JR, McGough A, Ono S (1999) Putting a new twist on actin: ADF/cofilins modulate actin dynamics. *Trends Cell Biol* 9(9):364–370.

23. Pollard TD, Cooper JA (1986) Actin and actin-binding proteins. A critical evaluation of mechanisms and functions. *Annu Rev Biochem* 55:987–1035.

24. Loisel TP, Boujemaa R, Pantaloni D, Carlier M-F (1999) Reconstitution of actin-based motility of Listeria and Shigella using pure proteins. *Nature* 401(6753):613–616.

25. Geese M, et al. (2002) Contribution of Ena/VASP Proteins to Intracellular Motility of Listeria Requires Phosphorylation and Proline-rich Core but Not F-Actin Binding or Multimerization. *Mol Biol Cell*:1–14.

26. Welch MD, Iwamatsu A, Mitchison TJ (1997) Actin polymerization induced by Arp2/3 protein complex at the surface of Listeria monocytogenes.pdf. *Nature* 385(6613):265–269.

27. Theriot JA, Mitchison TJ, Tilney LG, Portnoy DA (1992) The rate of actin-based motility of intracellular Listeria monocytogenes equals the rate of actin polymerization. *Nature* 357(6375):257–260.

28. Laurent V, et al. (1999) Role of proteins of the Ena/VASP family in actin-based motility of Listeria monocytogenes. *J Cell Biol* 144(6):1245–1258.

29. Kahn RA, Fu H, Roy CR (2002) Cellular hijacking: a common strategy for microbial infection. *Trends Biochem Sci* 27(6):308–314.

30. Machesky LM, Atkinson SJ, Ampe C, Vandekerckhove J, Pollard TD (1994) Purification of a cortical complex containing two unconventional actins from Acanthamoeba by affinity chromatography on profilin-agarose. *J Cell Biol* 127(1):107–115.

31. Rotty JD, Wu C, Bear JE (2013) New insights into the regulation and cellular functions of the ARP2/3 complex. *Nat Rev Mol Cell Biol* 14(1):7–12.

32. Pollard TD (2007) Regulation of actin filament assembly by Arp2/3 complex and formins. *Annu Rev Biophys Biomol Struct* 36:451–477.

33. Welch MD, Rosenblatt J, Skoble J, Portnoy DA, J MT (1998) Interaction of Human Arp2/3 Complex and the Listeria monocytogenes ActA Protein in Actin Filament Nucleation. *Science (80-)* 281(5373):105–108.

34. Goley ED, Welch MD (2006) The ARP2/3 complex: an actin nucleator comes of age. *Nat Rev Mol Cell Biol* 7(10):713–726.

35. Cooper JA, Schafer DA (2000) Control of actin assembly and disassembly at filament ends. *Curr Opin Cell Biol* 12(1):97–103.

36. Edwards M, et al. (2014) Capping protein regulators fine-tune actin assembly dynamics. *Nat Rev Mol Cell Biol* 15(10):677–689.

37. Akin O, Mullins RD (2008) Capping Protein Increases the Rate of Actin-Based Motility by Promoting Filament Nucleation by the Arp2/3 Complex. *Cell* 133(5):841–851.

38. Blanchoin L, Pollard TD, Mullins RD (2000) Interactions of ADF/cofilin, Arp2/3 complex, capping protein and profilin in remodeling of branched actin filament networks. *Curr Biol* 10(20):1273–1282.

39. Rosenblatt J, Agnew BJ, Abe H, Bamburg JR, Mitchison TJ (1997) Xenopus Actin Depolymerizing Factor/Cofilin (XAC) Is Responsible for the Turnover of Actin Filaments in Listeria monocytogenes Tails. *J Cell Biol* 136 (6):1323–1332.

40. Vinson VK, De La Cruz EM, Higgs HN, Pollard TD (1998) Interactions of Acanthamoeba Profilin with Actin and Nucleotides Bound to Actin. *Biochemistry* 37(31):10871–10880.

41. Yarmola EG, Bubb MR (2006) Profilin: emerging concepts and lingering misconceptions. *Trends Biochem Sci* 31(4):197–205.

42. Schluter K, Jockusch BM, Rothkegel M (1997) Profilins as regulators of actin dynamics. *Biochim Biophys Acta* 1359(2):97–109.

43. Goode BL, Eck MJ (2007) Mechanism and Function of Formins in the Control of Actin Assembly. *Annu Rev Biochem* 76(1):593–627.

44. Bear J, Gertler F (2009) Ena/VASP: towards resolving a pointed controversy at the barbed end. *J Cell Sci* 122(12):1947–1953.

45. Barzik M, et al. (2005) Ena/VASP proteins enhance actin polymerization in the presence of barbed end capping proteins. *J Biol Chem* 280(31):28653–28662.

46. Bear JE, et al. (2002) Antagonism between Ena/VASP proteins and actin filament capping regulates fibroblast motility. *Cell* 109(4):509–521.

47. Breitsprecher D, et al. (2011) Molecular mechanism of Ena/VASP-mediated actin-filament elongation. *EMBO J* 30(3):456–467.

48. Hansen S, Mullins R (2010) VASP is a processive actin polymerase that requires monomeric actin for barbed end association. *J Cell Biol* 191(3):571–584.

49. Auerbuch V, Loureiro JJ, Gertler FB, Theriot JA, Portnoy DA (2003) Ena/VASP proteins contribute to Listeria monocytogenes pathogenesis by controlling temporal and spatial persistence of bacterial actin-based motility. *Mol Microbiol* 49(5):1361–1375.

50. Lambrechts A, Gevaert K, Cossart P, Vandekerckhove J, Van Troys M (2008) Listeria comet tails: the actin-based motility machinery at work. *Trends Cell Biol* 18(5):220–227.

51. Krause M, Dent EW, Bear JE, Loureiro JJ, Gertler FB (2003) Ena/VASP proteins: regulators of the actin cytoskeleton and cell migration. *Annu Rev Cell Dev Biol* 19:541–564.

52. Gertler FB, Doctor JS, Hoffmann FM (1990) Genetic suppression of mutations in the Drosophila abl proto-oncogene homolog. *Sci* 248 (4957):857–860.

53. Gertler FB, et al. (1995) enabled, a dosage-sensitive suppressor of mutations in the Drosophila Abl tyrosine kinase, encodes an Abl substrate with SH3 domain-binding properties. *Genes Dev* 9(5):521–533.

54. Yu TW, Hao JC, Lim W, Tessier-Lavigne M, Bargmann CI (2002) Shared receptors in axon guidance: SAX-3/Robo signals via UNC-34/Enabled and a Netrin-independent UNC-40/DCC function. *Nat Neurosci* 5(11):1147–1154.

55. Bashaw GJ, Kidd T, Murray D, Pawson T, Goodman CS (2000) Repulsive axon

guidance: Abelson and Enabled play opposing roles downstream of the roundabout receptor. *Cell* 101(7):703–715.

56. Gertler FB, Niebuhr K, Reinhard M, Wehland J, Soriano P (1996) Mena, a relative of VASP and Drosophila Enabled, is implicated in the control of microfilament dynamics. *Cell* 87(2):227–239.

57. Halbrugge M, Walter U (1989) Purification of a vasodilator-regulated phosphoprotein from human platelets. *Eur J Biochem* 185(1):41–50.

58. Haffner C, et al. (1995) Molecular cloning, structural analysis and functional expression of the proline-rich focal adhesion and microfilament-associated protein VASP. *EMBO J* 14(1):19–27.

59. Hauser W, et al. (1999) Megakaryocyte hyperplasia and enhanced agonist-induced platelet activation in vasodilator-stimulated phosphoprotein knockout mice. *Proc Natl Acad Sci* 96 (14):8120–8125.

60. Aszódi A, et al. (1999) The vasodilator-stimulated phosphoprotein (VASP) is involved in cGMP- and cAMP-mediated inhibition of agonist-induced platelet aggregation, but is dispensable for smooth muscle function. *EMBO J* 18(1):37–48.

61. Han Y-H, et al. (2002) Requirement of a Vasodilator-stimulated Phosphoprotein Family Member for Cell Adhesion, the Formation of Filopodia, and Chemotaxis in Dictyostelium , . *J Biol Chem* 277 (51):49877–49887.

62. Niebuhr K, et al. (1997) A novel proline-rich motif present in ActA of Listeria monocytogenes and cytoskeletal proteins is the ligand for the EVH1 domain, a protein module present in the Ena/VASP family. *EMBO J* 16(17):5433–5444.

63. BRINDLE NPJ, HOLT MR, DAVIES JE, PRICE CJ, CRITCHLEY DR (1996) The focal-adhesion vasodilator-stimulated phosphoprotein (VASP) binds to the proline-rich domain in vinculin. *Biochem J* 318(3):753–757.

64. Drees B, et al. (2000) Characterization of the Interaction between Zyxin and Members of the Ena/Vasodilator-stimulated Phosphoprotein Family of Proteins. *J Biol Chem* 275 (29):22503–22511.

65. Krause M, et al. (2004) Lamellipodin, an Ena/VASP ligand, is implicated in the regulation of lamellipodial dynamics. *Dev Cell* 7(4):571–583.

66. Lafuente EM, et al. (2004) RIAM, an Ena/VASP and Profilin Ligand, Interacts with Rap1-GTP and Mediates Rap1-Induced Adhesion. *Dev Cell* 7(4):585–595.

67. Hansen SD, Mullins RD (2015) Lamellipodin promotes actin assembly by clustering Ena/VASP proteins and tethering them to actin filaments. *Elife* 4.

68. Boëda B, et al. (2007) Tes, a Specific Mena Interacting Partner, Breaks the Rules for EVH1 Binding. *Mol Cell* 28(6):1071–1082.

69. Lambrechts A, et al. (2000) cAMP-dependent Protein Kinase Phosphorylation of EVL, a Mena/VASP Relative, Regulates Its Interaction with Actin and SH3 Domains. *J Biol Chem* 275(46):36143–36151.

70. Reinhard M, et al. (1995) The proline-rich focal adhesion and microfilament protein VASP is a ligand for profilins. *EMBO J* 14(8):1583–1589.

71. Ferron F, Rebowski G, Lee SHHH, Dominguez R (2007) Structural basis for the recruitment of profilin-actin complexes during filament elongation by Ena/VASP. *EMBO J* 26(21):4597–4606.

72. Loureiro JJ, et al. (2002) Critical roles of phosphorylation and actin binding motifs, but not the central proline-rich region, for Ena/vasodilator-stimulated phosphoprotein (VASP) function during cell migration. *Mol Biol Cell* 13(7):2533–2546.

73. Bachmann C, Fischer L, Walter U, Reinhard M (1999) The EVH2 Domain of the Vasodilator-stimulated Phosphoprotein Mediates Tetramerization, F-actin Binding, and Actin Bundle Formation. *J Biol Chem* 274 (33):23549–23557.

74. Applewhite DA, et al. (2007) Ena/VASP Proteins Have an Anti-Capping Independent Function in Filopodia Formation. *Mol Biol Cell* 18(7):2579–2591.

75. Bear JE, Haugh JM (2014) Directed migration of mesenchymal cells: where signaling and the cytoskeleton meet. *Curr Opin Cell Biol* 30:74–82.

76. Law A-L, et al. (2013) Lamellipodin and the Scar/WAVE complex cooperate to promote cell migration in vivo. *J Cell Biol* 203:673–89.

77. Krause M, Gautreau A (2014) Steering cell migration: lamellipodium dynamics and the regulation of directional persistence. *Nat Rev Mol Cell Biol* 15(9):577–590.

78. Yang C, et al. (2007) Novel Roles of Formin mDia2 in Lamellipodia and Filopodia Formation in Motile Cells . *PLoS Biol* 5(11):e317.

79. Block J, et al. (2012) FMNL2 Drives Actin-Based Protrusion and Migration Downstream of Cdc42. *Curr Biol* 22(11):1005–1012.

80. Yang C, et al. (2005) Mammalian CARMIL Inhibits Actin Filament Capping by Capping Protein. *Dev Cell* 9(2):209–221.

81. Bugyi B, Carlier M-F (2010) Control of Actin Filament Treadmilling in Cell Motility.

Annu Rev Biophys 39(1):449–470.

82. Cai L, Makhov AM, Schafer DA, Bear JE (2008) Coronin 1B antagonizes cortactin and remodels Arp2/3-containing actin branches in lamellipodia. *Cell* 134(5):828–842.

83. Haynes EM, et al. (2015) GMFbeta controls branched actin content and lamellipodial retraction in fibroblasts. *J Cell Biol* 209(6):803–812.

84. Cai L, Marshall TW, Uetrecht AC, Schafer DA, Bear JE (2007) Coronin 1B Coordinates Arp2/3 Complex and Cofilin Activities at the Leading Edge. *Cell* 128(5):915–929.

85. Bryce NS, et al. (2005) Cortactin Promotes Cell Motility by Enhancing Lamellipodial Persistence. *Curr Biol* 15(14):1276–1285.

86. Bear JE, et al. (2000) Negative regulation of fibroblast motility by Ena/VASP proteins. *Cell* 101(7):717–728.

87. Rottner K, Behrendt B, Small J V, Wehland J (1999) VASP dynamics during lamellipodia protrusion. *Nat Cell Biol* 1(5):321–322.

88. Krause M, Bear JE, Loureiro JJ, Gertler FB (2002) The Ena/VASP enigma. *J Cell Sci* 115(Pt 24):4721–4726.

89. Gupton SL, Gertler FB (2007) Filopodia: The Fingers That Do the Walking. *Sci Signal* 2007(400):re5–re5.

90. Smith CL (1994) Cytoskeletal movements and substrate interactions during initiation of neurite outgrowth by sympathetic neurons in vitro. *J Neurosci* 14(1):384–398.

91. Dent EW, Tang F, Kalil K (2003) Axon Guidance by Growth Cones and Branches: Common Cytoskeletal and Signaling Mechanisms. *Neurosci* 9 (5):343–353.

92. Vasioukhin V, Bauer C, Yin M, Fuchs E (2000) Directed Actin Polymerization Is the Driving Force for Epithelial Cell–Cell Adhesion. *Cell* 100(2):209–219.

93. Galbraith CG, Yamada KM, Galbraith JA (2007) Polymerizing Actin Fibers Position Integrins Primed to Probe for Adhesion Sites. *Sci* 315 (5814):992–995.

94. Svitkina TM, et al. (2003) Mechanism of filopodia initiation by reorganization of a dendritic network. *J Cell Biol* 160:409–421.

95. Mejillano MR, et al. (2004) Lamellipodial versus filopodial mode of the actin nanomachinery: pivotal role of the filament barbed end. *Cell* 118(3):363–373.

96. Lebrand C, et al. (2004) Critical role of Ena/VASP proteins for filopodia formation in neurons and in function downstream of netrin-1. *Neuron* 42(1):37–49.

97. Barzik M, McClain LM, Gupton SL, Gertler FB (2014) Ena/VASP regulates mDia2-initiated filopodial length, dynamics, and function. *Mol Biol Cell* 25(17):2604–2619.

98. Bilancia CG, et al. (2014) Enabled Negatively Regulates Diaphanous-Driven Actin Dynamics In Vitro and In Vivo. *Dev Cell* 28(4):394–408.

99. Vaggi F, et al. (2011) The Eps8/IRSp53/VASP network differentially controls actin capping and bundling in filopodia formation. *PLoS Comput Biol* 7(7):e1002088.

100. Disanza A, et al. (2013) CDC42 switches IRSp53 from inhibition of actin growth to elongation by clustering of VASP. *EMBO J* 32(20):2735–50.

101. Kwiatkowski A V, et al. (2007) Ena/VASP Is Required for neuritogenesis in the developing cortex. *Neuron* 56(3):441–455.

102. Dent EW, Gupton SL, Gertler FB (2011) The Growth Cone Cytoskeleton in Axon Outgrowth and Guidance. *Cold Spring Harb Perspect Biol* 3(3):a001800.

103. Drees F, Gertler FB (2008) Ena/VASP: proteins at the tip of the nervous system. *Curr Opin Neurobiol* 18(1):53–9.

104. Citi S, Guerrera D, Spadaro D, Shah J (2014) Epithelial junctions and Rho family GTPases: the zonular signalosome. *Small GTPases* 5(4):1–15.

105. Van Itallie CM, Anderson JM (2014) Architecture of tight junctions and principles of molecular composition. *Semin Cell Dev Biol* 36:157–165.

106. Perez-Moreno M, Jamora C, Fuchs E (2003) Sticky Business: Orchestrating Cellular Signals at Adherens Junctions. *Cell* 112(4):535–548.

107. Yap AS, Gomez GA, Parton RG (2015) Adherens Junctions Revisualized: Organizing Cadherins as Nanoassemblies. *Dev Cell* 35(1):12–20.

108. Sheffield M, Loveless T, Hardin J, Pettitt J (2007) C. elegans Enabled Exhibits Novel Interactions with N-WASP, Abl, and Cell-Cell Junctions. *Curr Biol* 17(20):1791–1796.

109. Baum B, Perrimon N (2001) Spatial control of the actin cytoskeleton in Drosophila epithelial cells. *Nat Cell Biol* 3(10):883–890.

110. Gates J, et al. (2007) Enabled plays key roles in embryonic epithelial morphogenesis in Drosophila. *Development* 134:2027–2039.

111. Scott JA, et al. (2006) Ena/VASP proteins can regulate distinct modes of actin

organization at cadherin-adhesive contacts. *Mol Biol Cell* 17(3):1085–1095.

112. Leerberg JM, et al. (2014) Tension-Sensitive Actin Assembly Supports Contractility at the Epithelial Zonula Adherens. *Curr Biol*:1–11.

113. Furman C, et al. (2007) Ena/VASP is required for endothelial barrier function in vivo. *J Cell Biol* 179(4):761–775.

114. Geiger B, Yamada KM (2011) Molecular Architecture and Function of Matrix Adhesions. *Cold Spring Harb Perspect Biol* 3(5):a005033.

115. Hynes RO (2002) Integrins: Bidirectional, Allosteric Signaling Machines. *Cell* 110(6):673–687.

116. Zaidel-Bar R, Itzkovitz S, Ma'ayan A, Iyengar R, Geiger B (2007) Functional atlas of the integrin adhesome. *Nat Cell Biol* 9(8):858–867.

117. Huttenlocher A, Horwitz AR (2011) Integrins in cell migration. *Cold Spring Harb Perspect Biol* 3(9):a005074.

118. Gupton SL, et al. (2012) Mena binds α5 integrin directly and modulates α5β1 function. *J Cell Biol* 198(4):657–76.

119. Lagarrigue F, et al. (2015) A RIAM/lamellipodin-talin-integrin complex forms the tip of sticky fingers that guide cell migration. *Nat Commun* 6.

120. Coló GP, Lafuente EM, Teixidó J (2012) The MRL proteins: Adapting cell adhesion, migration and growth. *Eur J Cell Biol* 91(11–12):861–868.

121. Philippar U, et al. (2008) A Mena invasion isoform potentiates EGF-induced carcinoma cell invasion and metastasis. *Dev Cell* 15(6):813–828.

122. Di Modugno F, et al. (2012) Splicing program of human MENA produces a previously undescribed isoform associated with invasive, mesenchymal-like breast tumors. *Proc Natl Acad Sci* 109(47):19280–5.

123. Di Modugno F, et al. (2007) Molecular cloning of hMena (ENAH) and its splice variant hMena+11a: epidermal growth factor increases their expression and stimulates hMena+11a phosphorylation in breast cancer cell lines. *Cancer Res* 67(6):2657–65.

124. Roussos ET, et al. (2011) Mena invasive (Mena(INV)) and Mena11a isoforms play distinct roles in breast cancer cell cohesion and association with TMEM. *Clin Exp Metastasis* 28(6):515–527.

125. Roussos ET, et al. (2011) Mena invasive (MenaINV) promotes multicellular streaming motility and transendothelial migration in a mouse model of breast

cancer. *J Cell Sci* 124(Pt 13):2120–2131.

126. Pino MS, et al. (2008) Human Mena+11a isoform serves as a marker of epithelial phenotype and sensitivity to epidermal growth factor receptor inhibition in human pancreatic cancer cell lines. *Clin Cancer Res* 14(15):4943–50.

127. WALDMANN R, NIEBERDING M, WALTER U (1987) Vasodilator-stimulated protein phosphorylation in platelets is mediated by cAMP- and cGMP-dependent protein kinases. *Eur J Biochem* 167(3):441–448.

128. Benz PM, et al. (2008) Cytoskeleton assembly at endothelial cell–cell contacts is regulated by αII-spectrin–VASP complexes. *J Cell Biol* 180 (1):205–219.

129. Benz PM, et al. (2009) Differential VASP phosphorylation controls remodeling of the actin cytoskeleton. *J Cell Sci* 122(Pt 21):3954–3965.

130. Anton KA, et al. (2014) PKA-regulated VASP phosphorylation promotes extrusion of transformed cells from the epithelium. *J Cell Sci* 127(16):3425–3433.

131. Defawe OD, et al. (2010) VASP phosphorylation at serine239 regulates the effects of NO on smooth muscle cell invasion and contraction of collagen. *J Cell Physiol* 222(1):230–237.

132. Döppler HR, Bastea LI, Lewis-Tuffin LJ, Anastasiadis PZ, Storz P (2013) Protein Kinase D1-mediated Phosphorylations Regulate Vasodilator-stimulated Phosphoprotein (VASP) Localization and Cell Migration. *J Biol Chem* 288 (34):24382–24393.

133. Blume C, et al. (2007) AMP-activated Protein Kinase Impairs Endothelial Actin Cytoskeleton Assembly by Phosphorylating Vasodilator-stimulated Phosphoprotein. *J Biol Chem* 282 (7):4601–4612.

134. Thomson DM, Ascione MPA, Grange J, Nelson C, Hansen MDH (2011) Phosphorylation of VASP by AMPK alters actin binding and occurs at a novel site. *Biochem Biophys Res Commun* 414(1):215–219.

135. Janssens K, et al. (2009) Characterization of EVL-I as a protein kinase D substrate. *Cell Signal* 21(2):282–292.

136. Tani K, et al. (2003) Abl interactor 1 promotes tyrosine 296 phosphorylation of mammalian enabled (Mena) by c-Abl kinase. *J Biol Chem* 278(24):21685–21692.

137. Ahern-Djamali SM, et al. (1998) Mutations in Drosophila Enabled and Rescue by Human Vasodilator-stimulated Phosphoprotein (VASP) Indicate Important Functional Roles for Ena/VASP Homology Domain 1 (EVH1) and EVH2 Domains. *Mol Biol Cell* 9 (8):2157–2171.

138. Comer AR, Ahern-Djamali SM, Juang J-L, Jackson PD, Hoffmann FM (1998) Phosphorylation of Enabled by the Drosophila Abelson Tyrosine Kinase Regulates the In Vivo Function and Protein-Protein Interactions of Enabled. *Mol Cell Biol* 18(1):152–160.

139. Pula G, Krause M (2008) Role of Ena/VASP proteins in homeostasis and disease. *Handb Exp Pharmacol* (186):39–65.

140. Eigenthaler M, et al. (2003) Disruption of cardiac Ena-VASP protein localization in intercalated disks causes dilated cardiomyopathy. *Am J Physiol Heart Circ Physiol* 285(6):H2471–81.

141. Aguilar F, et al. (2011) Mammalian enabled (Mena) is a critical regulator of cardiac function. *Am J Physiol Heart Circ Physiol* 300(5):H1841–52.

142. Gertler F, Condeelis J (2011) Metastasis: tumor cells becoming MENAcing. *Trends Cell Biol* 21(2):81–90.

143. Mouneimne G, et al. (2012) Differential remodeling of actin cytoskeleton architecture by profilin isoforms leads to distinct effects on cell migration and invasion. *Cancer Cell* 22(5):615–630.

144. Dertsiz L, et al. (2005) Differential expression of VASP in normal lung tissue and lung adenocarcinomas. *Thorax* 60(7):576–581.

145. Doppler H, Bastea L, Borges S, Geiger X, Storz P (2015) The phosphorylation status of VASP at serine 322 can be predictive for aggressiveness of invasive ductal carcinoma. *Oncotarget* 6(30):29740–29752.

146. Di Modugno F, et al. (2004) Human Mena protein, a serex-defined antigen overexpressed in breast cancer eliciting both humoral and CD8+ T-cell immune response. *Int J cancer J Int du cancer* 109(6):909–918.

147. Di Modugno F, et al. (2006) The cytoskeleton regulatory protein hMena (ENAH) is overexpressed in human benign breast lesions with high risk of transformation and human epidermal growth factor receptor-2-positive/hormonal receptor-negative tumors. *Clin Cancer Res* 12(5):1470–8.

148. Toyoda A, et al. (2009) Aberrant expression of human ortholog of mammalian enabled (hMena) in human colorectal carcinomas: implications for its role in tumor progression. *Int J Oncol* 34(1):53–60.

149. Gurzu S, et al. (2008) The expression of cytoskeleton regulatory protein Mena in colorectal lesions. *Rom J Morphol Embryol* 49(3):345–349.

150. Gurzu S, Jung I, Prantner I, Chira L, Ember I (2009) The immunohistochemical

aspects of protein Mena in cervical lesions. *Rom J Morphol Embryol* 50(2):213–216.

151. Wang W, et al. (2007) Coordinated regulation of pathways for enhanced cell motility and chemotaxis is conserved in rat and mouse mammary tumors. *Cancer Res* 67(8):3505–3511.

152. Wang W, et al. (2004) Identification and testing of a gene expression signature of invasive carcinoma cells within primary mammary tumors. *Cancer Res* 64(23):8585–8594.

153. Lin EY, et al. (2003) Progression to malignancy in the polyoma middle T oncoprotein mouse breast cancer model provides a reliable model for human diseases. *Am J Pathol* 163(5):2113–26.

154. Roussos ET, et al. (2010) Mena deficiency delays tumor progression and decreases metastasis in polyoma middle-T transgenic mouse mammary tumors. *Breast Cancer Res* 12(6):R101.

155. Robinson BD, et al. (2009) Tumor microenvironment of metastasis in human breast carcinoma: a potential prognostic marker linked to hematogenous dissemination. *Clin Cancer Res* 15(7):2433–2441.

156. Rohan TE, et al. (2014) Tumor microenvironment of metastasis and risk of distant metastasis of breast cancer. *J Natl Cancer Inst* 106(8):1–11.

157. Yamaguchi H, Pixley F, Condeelis J (2006) Invadopodia and podosomes in tumor invasion. *Eur J Cell Biol* 85(3–4):213–218.

158. Hughes SK, et al. (2015) PTP1B-dependent regulation of receptor tyrosine kinase signaling by the actin-binding protein Mena. *Mol Biol Cell* .

159. Warzecha CC, Sato TK, Nabet B, Hogenesch JB, Carstens RP (2010) ESRP1 and ESRP2 Are Epithelial Cell-Type-Specific Regulators of FGFR2 Splicing. *Mol Cell* 33(5):591–601.

160. Warzecha CC, et al. (2010) An ESRP-regulated splicing programme is abrogated during the epithelial-mesenchymal transition. *EMBO J* 29(19):3286–300.

161. Shapiro IM, et al. (2011) An EMT–Driven Alternative Splicing Program Occurs in Human Breast Cancer and Modulates Cellular Phenotype. *PLoS Genet* 7(8):21.

162. Lovci MT, et al. (2013) Rbfox proteins regulate alternative mRNA splicing through evolutionarily conserved RNA bridges. *Nat Struct Mol Biol*.

163. Braeutigam C, et al. (2014) The RNA-binding protein Rbfox2: an essential

regulator of EMT-driven alternative splicing and a mediator of cellular invasion. *Oncogene* 33(9):1082–1092.

164. Yeo G, et al. (2009) An RNA code for the FOX2 splicing regulator revealed by mapping RNA-protein interactions in stem cells. *Nat Struct & Mol Biol* 16(2):130–137.

165. Yoshida T, et al. (2015) CLK2 Is an Oncogenic Kinase and Splicing Regulator in Breast Cancer. *Cancer Res* 75(7):1516–1526.

166. Lanier LM, et al. (1999) Mena is required for neurulation and commissure formation. *Neuron* 22(2):313–325.

167. Agarwal S, et al. (2012) Quantitative assessment of invasive mena isoforms (Menacalc) as an independent prognostic marker in breast cancer. *Breast Cancer Res* 14(5):R124.

168. Forse C, et al. (2015) Mena calc , a quantitative method of metastasis assessment, as a prognostic marker for axillary node-negative breast cancer. *BMC Cancer* 15(1):483.

Chapter 2: Mena11a is expressed in epithelia and muscle

Figures 2.2 A, B, and D contributed to the following manuscript: Balsamo and Mondal, et al. "Mena-dependent regulation of actin cytoskeleton organization and cell behavior is regulated by the alternatively-included 11a sequence." Manuscript submitted. Figures 2.4 and 2.5 were completed in collaboration with Sara Dubbury (Sharp Lab, MIT), and Dr. Eric Wang (University of Florida).

TABLE OF CONTENTS

2.1 Abstract

The evaluation of endogenous Mena11a expression, at both the mRNA and protein level, has been limited exclusively to epithelial cancer cell lines *in vitro* (1, 2), tumor cells collected from primary mammary tumors (3) and clinical samples (4–6). To understand the general functionality of Mena11a, we interrogated its expression and spatial distribution both during development in mouse embryonic tissues, as well as in normal adult mouse and human tissues. We find that Mena11a protein is strongly enriched in normal mouse and human epithelia (Balsamo and Mondal, submitted). In addition, Mena11a mRNA is highly expressed in normal human heart and skeletal muscle, and Mena11a protein is enriched in mouse embryonic muscle.

2.2 Introduction

Ena/VASP protein expression has been examined in both mouse and human tissues. Western blotting of whole tissue lysate demonstrated mouse Mena enrichment in both the brain and the whole body during mouse embryogenesis (E10 – E15) (7), and in total brain lysate of adult mice (8, 9). Further organ-specific analysis showed that Mena protein is highly expressed in the ovary, testes, and fat of adult mice (8), and in the lung, stomach, kidney, and large intestine in both neonates and adult mice (9). Immunocytochemistry of adult mouse tissue sections showed localization of Mena protein within some of these tissues; Mena localizes to areas of smooth muscle (e.g. lamina mucularis mucosae and lamina propria), as well as the epithelium in the gastrointestinal tract, glomerular mesangial cells in the kidney, and intercalated discs in the heart (9).

VASP, a mammalian paralog of Mena, is also expressed in the brain, lung, stomach, large intestine, kidney, and heart, and has marked colocalization with Mena in most of these tissues (9), suggesting potential compensatory function. However, VASP, which was first identified as a cGMP/cAMP-dependent kinase substrate in human platelets (10), is present in the adult and neonate mouse platelets, while Mena is not (9). Both Evl (another mammalian paralog of Mena) and VASP, but not Mena, are highly expressed in the spleen and thymus of adult mice (8), pointing to differential regulation in these organs.

The Mena11a isoform, which includes a sequence of 21 amino acids in the EVH2 domain between the FAB and CC (Figure 2.1), was first cloned from a human epithelial-like breast cancer cell line (1). Mena11a mRNA and protein expression levels have been examined to some extent in cancer cells *in vitro*, and various mammary tumors and patient samples *in vivo* (2–4), but the localization and functionality of Mena11a in normal tissues is unknown; thus, we evaluated Mena11a protein spatial distribution in embryonic and adult mouse / human tissues, and Mena11a mRNA expression in normal human tissues.

2.3 Results

2.3.1 Mena11a protein is enriched in epithelia *in vivo.*

Using antibodies that recognize all Mena isoforms ("pan-Mena") or Mena11a exclusively (Figure 2.1) for tissue immunofluorescence, we find that Mena11a is differentially distributed in normal tissues compared to pan-Mena (Balsamo and Mondal, submitted).

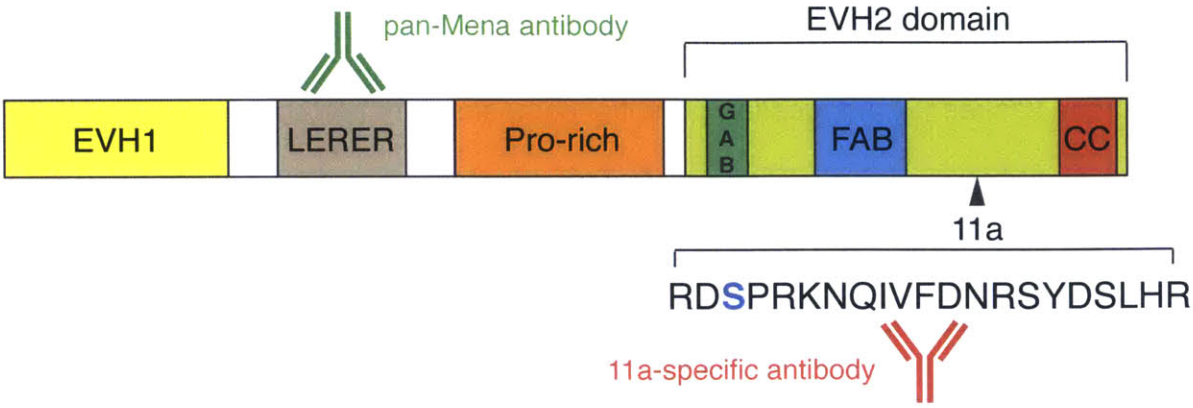

Figure 2.1: Mena11a domain structure. The 11a alternatively-included sequence is located in the EVH2 domain between the F-actin binding region (FAB) and the coiled-coil that mediates oligomerization (CC). The 11a sequence is 21 amino acids; the Mena11a-specific antibody only recognizes the Mena11a isoform; the pan-Mena antibody recognizes all Mena isoforms.

We first examined Mena11a protein expression during development in E15.5 embryos that express Mena, but lack VASP and EVL protein. Mice with at least one allele of Mena and another Ena/VASP allele (MMeevv, MmEevv, MmeeVv) produce viable and fertile mice, with no obvious morphological defects (11). We stained tissues from E15.5 MMeevv mouse embryos because they were readily available. In the E15.5 MMeevv mouse embryos, Mena11a localized to cells in the dermis (Figure 2.2 A) and lung epithelium (Figure 2.2 B), respectively, but was excluded from surrounding pan-Mena-expressing mesenchyme.

Mena11a expression was observed in adult mouse and human epithelial tissues, including adult mouse epidermis, adult mouse bronchioalveolar epithelium (Balsamo and Mondal, submitted), adult bladder epithelium (Figure 2.2 C) and human colon epithelium (Figure 2.2 D). Thus, we conclude that Mena11a is enriched in normal epithelial structures *in vivo* (Balsamo and Mondal, submitted).

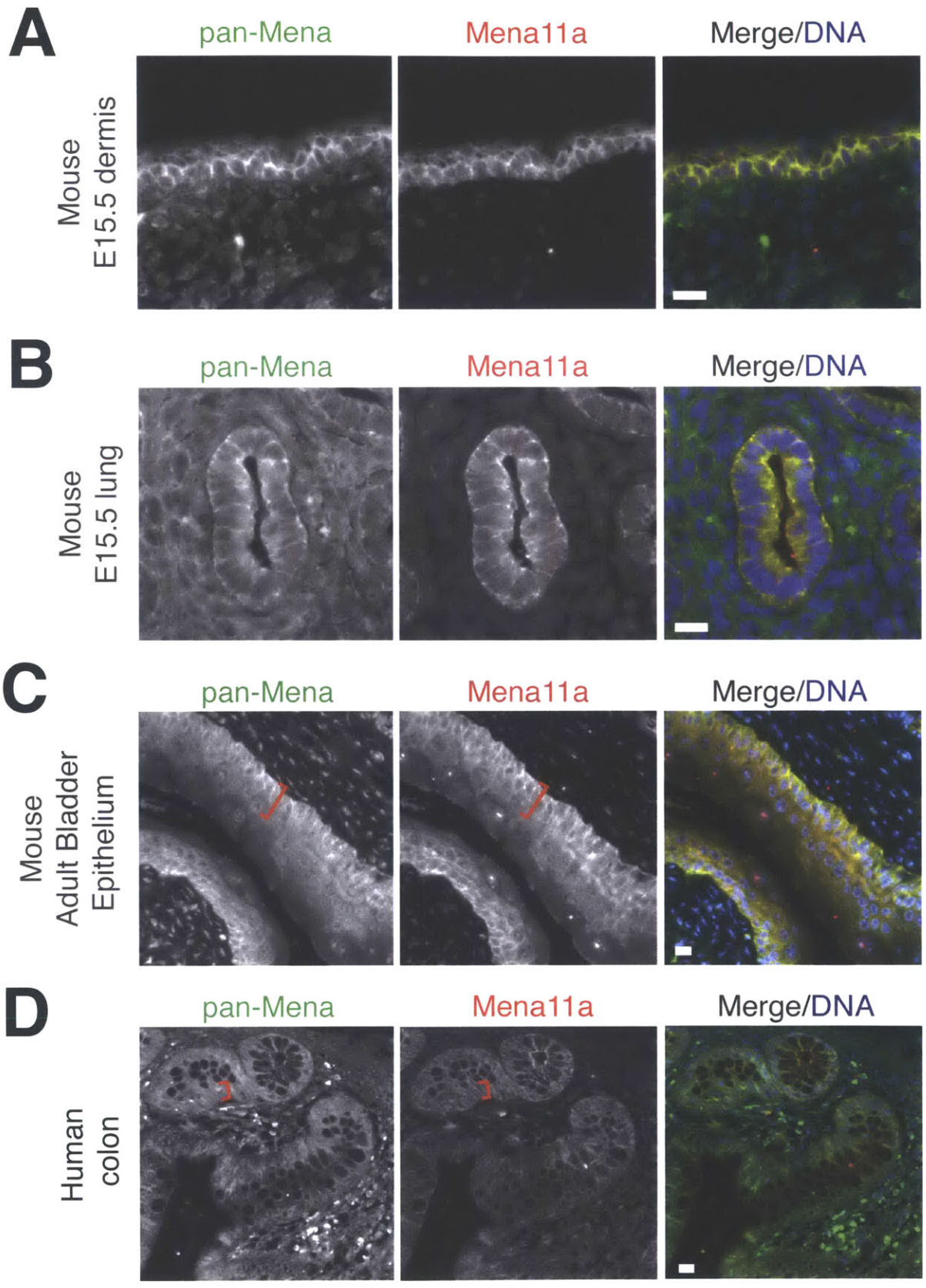
A
pan-Mena
Mena11a
Merge/DNA
Mouse
E15.5 dermis
B
pan-Mena
Mena11a
Merge/DNA
Mouse
E15.5 lung
C
pan-Mena
Mena11a
Merge/DNA
Mouse
Adult Bladder
Epithelium
D
pan-Mena
Mena11a
Merge/DNA
Human
colon

Figure 2.2: Mena11a protein expression in epithelia *in vivo*. Immunofluorescence of Mena11a and pan-Mena in (A) mouse E15.5 dermis, (B) mouse E15.5 lung, (C) mouse adult bladder, (D) adult human colon. DNA is visualized with Hoechst staining. Scale bar, 20 μm. Red brackets in (C) and (D) show epithelial layer where Mena11a is enriched.

2.3.2 Mena11a mRNA and protein is expressed in muscle.

Interestingly, in the same mouse embryos as above that express Mena, but lack VASP and EVL protein, we find that Mena11a is enriched in muscle; there are high levels of Mena11a in a sagittal cross-section of E15.5 mouse diaphragm (Figure 2.3). By E15.5, myofibers have formed in the diaphragm and are beginning to differentiate into the costal and crural skeletal muscles (12). This finding demonstrates Mena11a protein is present during mouse embryonic development in muscle.

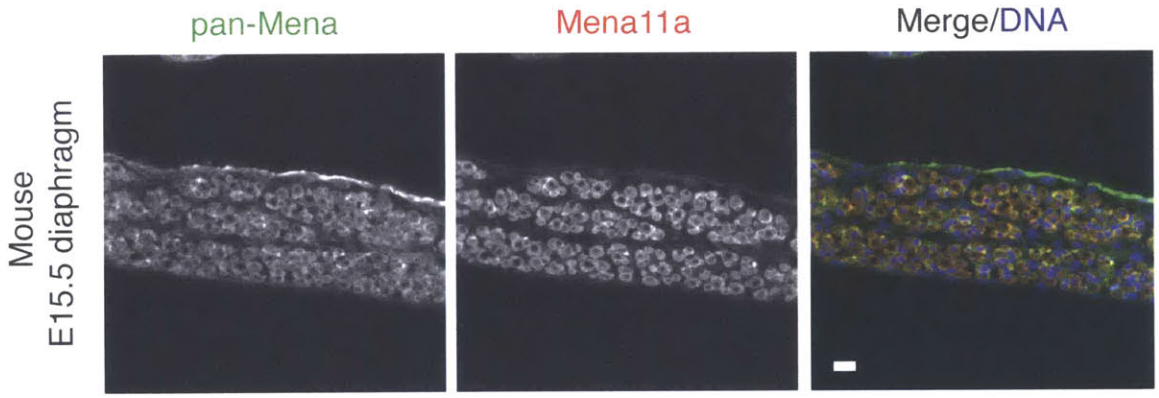

2.3 Mena11a protein is expressed in mouse embryonic muscle.
Immunofluorescence of Mena11a and pan-Mena in mouse E15.5 diaphragm. DNA is visualized with Hoechst staining. Scale bar, 20 μm.

To validate our muscle staining, we accessed publicly available RNAseq reads from the Illumina Body Map 2.0. The Illumina Body Map 2.0 is composed of 16 normal human tissues, including adipose, brain, breast, heart, liver, lung, and skeletal muscle, amongst others. Examining read density per million mapped reads of Mena constitutive

exons (i.e. Const 1 and Const 2), we find that ENAH (gene name for Mena protein) is expressed in adipose, brain, breast, heart, liver, lung, and skeletal muscle tissue, but only present at low levels in liver tissue (Figure 2.4).

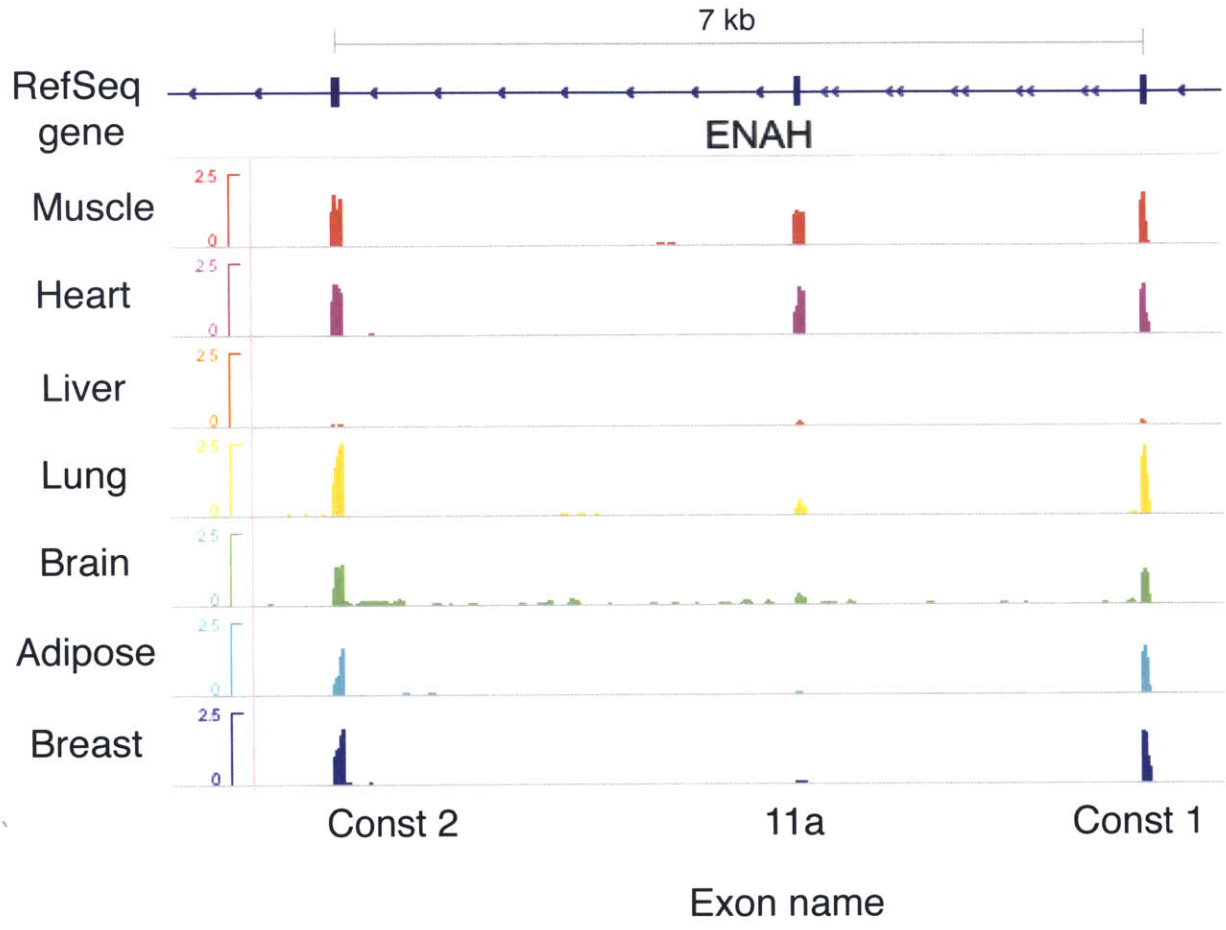

2.4 Relative Mena mRNA expression in human tissues. RNAseq data from the Illumina Body Map 2.0 aligned to hg18. RefSeq gene is ENAH (NCBI accession: NM_001008493.1). Y-axis values: read density/million mapped reads. Y-axis labels: Normal human tissue libraries. Exon name: Const1 and Const 2 are constitutive ENAH exons (chr1:223,762,276-223,762,342 and chr1:223,755,317-223,755,395, respectively), and 11a is an alternate exon (chr1:223,759,316-223,759,378). Directionality is right to left, 5' to 3'. kb = kilobases.

If we now examine the read density per million mapped reads of the alternate 11a exon relative to the constitutive Mena exons (Const 1 and Const 2), we find that most ENAH transcripts in the skeletal muscle and heart include the 11a exon (Figure

2.5). Taken together, this data suggests that Mena11a is expressed in the muscle *in vivo*.

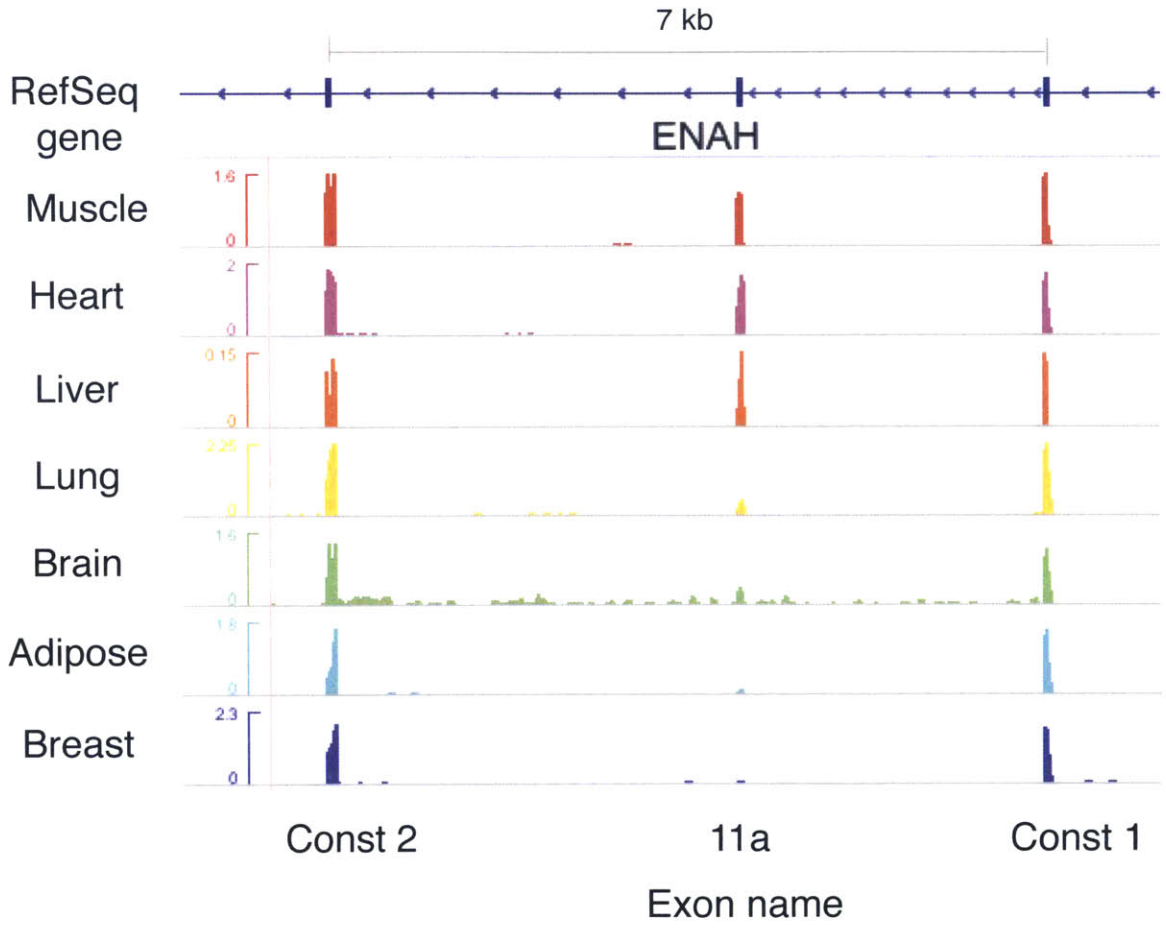

2.5 Mena11a mRNA is expressed in normal human muscle and heart. RNAseq data from the Illumina Body Map 2.0 aligned to hg18. RefSeq gene is ENAH (NCBI accession: NM_001008493.1). Y-axis values: read density/million mapped reads; y-axis ranges are not identical. Y-axis labels: Normal human tissue libraries. Exon name: Const1 and Const 2 are constitutive ENAH exons (chr1:223,762,276-223,762,342 and chr1:223,755,317-223,755,395, respectively), and 11a is an alternate exon (chr1:223,759,316-223,759,378). Directionality is right to left, 5' to 3'. kb = kilobases.

2.4 Conclusion

For the first time, we evaluate Mena11a isoform expression at the protein and mRNA level in normal tissues. We find that Mena11a protein is highly enriched in epithelia in E15.5 embryonic mouse tissues that express Mena but lack VASP and EVL, as well as normal adult mouse and human tissues. Previous work demonstrates that vertebrate Ena/VASP proteins localize to cell-cell junctions (13, 14), function in tension-regulated actin dynamics at epithelial zonula adherens (15), and are required for endothelial barrier function (15). This suggests that Mena11a may have isoform-specific functionality in maintaining epithelial architecture *in vivo* (Balsamo and Mondal, submitted). Interestingly, Evl-I, a splice isoform of Evl, is also enriched in epithelial layers within the mouse skin at the protein level (16).

We also have evidence that Mena11a protein is expressed in embryonic muscle (in the same E15.5 mouse embryos as above). To better characterize the distribution of Mena11a protein in muscle during development, further analysis in additional embryonic organ tissues must be conducted with skeletal, smooth, and cardiac muscle-specific markers. Although mRNA expression is not a surrogate for protein levels, analysis of publicly available RNAseq data of normal human tissues showed that the 11a exon is included in most ENAH transcripts in normal human skeletal muscle and heart, suggesting that Mena11a may function in different types of muscle. Additional analysis using the MISO tool will determine the percent spliced in, or fraction of mRNAs that have the 11a inclusion, providing quantitative information on the abundance of Mena11a mRNA in different tissues (17).

Recent evidence has demonstrated a role for Ena/VASP proteins in muscle function. VASP regulates actin polymerization and contraction of vascular smooth muscle cells (18) and airway smooth muscle (19). Mena and VASP are expressed in the mammalian heart and can interact with an αII-Spectrin splice variant at z-lines and intercalated disks in cardiomyocytes; deficiency of Mena and VASP in the heart causes cardiomyopathy (20, 21). An interesting question to examine is why Ena/VASP proteins are enriched at z-lines, considering that the F-actin that composes the z-line is capped by the CapZ protein (21).

Mena by itself has been examined extensively in cardiac function. Mena regulates normal cardiac function by maintaining the stability of intercalated disks through Cx43 and Rac-1 (22, 23), and overexpression of Mena results in susceptibility to cardiac injury and heart failure (24). Also, levels of Mena are substantially elevated in heart failure models (24). Thus, it will be interesting to further examine the role of Mena11a in the context of smooth muscle and cardiomyocyte function, where Ena/VASP proteins have been demonstrated to play key roles.

2.5 Materials and Methods

Tissues
E15.5 MMeevv embryos from a mixed background were obtained from the Gertler lab. Mice were sacrificed at the appropriate embryonic ages, dissected immediately, and fixed in 3.7% buffered formalin overnight at 4°C. Paraffin embedding of tissues was conducted in the Histology Core at the Swanson Biotechnology Center. Adult mouse tissue was a gift from the Hynes laboratory at the Koch Institute, MIT.

Immunofluorescence
5 µm sections of paraffin-embedded tissues were deparaffinized in xylene, treated with a graded series of alcohol, and rehydrated in PBS using a dewax program in the Histology Core, Swanson Biotechnology Center. Sections were subjected to heat-induced antigen retrieval in 1X Antigen Retrieval Plus Citra solution (Biogenex) using a pressure cooker system. Sections were incubated with 10% normal donkey or goat serum in 0.5% Tween-20 for 2 hours at room temperature. Primary antibodies in 1% donkey or goat serum in 0.5% Tween-20 buffer were added overnight at 4°C, and sections were subsequently washed three times in 1X PBS. Sections were incubated with fluorescently labeled secondary antibodies (AlexaFluor, Molecular Probes) for 2 hours at room temperature, and in 10 µg/ml Hoechst dye to stain the nucleus.

Antibodies
The rabbit polyclonal anti-Mena11a (2) and mouse monoclonal anti pan-Mena (8) antibodies were generated in our laboratory. CF405-Phalloidin was purchased (Biotium) and diluted 1:50.

Microscopy of Tissues
z-series of tissues were imaged with a Nikon Ti inverted microscope using NIS Elements acquisition software (Nikon), a 40X 1.15 NA Plan-Apochromat objective lens (Nikon), and an Andor Zyla4.2 sCMOS camera.

Illumina Human Body Map 2.0 RNA-Seq Data
RNAseq reads from the publicly available Illumina Body Map 2.0 RNAseq data, consisting of 16 human tissues (http://www.ebi.ac.uk/arrayexpress/experiments/E-MTAB-513/), were aligned to the hg18 reference genome using TopHat. Read density was calculated across the ENAH locus and scaled by the inverse of Million Mapped Reads in each tissue using Bedtools. Read density was visualized using the Integrative Genomic Viewer (IGV).

2.6 References

1. Di Modugno F, et al. (2007) Molecular cloning of hMena (ENAH) and its splice variant hMena+11a: epidermal growth factor increases their expression and stimulates hMena+11a phosphorylation in breast cancer cell lines. *Cancer Res* 67(6):2657–65.
2. Pino MS, et al. (2008) Human Mena+11a isoform serves as a marker of epithelial phenotype and sensitivity to epidermal growth factor receptor inhibition in human pancreatic cancer cell lines. *Clin Cancer Res* 14(15):4943–50.
3. Goswami S, et al. (2009) Identification of invasion specific splice variants of the cytoskeletal protein Mena present in mammary tumor cells during invasion in vivo. *Clin Exp Metastasis* 26(2):153–159.
4. Roussos ET, et al. (2011) Mena invasive (Mena(INV)) and Mena11a isoforms play distinct roles in breast cancer cell cohesion and association with TMEM. *Clin Exp Metastasis* 28(6):515–527.
5. Agarwal S, et al. (2012) Quantitative assessment of invasive mena isoforms (Menacalc) as an independent prognostic marker in breast cancer. *Breast Cancer Res* 14(5):R124.
6. Forse C, et al. (2015) Mena calc , a quantitative method of metastasis assessment, as a prognostic marker for axillary node-negative breast cancer. *BMC Cancer* 15(1):483.
7. Gertler FB, Niebuhr K, Reinhard M, Wehland J, Soriano P (1996) Mena, a relative of VASP and Drosophila Enabled, is implicated in the control of microfilament dynamics. *Cell* 87(2):227–239.
8. Lanier LM, et al. (1999) Mena is required for neurulation and commissure formation. *Neuron* 22(2):313–325.
9. Gambaryan S, Hauser W, Kobsar A, Glazova M, Walter U (2001) Distribution, cellular localization, and postnatal development of VASP and Mena expression in mouse tissues. *Histochem Cell Biol* 116(6):535–543.
10. Halbrugge M, Walter U (1989) Purification of a vasodilator-regulated phosphoprotein from human platelets. *Eur J Biochem* 185(1):41–50.
11. Kwiatkowski A V, et al. (2007) Ena/VASP Is Required for neuritogenesis in the developing cortex. *Neuron* 56(3):441–455.
12. Merrell AJ, Kardon G (2013) Development of the diaphragm, a skeletal muscle essential for mammalian respiration. *FEBS J* 280(17):10.1111/febs.12274.

13. Scott JA, et al. (2006) Ena/VASP proteins can regulate distinct modes of actin organization at cadherin-adhesive contacts. *Mol Biol Cell* 17(3):1085–1095.

14. Vasioukhin V, Bauer C, Yin M, Fuchs E (2000) Directed Actin Polymerization Is the Driving Force for Epithelial Cell–Cell Adhesion. *Cell* 100(2):209–219.

15. Leerberg JM, et al. (2014) Tension-Sensitive Actin Assembly Supports Contractility at the Epithelial Zonula Adherens. *Curr Biol*:1–11.

16. Janssens K, et al. (2009) Characterization of EVL-I as a protein kinase D substrate. *Cell Signal* 21(2):282–292.

17. Katz Y, Wang ET, Airoldi EM, Burge CB (2010) Analysis and design of RNA sequencing experiments for identifying isoform regulation. *Nat Meth* 7(12):1009–1015.

18. Kim HR, et al. (2010) Actin polymerization in differentiated vascular smooth muscle cells requires vasodilator-stimulated phosphoprotein. *Am J Physiol - Cell Physiol* 298(3):C559–C571.

19. Wu Y, Gunst SJ (2015) Vasodilator-stimulated Phosphoprotein (VASP) Regulates Actin Polymerization and Contraction in Airway Smooth Muscle by a Vinculin-dependent Mechanism. *J Biol Chem* 290 (18):11403–11416.

20. Eigenthaler M, et al. (2003) Disruption of cardiac Ena-VASP protein localization in intercalated disks causes dilated cardiomyopathy. *Am J Physiol Heart Circ Physiol* 285(6):H2471–81.

21. Benz PM, et al. (2013) Mena/VASP and αII-Spectrin complexes regulate cytoplasmic actin networks in cardiomyocytes and protect from conduction abnormalities and dilated cardiomyopathy. *Cell Commun Signal* 11(1):56.

22. Aguilar F, et al. (2011) Mammalian enabled (Mena) is a critical regulator of cardiac function. *Am J Physiol Heart Circ Physiol* 300(5):H1841–52.

23. Ram R, Wescott AP, Varandas K, Dirksen RT, Blaxall BC (2014) Mena associates with Rac1 and modulates connexin 43 remodeling in cardiomyocytes. *Am J Physiol - Hear Circ Physiol* 306(1):H154–H159.

24. Belmonte SL, Ram R, Mickelsen DM, Gertler FB, Blaxall BC (2013) Cardiac overexpression of Mammalian enabled (Mena) exacerbates heart failure in mice. *Am J Physiol - Hear Circ Physiol* 305(6):H875–H884.

Chapter 3: Mena11a dampens cell protrusion and reduces motility

The work from this chapter contributed to the following manuscript: Balsamo and Mondal, et al. "Mena-dependent regulation of actin cytoskeleton organization and cell behavior is regulated by the alternatively-included 11a sequence." Manuscript submitted. I contributed to Figures 3.2, 3.3, 3.4, and 3.6 in collaboration with the Swanson Bioinformatics and Microscopy core facilities. Figures 3.8 B-C and 3.9 D-E were equal contributions of Dr. Michele Balsamo and myself. Figures 3.1, 3.5, 3.7, 3.9, 3.10, and 3.11 were contributed by Dr. Michele Balsamo. Figure 3.8 A is a contribution from Dr. Leslie McClain.

TABLE OF CONTENTS

3.1 Abstract

During tumor progression, alternative splicing of Mena mRNA produces protein isoforms with distinct functions. We analyzed how Mena11a affects Mena-dependent regulation of actin dynamics and cell behavior. We found that Mena11a acts both antagonistically to, and independently of, other Mena isoforms: it reduces growth factor-stimulated lamellipodial protrusion, decreases G-actin incorporation at the leading edge of the cell, and slows mesenchymal-like cell motility. In cells lacking Mena (and its paralogs, VASP and EVL), expression of Mena11a cannot stimulate actin-driven intracellular motility of the bacterium *Listeria monocytogenes* and decreases growth-factor elicited abundance of the Arp2/3 complex within lamellipodia. Mena11a-specific depletion perturbs E-cadherin distribution at cell-cell junctions and increases the motility of epithelial-like breast cancer cells. By analyzing RNAseq data linked to patient cohorts from multiple cancer types, we find that the difference between the abundance of mRNAs encoding constitutive Mena sequences and those containing the 11a exon correlates with metastasis in colorectal cancer patients. Our findings explain how exclusion of 11a from Mena contributes to the aggressive, invasive phenotypes characteristic of metastatic carcinoma cells that lead to poor clinical outcomes (Balsamo and Mondal, submitted).

3.2 Introduction

Mena is upregulated in human epithelial tumors (1–5) and in invasive rodent mammary adenocarcinoma cells collected by *in vivo* EGF-elicited chemotaxis (6, 7). Mena function has been examined in mouse models of breast cancer and in breast cancer patients. In PyMT mammary tumors, Mena deficiency delays tumor progression and reduces invasion, intravasation, and metastasis formation (8), and in breast cancer patients, the density of a structure consisting of a cancer cell expressing Mena, an endothelial cell, and a macrophage is correlated with the risk of metastasis (9, 10).

Mena mRNA has 14 constitutive exons, and can contain one or more of 5 alternatively-included exons that produce in-frame proteins (11–13). One isoform, $Mena^{INV}$, is upregulated in chemotactic, invasive mammary carcinoma cells (14) and sensitizes them to EGF stimulation, increasing their invasive and metastatic capability (15–18). Another isoform, Mena11a, which includes 21 amino acids between the F-actin binding and tetramerization regions in EVH2 (12), is downregulated in invasive carcinoma cells (14) and retained in epithelial carcinoma cell lines - in part by activity of epithelial-specific splicing factors (19); its exclusion from mesenchymal cells (12, 20) is regulated by drivers of epithelial-to-mesenchymal transition (EMT) (21) (Balsamo and Mondal, submitted).

Ectopic expression of Mena11a in rat mammary adenocarcinoma cells decreases 3-D invasion of cells in a collagen matrix in response to EGF. Xenograft studies with these same cells results in the formation of mammary tumors that are poorly metastatic (16). Evaluation of Mena and Mena11a protein expression in clinical

samples using quantitative immunofluorescence reveals that low Mena11a expression and high overall Mena expression are associated with decreased survival (22, 23).

However, the cellular and molecular underpinnings of these phenotypes are unknown. Here we reveal isoform-specific roles for Mena11a that are functionally distinct from Mena in the control of actin cytoskeleton organization, cell-cell adhesion and motility in cancer cells (Balsamo and Mondal, submitted).

3.3 Results

3.3.1 Mena11a is expressed in MMTV-PyMT adenomas and early carcinomas in a heterogeneous manner.

Several epithelial human cancers express increased levels of Mena protein (1–5). Mena11a mRNA and protein expression levels have been examined in fine needle aspirates and tissues from clinical samples (17, 22, 23); however, Mena11a protein expression and spatial distribution during tumor progression has not yet been reported. Therefore, we examined Mena11a expression using the MMTV-PyMT mouse mammary tumor model for invasive breast cancer which temporally and morphologically recapitulates human pathology (24). We stained MMTV-PyMT tissues with antibodies for pan-Mena and Mena11a, allowing us to explore the relative distribution of Mena11a with respect to total Mena during tumor progression. In adenomas, which mimic ductal hyperplasia, and early carcinomas, which are similar to ductal carcinoma in situ (24) (Figure 3.1 A-B, respectively), pan-Mena and Mena11a had heterogeneous expression: while Mena11a and pan-Mena were enriched in the epithelia, Mena11a was excluded

from the pan-Mena positive stromal cells. The specificity of the antibodies was confirmed by staining PyMT-MMTV Mena -/- (null) tissues (Figure 3.1 C) (Balsamo and Mondal, submitted).

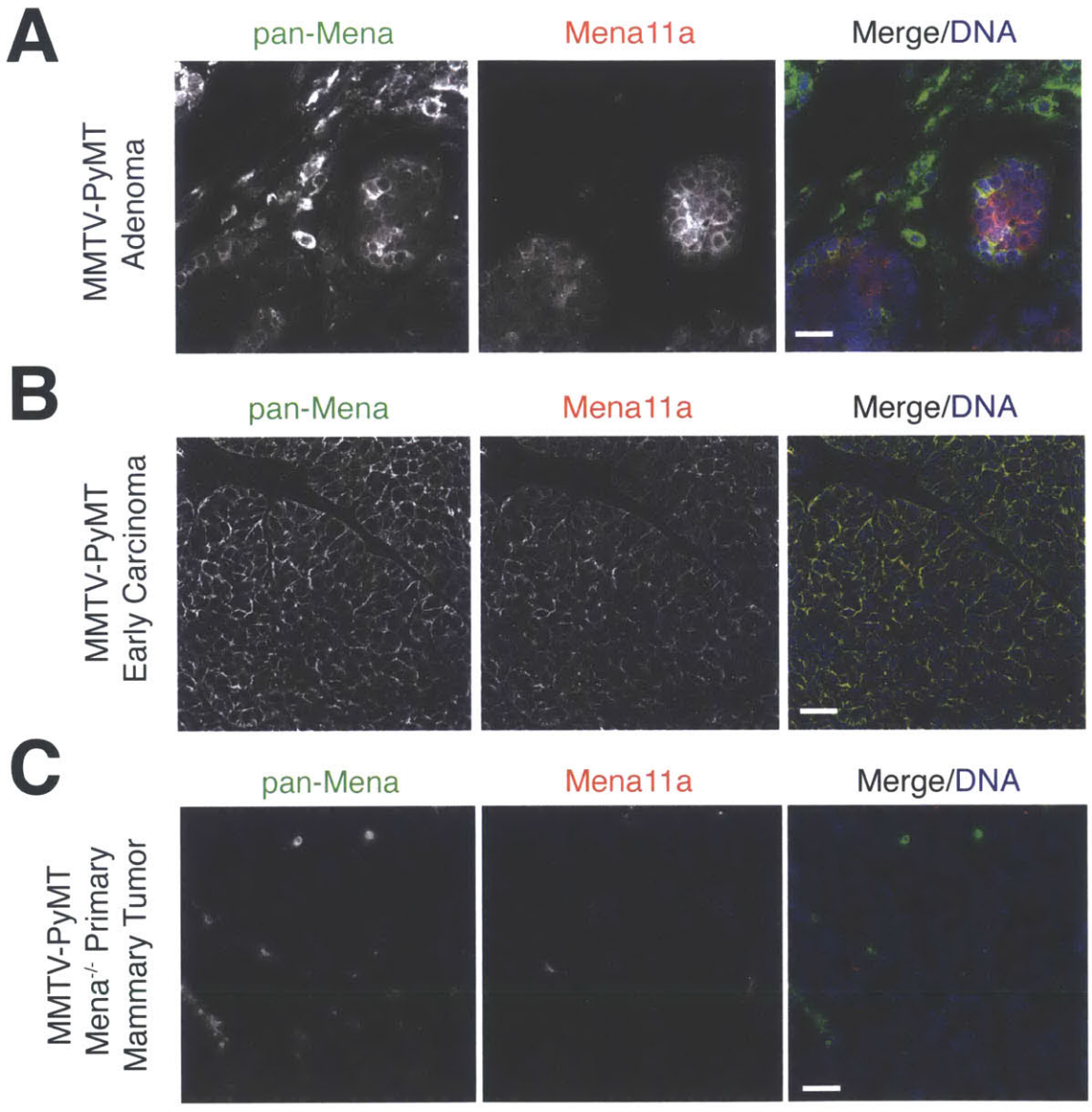

Figure 3.1: Mena11a is expressed in MMTV-PyMT adenomas and early carcinomas. Immunofluorescence of pan-Mena and Mena11a in primary mammary tumors from MMTV-PyMT transgenic mice at both the (A) adenoma and (B) early

carcinoma stages. (C) Primary mammary tumor section from MMTV-PyMT Mena$^{-/-}$ mice. DNA visualized with Hoechst staining. Scale bar, 20 μm. Images are representative of three independent experiments.

3.3.2 MenaCalc^{RNA} is associated with metastasis formation in the COAD cohort.

Both pan-Mena and Mena11a protein levels have been examined in clinical samples using multiplexed quantitative immunofluorescence (MQIF) of tissue microarrays. Previous studies using this method demonstrated that high values of MenaCalc^{PR}, a metric measuring the difference between all Mena isoforms and Mena11a protein levels (MenaCalc^{PR} = pan-MenaZ – Mena11aZ, where Z = z score, see (22) methods) were associated with decreased overall survival in three independent breast cancer patient cohorts (22, 23), although protein levels of either Mena or Mena11a alone were not. To investigate whether RNAseq transcriptome data from clinical samples could be used to develop a surrogate metric equivalent to MenaCalc^{PR}, we acquired exon-level gene expression data from the publicly available TCGA data portal and determined whether the abundance of mRNAs encoding constitutively included Mena exons, Mena11a, or an mRNA-based version of MenaCalc ^{PR} (MenaCalc^{RNA} = average RPKM constitutive Mena exons – RPKM alternate Mena11a exon, see Methods) were associated with overall survival. Due to the short follow-up time for patients (>10 years follow-up, n = 55 alive, n = 73 deceased, data not shown), we were unable to find a stable correlation between MenaCalc^{RNA} and overall survival in this TCGA breast cancer cohort (BRCA) (Balsamo and Mondal, submitted).

Since Mena11a is expressed in normal human colon epithelium (Figure 2.1 D), and Mena is upregulated in colorectal adenocarcinomas (3, 4), we investigated whether

MenaCalc^{RNA} levels correlated with overall survival or with annotated clinicopathological characteristics in the TCGA colon adenocarcinoma (COAD) cohort. While statistics failed to detect predictive value of MenaCalc^{RNA} in terms of overall survival (again, likely because of the relatively short follow-up time and small number of patients in the cohort, >1 year follow-up, n = 110 alive, n = 33 deceased), patients with evidence of distant metastasis (M1) had, on average, significantly higher MenaCalc^{RNA} values compared to patients with no evidence of distant metastasis (M0) (Figure 3.2 A). Logistic regression analysis demonstrated that MenaCalc^{RNA} (coefficient = 0.349, p = 0.003), but neither Mena (coefficient = 0.176, p = 0.168) nor Mena11a (coefficient = -0.033, p = 0.808) alone, was significantly associated with metastasis in the COAD cohort. These data support the idea that MenaCalc^{RNA} is associated with malignant progression in at least some carcinomas (Balsamo and Mondal, submitted).

Interestingly, gene ontology (GO) and gene set enrichment analysis (GSEA) analyses of genes whose expression levels correlated with those of Mena, Mena11a, or MenaCalc^{RNA} showed that a distinct set of functional annotations were enriched in the MenaCalc^{RNA}, but not the Mena or Mena11a correlating gene lists (Figure 3.2 B, Table 3.3). The top 50 genes correlating with MenaCalc^{RNA} in the COAD cohort (Table 3.4) were enriched in gene sets related to EMT (Table 3.3) and were associated with GO terms such as cell-substrate adhesion (GO:0031589) and cell-matrix adhesion (GO:0007160) (Figure 3.2 B), whereas genes correlating with Mena and Mena11a alone (Table 3.4) were not enriched in, or associated with key biological processes directly involved in cancer invasion and metastasis. These findings are consistent with the idea that MenaCalc^{RNA}, which represents the abundance of Mena isoforms lacking

the 11a exon, is more associated with pro-metastatic phenotypes than either total Mena or Mena11a levels, providing potential insight into why MenaCalc^{RNA}, but not Mena nor Mena11a levels were associated with poor clinical outcome in appropriately powered analyses of multiple breast cancer patient cohorts (22, 23) (Balsamo and Mondal, submitted).

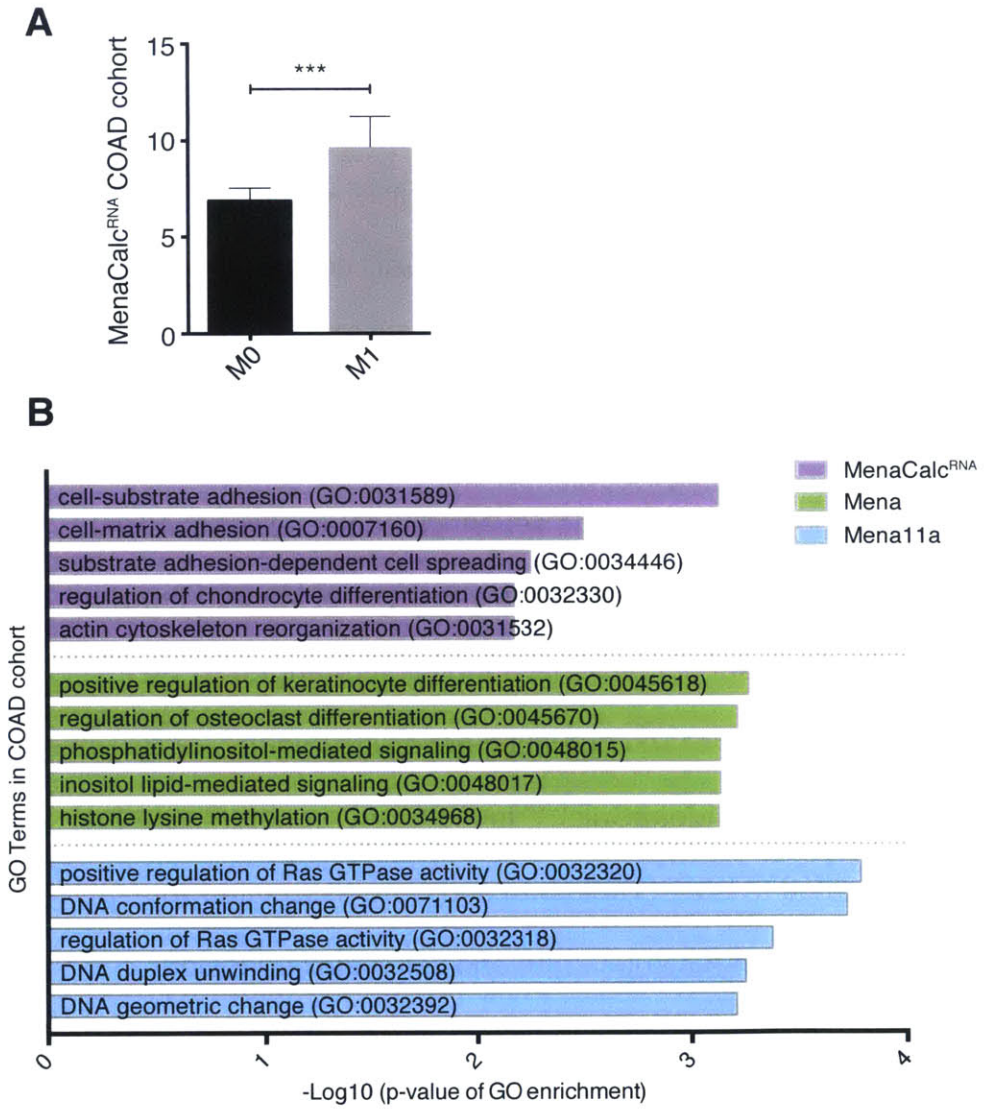

Figure 3.2: High MenaCalc^{RNA} values are associated with metastasis formation. (A) Association between metastatic stage and MenaCalc^{RNA} in COAD patient cohort; M0 = no evidence of distant metastasis, M1 = evidence of distant metastasis. n = 453 patients. Error bars: 95% CI. Wilcoxon rank-sum test ***p< 0.005. (B) GO term

enrichment categories of the top 50 genes correlated with MenaCalc^{RNA}, Mena, and Mena11a in the COAD cohort.

MenaCalc^{RNA}		
Gene Set Name	*# of Genes in Overlap (k) / # Genes in Gene Set (K)*	*FDR q-value*
HALLMARK_EPITHELIAL_MESENCHYMAL_TRANSITION	6/200	1.88E-04
Mena		
Gene Set Name	*# of Genes in Overlap (k) / # Genes in Gene Set (K)*	*FDR q-value*
BIOPOLYMER_METABOLIC_PROCESS	12/1684	3.26E-04
REACTOME_YAP1_AND_WWTR1_TAZ_STIMULATED_GENE_EXPRESSION	3/24	2.50E-03
REACTOME_DEVELOPMENTAL_BIOLOGY	6/396	2.67E-03
REACTOME_PPARA_ACTIVATES_GENE_EXPRESSION	4/104	2.67E-03
REACTOME_CIRCADIAN_CLOCK	3/53	1.13E-02
Mena11a		
Gene Set Name	*# of Genes in Overlap (k) / # Genes in Gene Set (K)*	*FDR q-value*
BIOPOLYMER_METABOLIC_PROCESS	12/1684	4.14E-04
RNA_METABOLIC_PROCESS	7/841	2.77E-02
TRANSCRIPTION_DNA_DEPENDENT	6/636	2.77E-02
RNA_BIOSYNTHETIC_PROCESS	6/638	2.77E-02
BIOPOLYMER_MODIFICATION	6/650	2.77E-02

Table 3.3 Gene Set Enrichment Analysis of top 50 genes correlated with Mena11a, Mena, and MenaCalc^{RNA} expression in the TCGA COAD cohort. The top five gene sets, based on False Discovery rate (FDR) q-values, are listed for Mena11a, Mena, and MenaCalc^{RNA}. Genes correlating with MenaCalc^{RNA} are only enriched in one gene set.

ENAH (Mena)			**Mena11a**			**MenaCalc** RNA		
Gene Symbol	Spearman Correlation	p-value	Gene Symbol	Spearman Correlation	p-value	Gene Symbol	Spearman Correlation	p-value
ENAH	0.8867991	2.41E-162	ENAH	0.7629603	1.30E-92	CALD1	0.6640587	2.37E-62
ZNF281	0.5810896	1.08E-44	C1orf107	0.539385	1.39E-37	PKD2	0.6537702	7.40E-60
DSTYK	0.5694362	1.33E-42	HEATR1	0.5154953	6.11E-34	ZNF281	0.6474207	2.29E-58
ASH1L	0.5675036	2.89E-42	SMARC C1	0.501792	5.62E-32	FILIP1L	0.6462844	4.20E-58
CAMS AP1L1	0.5620149	2.57E-41	POGK	0.4925214	1.07E-30	CSGALN ACT2	0.6444578	1.11E-57
TEAD1	0.5564399	2.27E-40	PIGM	0.4852444	1.01E-29	ZEB1	0.6425433	3.03E-57
TRIM44	0.5560091	2.68E-40	PRKDC	0.4762818	1.50E-28	MPDZ	0.6337974	2.77E-55
ARID4B	0.553618	6.73E-40	DHX9	0.4728266	4.16E-28	LPHN2	0.6316911	8.04E-55
TAOK1	0.5534387	7.21E-40	RBBP5	0.4703961	8.46E-28	FERMT2	0.6292753	2.70E-54
RIF1	0.5519777	1.26E-39	NUP133	0.4692696	1.17E-27	TCF4	0.6274438	6.73E-54
RBBP5	0.5508919	1.90E-39	ZMYM4	0.4674431	1.99E-27	MSRB3	0.6255772	1.69E-53
ZMYM4	0.5492989	3.48E-39	NF1	0.4671857	2.14E-27	MLLT11	0.6212963	1.37E-52
POGK	0.5428187	3.92E-38	TOP2B	0.4608259	1.31E-26	AKT3	0.6192999	3.61E-52
UBXN7	0.5415125	6.35E-38	ASH1L	0.4597444	1.78E-26	SGCD	0.6179446	6.92E-52
ASXL2	0.5378015	2.47E-37	FNBP1L	0.4595945	1.85E-26	QKI	0.6175084	8.53E-52
RAB3GAP2	0.5372645	3.00E-37	RAB3GA P2	0.4587152	2.37E-26	DDR2	0.6165999	1.32E-51
SP3	0.5369939	3.31E-37	VPS54	0.4586967	2.38E-26	FSTL1	0.6139383	4.66E-51
LAMC1	0.5366477	3.75E-37	DARS2	0.4573969	3.43E-26	RAI14	0.612509	9.14E-51
ATRX	0.5346673	7.67E-37	BRWD3	0.4560308	5.01E-26	CEP170	0.6110002	1.85E-50
HEATR1	0.5340714	9.50E-37	MED1	0.4523662	1.38E-25	ZNF521	0.6103424	2.52E-50
MED1	0.5328019	1.50E-36	NLN	0.4512239	1.88E-25	ZEB2	0.6088298	5.10E-50
CEP350	0.5306643	3.20E-36	ZNF146	0.4501354	2.53E-25	KIAA1462	0.6087883	5.20E-50
NF1	0.5299924	4.07E-36	TEX2	0.4498268	2.75E-25	SYT11	0.6082975	6.52E-50

MAP3K2	0.5194514	1.59E-34	STT3B	0.4475113	5.15E-25	FRMD6	0.6066077	1.42E-49
MAN1A2	0.5184371	2.25E-34	IPO7	0.4446912	1.10E-24	DZIP1	0.6044797	3.78E-49
HIP1	0.5156911	5.72E-34	MEX3A	0.4445543	1.14E-24	FAM171B	0.6040564	4.58E-49
PIK3C2A	0.5155533	5.99E-34	RIF1	0.4437531	1.41E-24	AKAP12	0.6034847	5.95E-49
C1orf107	0.5155432	6.01E-34	HOOK1	0.4416415	2.47E-24	ELK3	0.6028755	7.85E-49
CLASP2	0.5145639	8.36E-34	TRIM44	0.4394753	4.37E-24	NEXN	0.6008463	1.97E-48
EPC2	0.5139951	1.01E-33	RBM12	0.4391192	4.80E-24	STON1	0.6007781	2.03E-48
MYO9A	0.5124311	1.71E-33	LASS6	0.4387483	5.29E-24	ANTXR1	0.5976856	8.12E-48
ZBTB41	0.5110114	2.74E-33	CDK12	0.4386625	5.41E-24	ECM2	0.596856	1.17E-47
ATF6	0.5105098	3.24E-33	WDR3	0.4384936	5.65E-24	FGF7	0.5967471	1.23E-47
MTR	0.510026	3.81E-33	FLVCR1	0.437578	7.18E-24	FBN1	0.5962858	1.51E-47
CREB1	0.5077297	8.12E-33	ZNF704	0.4372042	7.91E-24	VGLL3	0.5960098	1.71E-47
TOP2B	0.5072629	9.47E-33	QTRTD1	0.4359579	1.09E-23	COL8A1	0.5948843	2.82E-47
SBF2	0.5052337	1.84E-32	SBF2	0.4332465	2.20E-23	CACNA2D1	0.5947858	2.94E-47
MED13L	0.5041151	2.65E-32	RALGAPA2	0.43319	2.24E-23	ZNF532	0.5944417	3.42E-47
RAB11FIP2	0.5014646	6.25E-32	GPATCH2	0.4320931	2.96E-23	MAP1B	0.5940817	4.01E-47
CDK12	0.4995023	1.17E-31	ZBTB41	0.4313891	3.55E-23	LRCH2	0.592012	9.95E-47
PTPN11	0.4991686	1.30E-31	CLASP2	0.4299872	5.08E-23	OSMR	0.5919146	1.04E-46
KLHDC10	0.4991525	1.31E-31	SP3	0.4278646	8.69E-23	TRPS1	0.5917651	1.11E-46
BAT2L2	0.4974871	2.23E-31	MBTD1	0.4269689	1.09E-22	ADAMTS12	0.5916919	1.14E-46
WNK1	0.497445	2.26E-31	SMC6	0.426631	1.19E-22	CLIC4	0.5916721	1.15E-46
UBR3	0.4970471	2.57E-31	SYDE2	0.4260287	1.38E-22	GUCY1A3	0.5914269	1.29E-46
ABI2	0.4966007	2.96E-31	SRPK2	0.4257125	1.49E-22	FKBP14	0.5896336	2.80E-46
DHX36	0.49428	6.15E-31	ATRX	0.4250373	1.77E-22	ELOVL4	0.5894086	3.09E-46
NCOA3	0.4942151	6.28E-31	SUZ12	0.42487	1.85E-22	GPR116	0.5893575	3.16E-46
STRN	0.4931527	8.77E-31	UBR3	0.4246908	1.93E-22	MCC	0.5888054	4.01E-46
RPS6KC1	0.4929127	9.45E-31	GSK3B	0.422981	2.96E-22	ASAM	0.5886541	4.29E-46

Table 3.4 Top 50 genes correlated with Mena11a, Mena, and MenaCalc^{RNA} in COAD cohort. Genes are ranked by the Spearman correlation coefficient.

3.3.3 Mena11a maintains cell-cell junctions by regulating F-actin structure.

Mena11a is enriched in epithelia; we find it preferentially targets to cell-cell contacts *in vivo* (Figure 2.1), and co-localizes with ZO-1 at tight junctions as well as E-cadherin at adherens junctions in cultured human breast cancer MCF7 cells (Balsamo and Mondal, submitted, data not shown). Previous studies demonstrated that ectopic expression of Mena11a in mouse mammary tumors is associated with cohesive cell-cell contacts (17); however, these overexpression assays did not address the specific requirements for Mena11a because 1) additional endogenous Mena isoforms are co-expressed in the cell lines used and can form mixed tetramers with Mena11a, and 2) endogenously expressed Mena11a was still expressed in these experiments. To assess whether the 11a sequence endows Mena11a with specific functions distinct from Mena, we designed shRNAs targeting the 63 bases of the 11a insertion (sh-1, sh-2, hereafter Mena11a-KD) and paired control shRNAs (sh-1C, sh-2C, hereafter control-KD). In MCF7 cells, Mena11a shRNAs efficiently downregulated Mena11a, but did not affect protein levels of Mena lacking the 11a insertion (Figure 3.5 A-B) (Balsamo and Mondal, submitted).

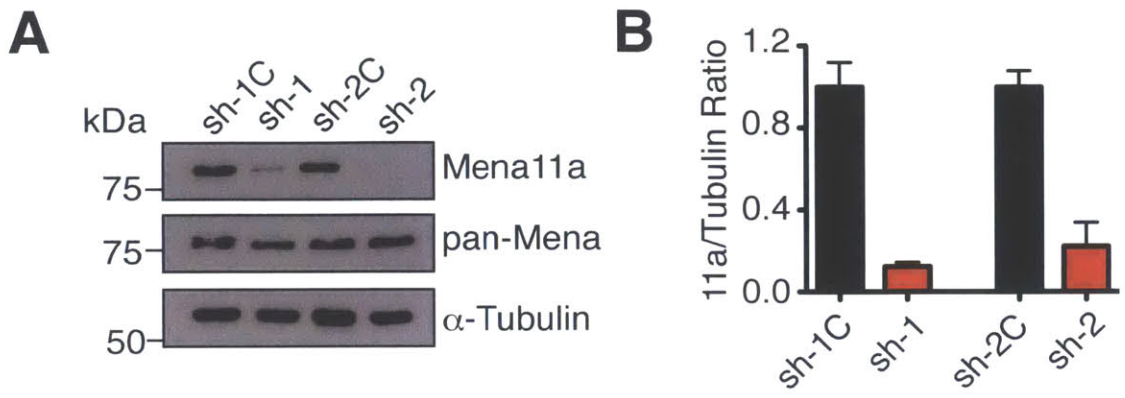

Figure 3.5: Isoform-specific depletion of Mena11a. (A) Western blot analysis. Membranes probed with anti Mena11a and anti pan-Mena antibodies. *α*-Tubulin: loading control. Sh-1C and sh-2C are distinct control scrambled hairpins; sh-1 and sh-2 are distinct Mena11a-specific hairpins. (D) Quantitative analysis of relative ratio of Mena11a:*α*-Tubulin, determined by densitometry. Fold change in expression is relative to appropriate control. Error bars: SEM. Results represent triplicates.

To investigate Mena11a-isoform specific function at cell-cell contacts, we used super-resolution three dimensional structured illumination microscopy (3D-SIM) to image monolayers of MCF7 Mena11a-KD cells and control-KD cells that were stained with phalloidin and E-cadherin to visualize F-actin and adherens junctions (Figure 3.6 A), respectively. Mena11a-KD cells had reduced E-Cadherin accumulation at the adherens junctions, as shown by fluorescence intensity quantitation (Figure 3.6 B). A circumferential belt of F-actin is normally present adjacent to tight and adherens junctions in epithelial sheets (25); in control-KD cells, this structure appeared normal; however, in Mena11a-KD cells the F-actin appeared to be disorganized at the adherens junctions (Figure 3.6 A). Together, these data indicate that the Mena11a isoform has a role in regulating the architecture of cell-cell contacts that is distinct from other Mena isoforms (whose expression is not affected by isoform-specific depletion of Mena11a) or Ena/VASP family members (Balsamo and Mondal, submitted).

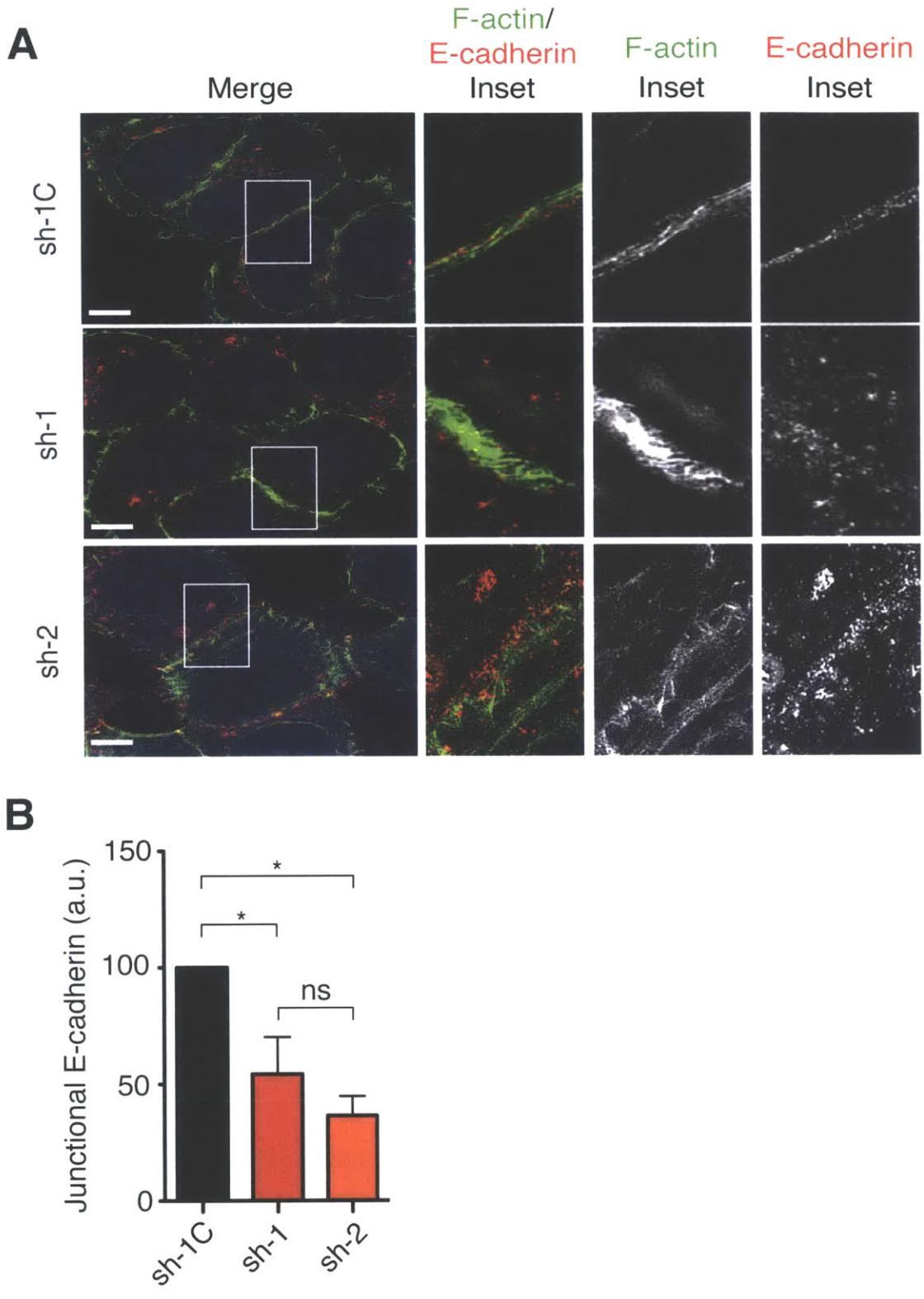

Figure 3.6: Mena11a isoform-specific depletion alters actin organization. (A) 3D-SIM images showing E-cadherin localization in MCF7 cells with isoform-specific

knockdown of Mena11a, using two different shRNAs (sh-1, sh-2) and control shRNAs (sh-1C). F-actin is visualized by phalloidin staining. Insets: 7X magnification. Scale bar, 10 μm. (B) Quantitation of junctional E-cadherin. a.u. = arbitrary units. >30 cells analyzed. Error bars: SEM. Results represent triplicates. One-way ANOVA *$p<0.05$, n.s., not significant.

3.3.4 Mena11a-specific depletion enhances cell migration.

Previously, the effects of Mena11a on cancer cell motility were evaluated in assays utilizing ectopic expression (16). To study the role of endogenously expressed Mena11a on cancer cell motility, we used T47D cells with Mena11a-specific knockdown (>80% reduction of Mena11a protein levels, data not shown) in wound closure assays. 48 hours after exposing a gap in a monolayer of T47D control-KD cells, approximately 45% of the initially cell-free region was filled (sh-1C: 50.41% ± 3.7; sh-2C: 40.38% ± 4.2), while T47D Mena11a-KD cells filled approximately 74% of the gap (sh-1: 78.39% ± 4.8; sh-2: 70.20% ± 8.8) (Figure 3.7 A-B). Therefore, depletion of the Mena11a isoform from cells that normally express both Mena and Mena11a increased the rate of cell migration (Balsamo and Mondal, submitted).

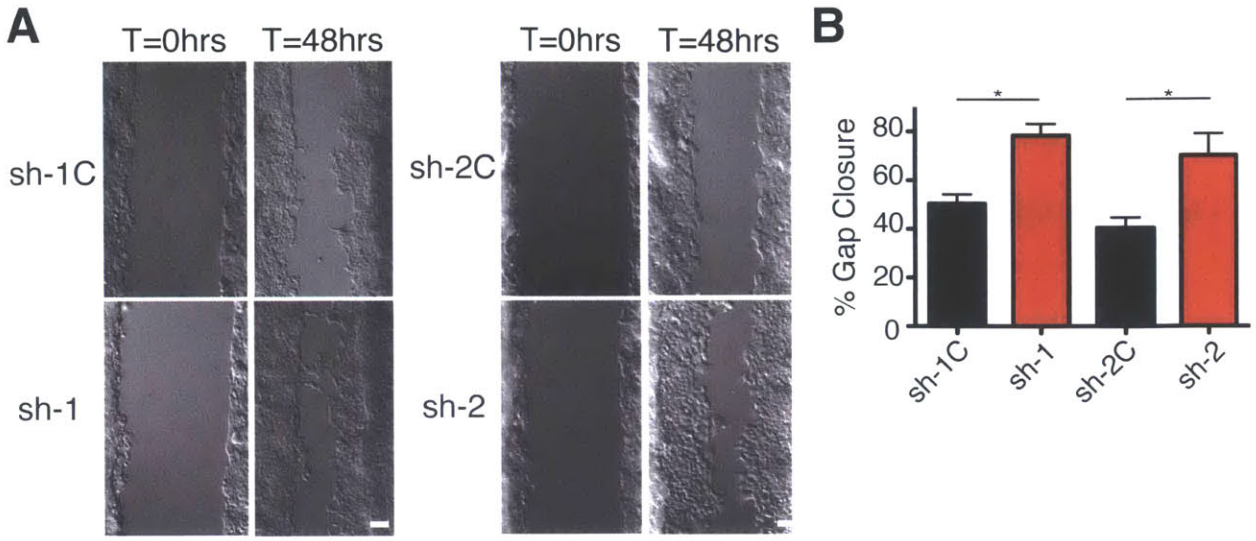

Figure 3.7 Mena11a downregulation increases 2D cell migration. (A) Wound healing assay using T47D control (sh-1C, sh-2C) and Mena11a-specific knockdown (sh-1, sh-2) cells. DIC images of cells after 0 and 48 hours in complete media. Scale bar, 50 μm. (B) Percent gap closure of cells after 48 hours in complete media.

3.3.5 Effect of Mena11a on actin cytoskeletal organization.

The Mena11a isoform-specific phenotypes at cell-cell junctions and membrane protrusions raise the possibility that Mena11a may differently affect actin cytoskeleton remodeling compared to Mena. We explored the contribution of Mena11a to actin cytoskeletal organization in established models used to study Ena/VASP function in cultured cells. An embryonic fibroblast cell line derived from a Mena/VASP double knockout mouse that lacks detectable expression of EVL (MV^{D7} cells) (26) was used to generate a panel of cell lines expressing equivalent levels of GFP, GFP-Mena, or GFP-Mena11a (hereafter GFP, Mena and Mena11a cells). Expression of Mena or Mena11a individually in an Ena/VASP "null" background cell line simplifies the interpretation of

results potentially arising from heterotetramers of Mena isoforms expressed endogenously or exogenously in the cell (Balsamo and Mondal, submitted).

The known role of Ena/VASP proteins in controlling the actin network architecture of MV^{D7} cells (27) led us to compare how actin networks were assembled in cells expressing Mena11a to those in cells expressing Mena, or to those lacking all Mena isoforms. We used platinum replica electron microscopy to examine the supramolecular organization of the actin filament network in lamellipodia of GFP, Mena and Mena11a MV^{D7} cell lines stimulated for 180 seconds with 100 ng/ml PDGF-BB to induce lamellipodium protrusion. Compared to GFP control cells, the actin network density did not appear to be altered grossly by Mena expression, but appeared to be substantially diminished in the lamellipodia of Mena11a expressing cells (Figure 3.8 A).

Because the actin network density at the lamellipodium leading edge depends upon Arp2/3, a complex that nucleates branched F-actin networks (28, 29), we reasoned that Mena11a expression could affect Arp2/3 abundance within lamellipodia. MV^{D7} cells expressing GFP, Mena, or Mena11a were stimulated with 100 ng/ml of PDFG-BB for 180 seconds and imaged by 3D-SIM. Mena11a cells exhibited significantly reduced levels of the Arp2/3 complex at the lamellipodium leading edge, compared to both GFP and Mena cells (Figure 3.8 B). A contour-based analysis method used to quantify Arp2/3 distribution and density within 0.65 μm of the lamellipodium edge (30) indicated that expression of Mena11a reduced Arp2/3 abundance significantly compared to both Mena-expressing cells and to cells lacking all Ena/VASP proteins (Figure 3.8 C). Thus, Mena11a exerts a distinct, inhibitory effect on Arp2/3-mediated

actin polymerization independent of other Mena isoforms and of VASP and EVL (Balsamo and Mondal, submitted).

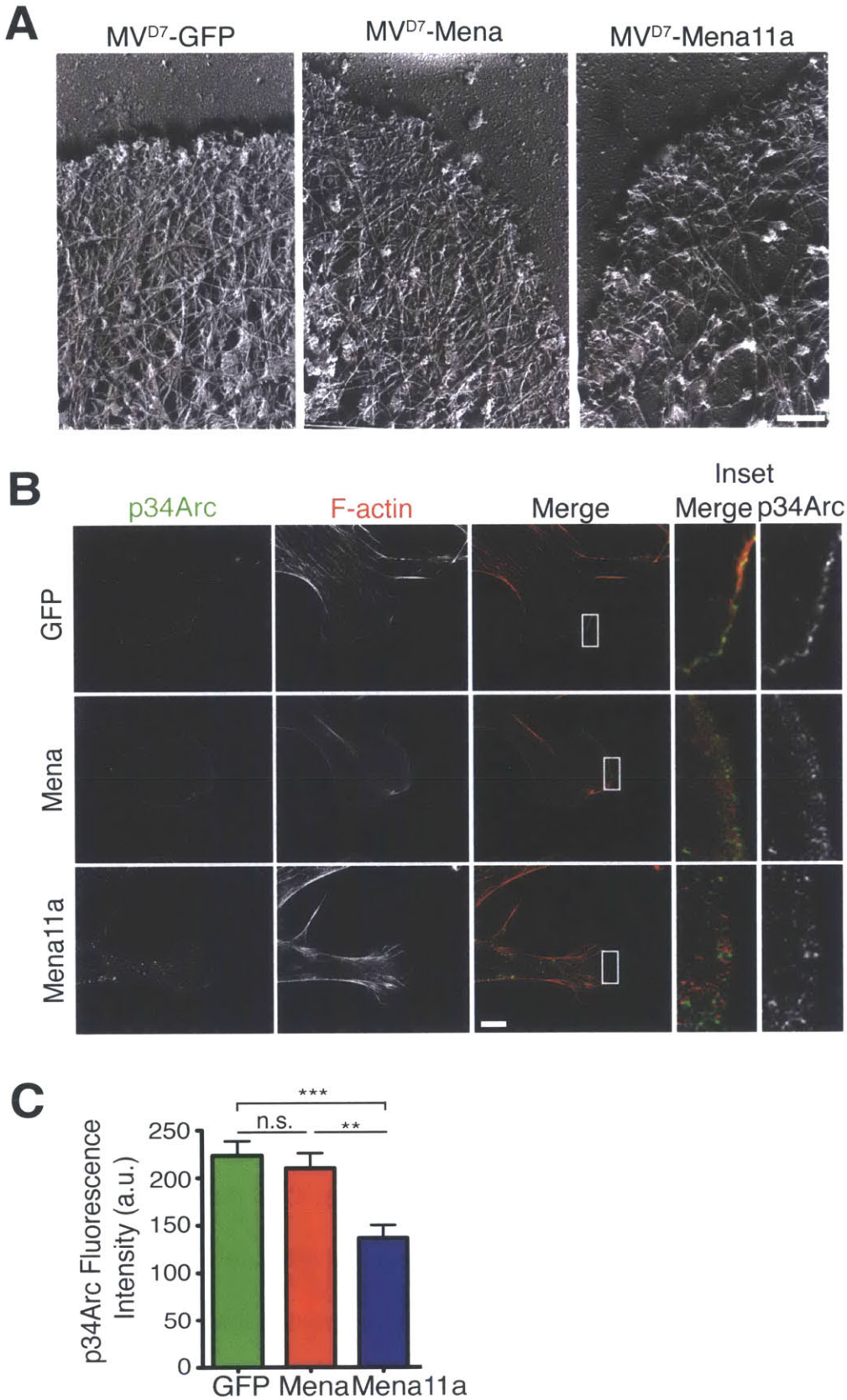
A
MV[D7]-GFP
MV[D7]-Mena
MV[D7]-Mena11a
B
p34Arc
F-actin
Merge
Inset
Merge p34Arc
GFP
Mena
Mena11a
C
p34Arc Fluorescence Intensity (a.u.)
250
200
150
100
50
0
***
n.s.
**
GFP
Mena
Mena11a

Figure 3.8: Expression of Mena11a decreases Arp2/3 abundance and alters F-actin organization at the leading edge.
(A) Platinum replica EM of actin cytoskeleton in MV^{D7} cells expressing GFP, Mena and Mena11a, stimulated with 100 ng/ml PDGF-BB for 5 minutes. Scale bar, 250 nm. Images representative of seven independent experiments. (B) 3D-SIM images of endogenous p34Arc in MV^{D7} cells expressing GFP, Mena and Mena11a, stimulated with 100 ng/ml PDGF-BB for 180 seconds. F-actin visualized by phalloidin staining. Scale bar, 10 μm. Insets are 28X magnification. (C) Quantification of p34Arc fluorescence intensity sum of initial 0.65 μm from the leading edge. a.u.= arbitrary units. >30 cells analyzed per condition. Results represent triplicates. One-way ANOVA **$p<0.01$, ***$p<0.005$, n.s., not significant.

3.3.6 Mena11a does not promote *Listeria* F-actin tail elongation.

Due to the complex signaling network controlling actin polymerization in cancer cells and fibroblasts, we chose to study Mena11a function in the context of *Listeria monocytogenes,* which recruits a limited set of host cell proteins to support its actin polymerization-driven intracellular motility (31, 32). Mena and other Ena/VASP proteins directly bind the *Listeria* surface protein ActA (33, 34), enhancing F-actin tail formation and elongation. Ena/VASP is not essential for *Listeria* motility, but does regulate intracellular actin-polymerization propulsion of *Listeria* (35, 36) increasing velocity and tuning the temporal and spatial persistence of bacterial movement, thereby contributing to cell-to-cell spread and virulence *in vivo* (37). *Listeria* F-actin tail length correlates with the rate of actin polymerization and bacterial intracellular velocity (38). Tail formation is initiated by ActA-activated Arp2/3 mediated actin nucleation (32, 39). To determine whether Mena11a affects *Listeria* F-actin tail formation and length, we infected GFP, Mena and Mena11a MV^{D7} cells with *Listeria*, and after 5 hours, fixed the cells and stained with phalloidin to visualize the F-actin tails. Consistent with previous reports (35, 37), Mena expressed in MV^{D7} cells infected with *Listeria* localized at the interface between the bacteria and the F-actin tail (11), rescued the loss-of-tail phenotype

observed in in the absence of Ena/VASP expression (in GFP MV^{D7} cells) and increased F-actin tail length (Figure 3.9 A-C). Mena11a was localized at the interface between the bacterium and the F-actin tail and increased frequency of F-actin tail formation, but failed to increase F-actin tail length beyond that observed in the absence of Ena/VASP expression (in GFP MV^{D7} cells) (Figure 3.9 A-C). These data suggest that Mena11a is unable to support efficient *Listeria* intracellular motility, perhaps due to effects on Arp2/3-mediated actin nucleation and polymerization (Balsamo and Mondal, submitted).

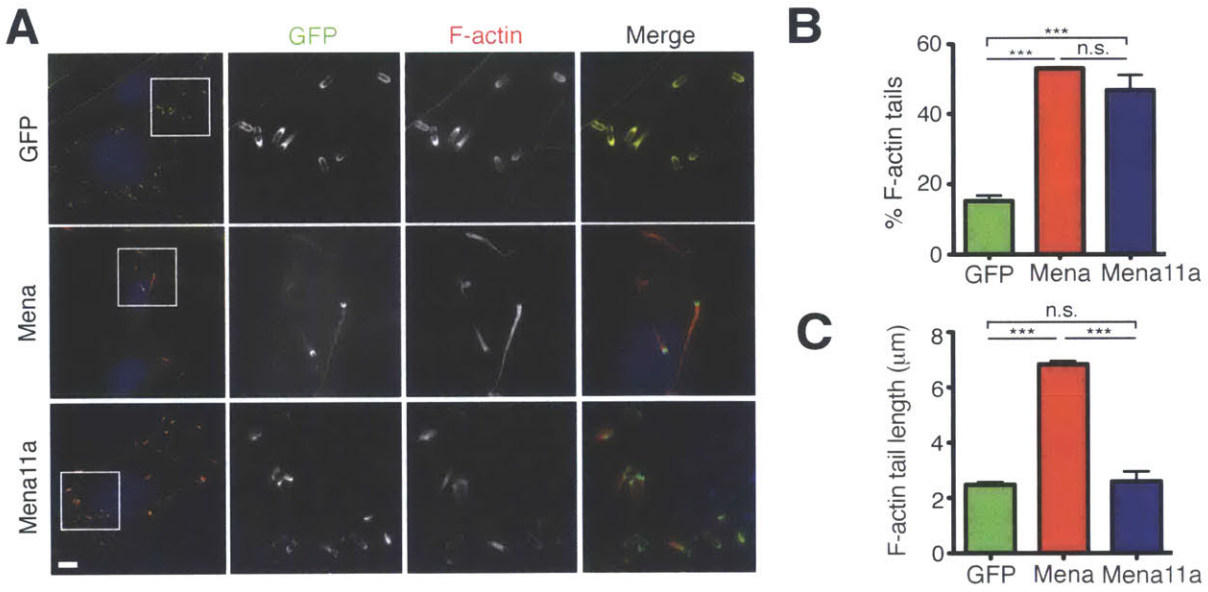

Figure 3.9: Expression of Mena11a does not support *Listeria* tail elongation. (A)-(C): MV^{D7} cells expressing GFP, Mena and Mena11a infected with *Listeria*. (A) Cells stained with phalloidin and Hoechst to visualize F-actin and DNA, respectively. Scale bar, 10 μm. Insets are 9X magnification. (B) Percent of F-actin tail formation induced by *Listeria*; >540 bacteria analyzed. (C) F-actin tail length of *Listeria* in >540 cells.

3.3.7 Expression of Mena11a dampens cancer cell membrane protrusion.

The effects of Mena11a expression in lamellipodia and on tumor cell behavior *in vivo* (16, 17) prompted us to investigate the role of Mena11a in the regulation of lamellipodial behavior in MTLn3 mammary carcinoma cells. MTLn3 cells respond to bath application of EGF by extending their membranes using a mechanism driven by actin assembly at free barbed ends created by cofilin-mediated severing of capped F-actin filaments (40). In MTLn3 cells, ectopic Mena and Mena^{INV} expression potentiate membrane protrusion during bath application of EGF (15, 16). To test the contribution of Mena11a during EGF-elicited membrane protrusion, we expressed (at the same protein levels) different GFP-Mena isoforms and GFP control ectopically in MTLn3 cells. Cells were serum-starved, stimulated with different concentrations of EGF, and membrane protrusion was imaged by time-lapse microscopy (Figure 3.10 A). At 0.5nM EGF (sub-saturating dose for the EGF receptor (EGFR)), expression of Mena potentiated membrane protrusion, as expected (see (15, 17)), while expression of Mena11a had no effect (3.10 C). Increasing the EGF concentration to 5nM (saturating dose, optimal for maximum membrane extension in MTLn3 (41)) eliminated the ability of Mena to increase membrane protrusion compared to GFP cells (Figure 3.10 A-B), while Mena11a expression had a strong negative effect on membrane protrusion (Figure 3.10 A-B), with cells that failed to extend a flat lamellipodium or showed several failed protrusions (Figure 3.10 A).

The negative effect of Mena11a on growth factor elicited protrusion could arise either from a direct effect on the actin cytoskeleton or from an effect on EGFR activation

and downstream signaling. Use of phospho-specific antibodies against pY-1068 or pY-1173 of EGFR (rapidly phosphorylated after EGF binds the EGFR) on Western blots of cell lysates from the three MTLn3 lines at various times after EGF stimulation revealed no statistically significant differences in the kinetics of EGFR phosphorylation (Figure 3.10 D-E). We conclude that the inhibitory effect of Mena11a on EGF elicited membrane protrusion in carcinoma cells derives mainly from the regulation of actin cytoskeleton remodeling.

Acute EGF elicited lamellipod extension in mammary carcinoma cells depends on cofilin-generated actin filament barbed end formation and Arp2/3 dependent nucleation of F-actin branches near the newly formed ends (42). We fixed the MTLn3 cells 180 seconds after 5nM EGF stimulation and confirmed that Arp2/3 was recruited to the leading edge of lamellipodia: in control GFP and Mena cell lines, Arp2/3 accumulated within 0.65 μm from the edge, but in Mena11a cells was significantly less abundant at the leading edge (Figure 3.10 F).

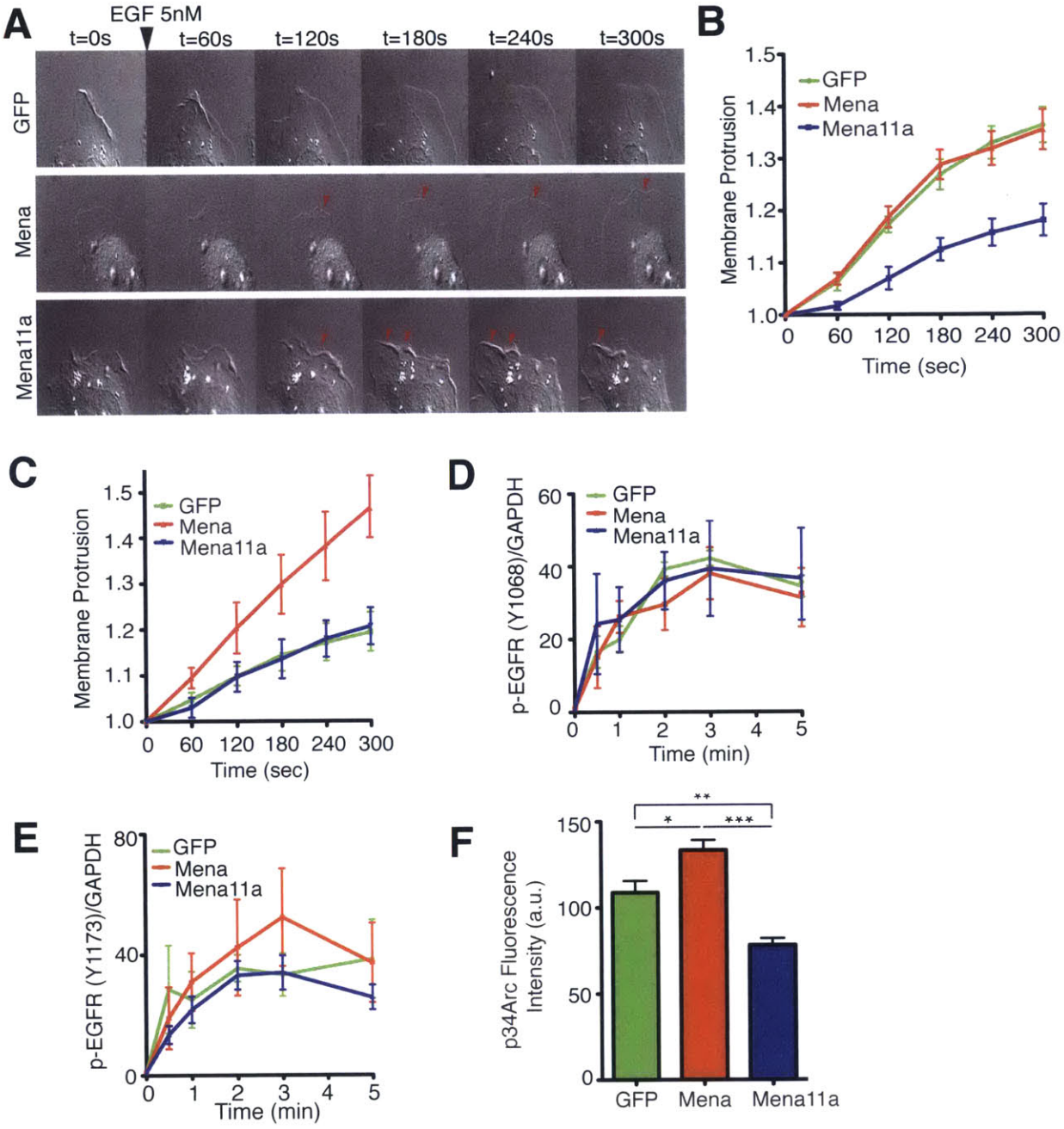

Figure 3.10 Mena11a expression dampens membrane protrusion and Arp2/3 recruitment to leading edge. (A)-(B): MTLn3 cells stably expressing GFP, Mena and Mena11a, stimulated with 5 nM EGF. (A) DIC images of membrane protrusion during stimulation. Red arrowheads: lamellipodial protrusions. (B) Membrane protrusion kinetics of cells after EGF stimulation. Error bars: SEM. (C) Membrane protrusion kinetics of MTLn3 cells stably expressing GFP, Mena, or Mena11a following 0.5 nM EGF stimulation. Error bars: SEM. (D)-(E): Western blot analysis of MTLn3 cells stably expressing GFP, Mena and Mena11a. Cells were starved for 4 hours, then stimulated

for 0, 0.5, 1, 2, 3, and 5 minutes with 5 nM EGF. Membranes were probed with (D) anti-EGFR pY1068 and (E) anti-EGFR pY1173. GAPDH was used as a loading control. Densitometry of the relative ratio of (D) EGFR pY1068/GAPDH and (E) EGFR pY1173/GAPDH as determined by densitometry. Fold increase is over baseline (no EGF stimulation). (F) Quantification of p34Arc fluorescence intensity sum of the initial 0.65 μm from the leading edge of cells after stimulation with 5 nM EGF for 180 seconds. a.u., arbitrary units. Error bars: SEM. Results represent triplicates, >50 cells analyzed. One-way ANOVA *$p<0.05$, **$p<0.01$, ***$p<0.005$. Error bars: SEM.

3.3.8 Mena11a affects cofilin- and Arp2/3-mediated barbed end formation.

Generation of actin filament free barbed ends correlates directly with EGF-stimulated membrane protrusion in carcinoma cells (41, 43). EGF-stimulation of MTLn3 cells increased the number of free barbed ends at the lamellipodial periphery, which are temporally regulated by cofilin severing activity at 60 seconds and Arp2/3 at 180 seconds post stimulation (44). Upon EGF stimulation, Mena is recruited to nascent lamellipodia within 30 seconds (preceding Arp2/3 accumulation, which begins after ~60 seconds) and potentiates barbed end formation after 60 seconds (15). To determine whether reduced lamellipodium protrusion in Mena11a-expressing cells in response to EGF resulted from decreased formation of free F-actin barbed ends at the leading edge, we measured the relative number of free barbed ends after stimulation with different EGF concentrations. After 60 seconds of stimulation with 0.5 nM EGF, Mena increased the incorporation of free barbed ends over control GFP cells whereas Mena11a did not (Figure 3.11 A-C). Conversely, Mena11a expression reduced G-actin incorporation at the leading edge below that of control GFP or Mena expressing MTLn3 cells after 60 (Figure 3.11 D-F) and 180 seconds (Figure 3.11 G-I) of 5 nM EGF treatment. Hence, Mena11a reduces both cofilin-dependent (at 60 seconds) and Arp2/3-dependent (at 180

seconds) F-actin free barbed ends abundance within lamellipodia of carcinoma cells (Balsamo and Mondal, submitted).

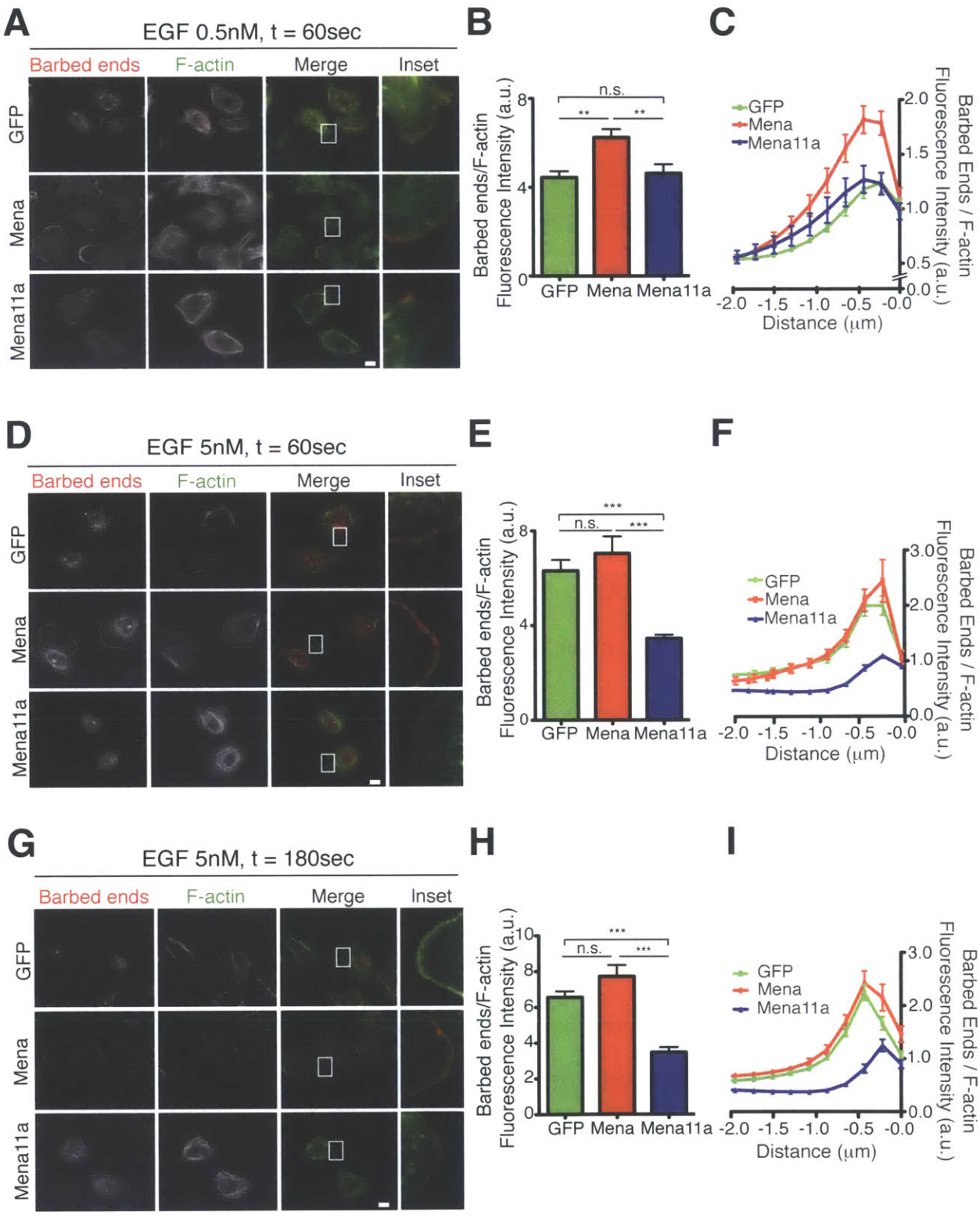
A
EGF 0.5nM, t = 60sec
Barbed ends
F-actin
Merge
Inset
GFP
Mena
Mena11a
B
Barbed ends/F-actin Fluorescence Intensity (a.u.)
n.s.
**
**
GFP Mena Mena11a
C
GFP
Mena
Mena11a
Barbed Ends / F-actin Fluorescence Intensity (a.u.)
Distance (μm)
D
EGF 5nM, t = 60sec
E
***
n.s.
***
F
G
EGF 5nM, t = 180sec
H
I

3.11 Mena11a expression decreases G-actin incorporation to F-actin barbed ends at the leading edge. All experiments done on MTLn3 cells stably expressing GFP, Mena and Mena11a. (A), (D), (G): Barbed end incorporation after stimulation with (A) 0.5 nM EGF for 60 seconds, (D) 5 nM EGF for 60 seconds, and (G) 5 nM EGF for 180 seconds. Barbed ends and F-actin visualized with rhodamine-G-actin and phalloidin labeling, respectively. Scale bar, 10 μm. Insets at (A) 27X, (D) 31X, and (G) 25X magnification show barbed end distribution at the leading edge. (B), (E), (H): Quantification of relative number of barbed ends at leading edge, after stimulation with (B) 0.5 nM EGF for 60 seconds, (E) 5 nM EGF for 60 seconds, and (H) 5 nM EGF for 180 seconds. Error bars: SEM. Results represent triplicates, >30 cells analyzed for (B) and (E), >50 cells for (H). One-way ANOVA **$p<0.01$, ***$p<0.005$, n.s not significant. (C), (F), (I): Normalized pixel intensities of relative number of barbed ends, plotted as a function of distance from the cell edge (mean ± SEM), after stimulation with (C) 0.5 nM EGF for 60 seconds, (F) 5 nM EGF for 60 seconds, and (I) 5 nM EGF for 180 seconds.

3.4 Conclusion

In epithelial-like breast cancer cells, we find that Mena11a localizes to cell-cell junctions. Mena11a-specific knockdown disrupts E-cadherin distribution at cell-cell junctions and alters the junctional actin organization. In addition, depletion of Mena11a increases 2D migration of these cells, suggesting a role for Mena11a in maintaining cell-cell junctions and antagonizing cell motility.

Our results demonstrate that Mena11a has functions distinct from Mena. In MV^{D7} cells, which are Ena/VASP-deficient, Mena11a expression does not support efficient *Listeria* tail F-actin elongation, is able to decrease accumulation of Arp2/3 complex at the leading edge and alter the F-actin network density in lamellipodia. In cells with both isoforms, Mena11a also acts antagonistically to Mena, potentially through formation of mixed Mena/Mena11a heterotetramers (45). Co-expression of Mena11a with Mena reduces the levels of F-actin barbed ends at the leading edge of lamellipodia and

impairs lamellipodial protrusion. Acute EGF-elicited EGFR activation and downstream signaling were not affected in Mena11a-expressing cells. This suggests that Mena11a-dependent dampening of growth factor elicited lamellipodial protrusion could be a due to reduced actin assembly rather than dysregulated signal transduction (Balsamo and Mondal, submitted).

Transcriptome data from cancer cohorts in the Cancer Genome Atlas demonstrated that neither Mena nor Mena11a expression alone had correlation with clinicopathological features of patients. MenaCalc^{RNA}, a metric examining the difference between Mena and Mena11a expression levels had greater predictive power; patients with a high MenaCalc^{RNA} in the colorectal adenocarcinoma cohort had increased metastasis formation (Balsamo and Mondal, submitted).

3.5 Materials and Methods

Tissues
Serial sections of mammary tumors from different stages of progression were obtained from MMTV-PyMT mice in an FVB background (gifts from Patrick Stern and John Lamar of the Hynes laboratory at the Koch Institute at MIT, and Evanthia Roussos of the Condeelis laboratory at Albert Einstein SOM).

Immunofluorescence of Tissues
5 µm sections of paraffin-embedded tissues were deparaffinized in xylene, treated with a graded series of alcohol, and rehydrated in PBS using a deparaffinization program in the Histology Core, Swanson Biotechnology Center. Sections were subjected to heat-induced antigen retrieval in 1X Antigen Retrieval Plus Citra solution (Biogenex). Sections were incubated with 10% normal donkey or goat serum in 0.5% Tween-20 for 2 hours at room temperature. Primary antibodies in 1% donkey or goat serum in 0.5% Tween-20 buffer were added overnight at 4°C, and sections were subsequently washed three times in 1X PBS. Sections were incubated with fluorescently labeled secondary antibodies (AlexaFluor, Molecular Probes) for 2 hours at room temperature, and in 10 µg/ml Hoechst dye to stain the nucleus.

Microscopy of Tissues
z-series of tissues were imaged with either a Deltavision microscope using SoftWoRx acquisition software (Applied Precision), a 40X and 60X 1.4 NA Plan-Apochromat objective lens (Olympus), and a camera (CoolSNAP HQ). Images taken with the Deltavision microscope were deconvolved using Deltavision SoftWoRx software and objective-specific point spread function.

Clinical Data and Analysis
Exon-level gene expression data (RNAseqV2) and clinical data for the 1098 breast cancer patients (BRCA) and 461 colorectal adenocarcinoma patients (COAD) were accessed from The Cancer Genome Atlas (TCGA) public data portal (https://tcga-data.nci.nih.gov/tcga/). MenaCalc^{RNA} was calculated with the following formula:

MenaCalc^{RNA} = average RPKM constitutive Mena exons (hg19 225695653:225695719 and 225688694: 225688772) – RPKM alternate exon 11a (hg19 225692693: 225692755)

For measure of pairwise gene association in the COAD cohort, Spearman's rank correlation coefficients and two-tailed p-values were estimated. The top 50 genes significantly correlating with Mena, Mena11a, and MenaCalc^{RNA} were run through GO analysis using the Enrichr analysis tool (http://amp.pharm.mssm.edu/Enrichr/) (46) and GSEA using the MsigDb (http://www.broadinstitute.org/gsea/msigdb/index.jsp) (47).

The association between MenaCalc^{RNA}, Mena, and Mena11a and metastasis in the COAD cohort was evaluated by a Wilcoxon rank-sum test and logistic regression in R 2.15.3. We excluded subjects without the pathological stage of metastasis assigned, or with an MX pathological stage (where presence of distant metastasis cannot be

assessed). For the logistic regression, in order to compare coefficients across tests, we standardized MenaCalc^{RNA}, Mena, and Mena11a RPKM values with mean zero and standard deviation one. The logistic regressions were carried with the stage of metastasis as the dependent variable (M0 as no evidence of distant metastasis, M1 as evidence with distant metastasis). The only independent variable fitted in the model was MenaCalc^{RNA}, or Mena, or Mena11a respectively. p values and coefficients corresponding to the independent variables were used to judge the level of association.

Cell lines

Human cancer cell lines (MCF7 and T47D) were obtained from ATCC. MCF7 and T47D cell lines, and HEK293 cells were cultured in DMEM supplemented with 10% Fetal Bovine Serum (FBS, Hyclone), L-glutamine, and antibiotics (penicillin/streptomycin; Invitrogen). MTLn3 cells were maintained in alpha-MEM media supplemented with 5% heat-inactivated fetal bovine serum (HyClone), L-glutamine, and antibiotics (penicillin/streptomycin; Invitrogen). MV^{D7}, Ena/VASP-deficient mouse embryonic fibroblastic cells were isolated as described (26), and cultured at 32°C in DMEM with 15% FBS, penicillin/streptomycin, L-glutamine, and 50 U/mL recombinant mouse IFN-γ (Invitrogen). Adherent cultures were incubated at 37°C in 5% CO_2. Cell lines were tested routinely for Mycoplasma contamination (Universal Mycoplasma Detection Kit, ATCC).

Molecular Cloning

GFP-Mena splice isoforms were subcloned into the pMSCV retroviral vector using standard techniques. shRNAs were designed with the following web tool: http://euphrates.mit.edu/cgi-bin/shRNA/index.pl (Hemann laboratory, Koch Institute, MIT). 97-mer oligos were synthesized by Invitrogen, PCR-amplified with primers having EcoRI/XhoI sites, and cloned in the pMSCV-miR30-MLS-GFP vector (gift of Michael Hemann, Koch Institute, MIT).

sh-1

TGCTGTTGACAGTGAGCG*CATGATTCATTACACAGACCAA*TAGTGAAGCCACAGAT
GTA*TTGGTCTGTGTAATGAATCATA*TGCCTACTGCCTCGGA

sh-1C

TGCTGTTGACAGTGAGCG*AATGATTCCTTAAACAGCCCAA*TAGTGAAGCCACAGAT
GTA*TTGGGCTGTTTAAGGAATCATG*TGCCTACTGCCTCGGA

sh-2

TGCTGTTGACAGTGAGCG*CAACAGGTCCTATGATTCATTA*TAGTGAAGCCACAGAT
GTA*TAATGAATCATAGGACCTGTTA*TGCCTACTGCCTCGGA

sh2-C

TGCTGTTGACAGTGAGCG*AAACAGGTCATAGGATTAATTA*TAGTGAAGCCACAGAT
GTA*TAATTAATCCTATGACCTGTTC*TGCCTACTGCCTCGGA

Retroviral packaging, infection and fluorescence-activated cell sorting

Retroviral packaging, infection, and fluorescence-activated cell sorting were performed as previously described (26). Retroviral plasmids and plasmids containing VSV-g and GAG-Pol cDNA were transiently transfected with X-tremeGENE 9 DNA transfection reagent (Roche) into HEK 293T cells to package virus. Virus was packaged at 32°C and supernatant was collected after 48 hours. MCF7, T47D, MV^{D7}, and MTLn3 cells were infected with virus for 24 hours in the presence of 1 mg/ml polybrene (Invitrogen) and cultured to 80% confluence. Cells were then trypsinized, filtered with 40 µm cell strainers, and fluorescence-activated cell sorted (FACS) in PBS + 5% Fetal Bovine Serum (FBS). Cells expressing GFP-shRNAs or GFP-Mena isoforms were sorted to expression levels as described (15) (Balsamo and Mondal, submitted).

Antibodies and Growth Factors

The rabbit polyclonal anti-Mena11a (20) and mouse monoclonal anti pan-Mena (48) antibodies were generated in our laboratory. Commercially available antibodies are: mouse monoclonal anti-E-Cadherin (BD, dilution 1:1000), rabbit polyclonal anti-p34Arc (Millipore, dilution 1:100), chicken IgY anti-GFP (Aves labs, dilution 1:500), mouse monoclonal anti-Tubulin (BD biosciences, dilution 1:5000), rabbit polyclonal anti-GAPDH (Cell Signaling Technology, dilution 1:1000), rabbit polyclonal anti-EGFR pY1068 (Cell Signaling Technology, dilution 1:1000), rabbit monoclonal anti-EGFR pY1173 (Epitomics, dilution 1:1000). CF405-Phalloidin was purchased (Biotium) and diluted 1:50. Hoechst 33342 (used at 10 µg/ml) was from Invitrogen. Mouse recombinant Epidermal Growth Factor (EGF) was from Invitrogen, and Platelet Derived Growth Factor-BB (PDGF-BB) was from Peprotech. Concentrations of growth factors are indicated in text.

Western Blots

Cells were lysed in NP-40 buffer (1% NP-40, 150 mM NaCl, and 50 mM Tris, pH 8.0) containing protease inhibitors (Complete Mini tablets; Roche) and phosphatase inhibitors (1 mM sodium orthovanadate, 50 mM sodium fluoride, 40 mM beta-glycerolphosphate, 15 mM sodium pyrophosphate). Protein concentrations were measured with a Bradford Assay (BioRad), and 25-40 µg of protein were run on 8% SDS-PAGE gels. Protein was transferred to nitrocellulose membrane (Biorad), blocked for 1 hour at room temperature in 5% nonfat milk in 1x TBSxT, and probed with antibodies diluted in 1x TBSxT as indicated in figures and legends. Mouse and rabbit HRP-conjugated secondaries (diluted 1:5000) from Jackson Immunoresearch were added for 1 hour at room temperature. The membrane was subsequently washed in 1x TBSxT, and developed with a BM Chemiluminescence Western Blotting Kit (Roche) on film.

3-Dimensional Structural Illumination Microscopy.

Cells were imaged with an OMX-3D Super-resolution microscope (Applied Precision/GE) equipped with 405 nm, 488 nm, 594 nm lasers and 3 Photometrics Cascade II, EMCCD cameras. Images were acquired with a 100X, NA 1.4 oil objective, at 0.125 µm z step, using 1.512 immersion oil. All images were acquired under the same illumination settings (405 nm laser at 19% strength, for 100 msec, 488 nm laser at 1% strength for 150 msec, and 594 nm laser at 50% strength for 100 msec) and then

processed with OMX softWoRx software (Applied Precision). Images were saved as .tiff of maximum projections of 8 x 0.125 micron z section stack.

Image quantification

Quantitative analysis of fluorescence intensity at contacts was performed as described in (49), with modifications. Using the line scan function of ImageJ, a line 4 μm in length (averaged over 20 pixels) was positioned upon randomly chosen contacts. The plot profile feature of ImageJ was used to obtain numerical values for the fluorescence intensity profile along this line; the baseline of each independent profile was corrected by subtracting a constant value from each of the intensity profiles. A minimum of 30 contacts from three individual experiments was measured. The data were imported into Prism 5 and fitted to a Gaussian function with an offset variable. Peak values and their SEs were obtained by nonlinear regression.

Wound Closure assay

Cells were plated on silicone cell culture inserts with a defined cell-free gap (Ibidi) in 8 well slides (Ibidi) following manufacturer's instructions. Control and knockdown cells were plated in the same 8 well slide and processed concurrently, with the same culture conditions. To avoid effects related to cell proliferation, we treated T47D cells with 5 mg/ml of mitomycin-C (Sigma), a proliferation inhibitor, 30 minutes prior to the start of the assay. DIC imaging was performed as above, with a 10X DIC objective. Gap area was quantified after 48 hours by manual tracing with ImageJ.

Platinum replica electron microscopy

Platinum Replica Electron Microscopy was performed as described (50). MV^{D7} cells were cultured on coverslips and immediately extracted with 1% Triton X-100 in PEM buffer (100 mM PIPES, pH 6.8, 1 mM EGTA, 1 mM $MgCl_2$) containing 10 μM phalloidin, 0.2% glutaraldehyde, and 4.2% sucrose as an osmotic buffer. Coverslips were washed with PEM containing 1 μM phalloidin, and 1% sucrose, fixed in 0.1 M Na-cacodylate buffer (pH 7.3), 2% glutaraldehyde, 1% sucrose, and processed for electron microscopy. Images were captured on film using a TEM JEOL 200CX. Films were scanned and an unsharp mask filter was applied to the pictures in Adobe Photoshop.

***Listeria* infections**

Infection of MV^{D7} cells with *Listeria monocytogenes* was done according to (35). Briefly, the *Listeria 10403S* was used to infect MV^{D7} cells using an MOI of 200:1 (bacteria:cell), and taking 1 O.D. = 10^9 bacteria/ml. After 1 hour of incubation time for bacterial entry at 37°C, cells were washed in PBS and media containing 10 mg/ml of gentamicin was added for 5 hours to kill extracellular *Listeria*, allowing for F-actin tail growth. After 5 hours, cells were washed in PBS, fixed in 4% paraformaldehyde in cytoskeleton buffer (20 minutes) and stained with phalloidin and Hoechst to visualize F-actin and DNA, respectively. Images were taken with a deconvolution microscope as above. F-actin tail length was quantified by manual tracing with ImageJ.

Membrane Protrusion Assay

MTLn3 cells were starved for 4 hours in L15 medium (Gibco) supplemented with 0.35% BSA. Cells were stimulated with a bath application of EGF at 37°C, at either 0.5 nM or 5 nM. DIC time-lapse movies were recorded for 5 minutes, with 10 second intervals, after addition of EGF. For MTLn3 cells, area fold change was quantified by cell tracing, and cell area was measured using ImageJ software. Area measurements of each cell were standardized to area at time = 0, averaged, and plotted over time after EGF stimulation.

For MV^{D7} cells, cells were starved as above, but stimulated with 100 ng/ml of PDGF-BB at 37°C, respectively. Cells were plated on glass coverslips coated with 10 µg/ml bovine plasma fibronectin (Sigma), stimulated for 3 minutes with PDGF-BB, fixed in 4% paraformaldehyde in cytoskeleton buffer (10 mM MES, pH 8.0, 3 mM $MgCl_2$, 138 mM KCl, 2 mM EGTA, pH 6.1, 0.32 M sucrose) for 20 minutes at room temperature, permeabilized in 0.2% Triton X-100 in PBS, blocked in 10% BSA in PBS for 1 hour; incubated with antibodies (indicated in figures and legends) for 1 hour at 37°C, washed 3 times in 1X PBS and incubated with fluorescently labeled secondary antibodies and phalloidin to visualize F-actin.

Barbed Ends Assay

Barbed ends assay was performed as described (51) with some modifications. MTLn3 cells were starved for 4 hours in L15 medium supplemented with 0.35% BSA. For stimulation, cells were treated with bath application of 0.5 nM or 5 nM EGF at 37°C, and 60 or 180 seconds later were permeabilized with 0.125 mg/ml saponin (Sigma) in the presence of 0.5 mM rhodamine–conjugated G-actin. After 1 minute of labeling, samples were fixed in 0.5% glutaraldehyde in cytoskeleton buffer, permeabilized with 0.5% Triton X-100 in cytoskeleton buffer, quenched in 100mM Na-Borohydride in PBS, and blocked in the presence of CF405–phalloidin (Biotium). Images were taken with a deconvolution microscope. The ratio of barbed end intensity to phalloidin intensity along the edge was quantified. Signal intensities from rhodamine-labeled barbed ends along the cell edge were quantified with a published contour-based ImageJ macro (52). We measured the distribution of signal along the membrane plotted as a function of distance from the cell edge (mean ± SEM) and the sum of the intensities in the first 0.65 µm from the cell edge.

Statistical Analysis

Statistical differences between two conditions were determined using student's unpaired t-test. For multiple conditions, means were compared by analysis of variance (ANOVA). All data found to be significant ($p < 0.05$) by ANOVA were compared with Tukey's honestly significant difference *post hoc* test.

3.6 References

1. Di Modugno F, et al. (2004) Human Mena protein, a serex-defined antigen overexpressed in breast cancer eliciting both humoral and CD8+ T-cell immune response. *Int J cancer J Int du cancer* 109(6):909–918.
2. Di Modugno F, et al. (2006) The cytoskeleton regulatory protein hMena (ENAH) is overexpressed in human benign breast lesions with high risk of transformation and human epidermal growth factor receptor-2-positive/hormonal receptor-negative tumors. *Clin Cancer Res* 12(5):1470–8.
3. Toyoda A, et al. (2009) Aberrant expression of human ortholog of mammalian enabled (hMena) in human colorectal carcinomas: implications for its role in tumor progression. *Int J Oncol* 34(1):53–60.
4. Gurzu S, et al. (2008) The expression of cytoskeleton regulatory protein Mena in colorectal lesions. *Rom J Morphol Embryol* 49(3):345–349.
5. Gurzu S, Jung I, Prantner I, Chira L, Ember I (2009) The immunohistochemical aspects of protein Mena in cervical lesions. *Rom J Morphol Embryol* 50(2):213–216.
6. Wang W, et al. (2007) Coordinated regulation of pathways for enhanced cell motility and chemotaxis is conserved in rat and mouse mammary tumors. *Cancer Res* 67(8):3505–3511.
7. Wang W, et al. (2004) Identification and testing of a gene expression signature of invasive carcinoma cells within primary mammary tumors. *Cancer Res* 64(23):8585–8594.
8. Roussos ET, et al. (2010) Mena deficiency delays tumor progression and decreases metastasis in polyoma middle-T transgenic mouse mammary tumors. *Breast Cancer Res* 12(6):R101.
9. Robinson BD, et al. (2009) Tumor microenvironment of metastasis in human breast carcinoma: a potential prognostic marker linked to hematogenous dissemination. *Clin Cancer Res* 15(7):2433–2441.
10. Rohan TE, et al. (2014) Tumor microenvironment of metastasis and risk of distant metastasis of breast cancer. *J Natl Cancer Inst* 106(8):1–11.
11. Gertler FB, Niebuhr K, Reinhard M, Wehland J, Soriano P (1996) Mena, a relative of VASP and Drosophila Enabled, is implicated in the control of microfilament dynamics. *Cell* 87(2):227–239.

12. Di Modugno F, et al. (2007) Molecular cloning of hMena (ENAH) and its splice variant hMena+11a: epidermal growth factor increases their expression and stimulates hMena+11a phosphorylation in breast cancer cell lines. *Cancer Res* 67(6):2657–65.

13. Di Modugno F, et al. (2012) Splicing program of human MENA produces a previously undescribed isoform associated with invasive, mesenchymal-like breast tumors. *Proc Natl Acad Sci* 109(47):19280–5.

14. Goswami S, et al. (2009) Identification of invasion specific splice variants of the cytoskeletal protein Mena present in mammary tumor cells during invasion in vivo. *Clin Exp Metastasis* 26(2):153–159.

15. Philippar U, et al. (2008) A Mena invasion isoform potentiates EGF-induced carcinoma cell invasion and metastasis. *Dev Cell* 15(6):813–828.

16. Roussos ET, et al. (2011) Mena invasive (MenaINV) promotes multicellular streaming motility and transendothelial migration in a mouse model of breast cancer. *J Cell Sci* 124(Pt 13):2120–2131.

17. Roussos ET, et al. (2011) Mena invasive (Mena(INV)) and Mena11a isoforms play distinct roles in breast cancer cell cohesion and association with TMEM. *Clin Exp Metastasis* 28(6):515–527.

18. Pignatelli J, et al. (2014) Invasive breast carcinoma cells from patients exhibit MenaINV- and macrophage-dependent transendothelial migration. *Sci Signal* 7(353):ra112–ra112.

19. Warzecha CC, Sato TK, Nabet B, Hogenesch JB, Carstens RP (2010) ESRP1 and ESRP2 Are Epithelial Cell-Type-Specific Regulators of FGFR2 Splicing. *Mol Cell* 33(5):591–601.

20. Pino MS, et al. (2008) Human Mena+11a isoform serves as a marker of epithelial phenotype and sensitivity to epidermal growth factor receptor inhibition in human pancreatic cancer cell lines. *Clin Cancer Res* 14(15):4943–50.

21. Shapiro IM, et al. (2011) An EMT–Driven Alternative Splicing Program Occurs in Human Breast Cancer and Modulates Cellular Phenotype. *PLoS Genet* 7(8):21.

22. Agarwal S, et al. (2012) Quantitative assessment of invasive mena isoforms (Menacalc) as an independent prognostic marker in breast cancer. *Breast Cancer Res* 14(5):R124.

23. Forse C, et al. (2015) Mena calc , a quantitative method of metastasis assessment, as a prognostic marker for axillary node-negative breast cancer.

BMC Cancer 15(1):483.

24. Lin EY, et al. (2003) Progression to malignancy in the polyoma middle T oncoprotein mouse breast cancer model provides a reliable model for human diseases. *Am J Pathol* 163(5):2113–26.

25. Takeichi M (2014) Dynamic contacts: rearranging adherens junctions to drive epithelial remodelling. *Nat Rev Mol Cell Biol* 15(6):397–410.

26. Bear JE, et al. (2000) Negative regulation of fibroblast motility by Ena/VASP proteins. *Cell* 101(7):717–728.

27. Bear JE, et al. (2002) Antagonism between Ena/VASP proteins and actin filament capping regulates fibroblast motility. *Cell* 109(4):509–521.

28. Svitkina TM, Borisy GG (1999) Arp2/3 Complex and Actin Depolymerizing Factor/Cofilin in Dendritic Organization and Treadmilling of Actin Filament Array in Lamellipodia. *J Cell Biol* 145(5):1009–1026.

29. Bisi S, et al. (2013) Membrane and actin dynamics interplay at lamellipodia leading edge. *Curr Opin Cell Biol* 25(5):565–573.

30. Cai L, Marshall TW, Uetrecht AC, Schafer DA, Bear JE (2007) Coronin 1B Coordinates Arp2/3 Complex and Cofilin Activities at the Leading Edge. *Cell* 128(5):915–929.

31. Lambrechts A, Gevaert K, Cossart P, Vandekerckhove J, Van Troys M (2008) Listeria comet tails: the actin-based motility machinery at work. *Trends Cell Biol* 18(5):220–227.

32. Welch MD, Iwamatsu A, Mitchison TJ (1997) Actin polymerization induced by Arp2/3 protein complex at the surface of Listeria monocytogenes.pdf. *Nature* 385(6613):265–269.

33. Chakraborty T, Ebel F, Domann E (1995) A focal adhesion factor directly linking intracellularly motile Listeria monocytogenes and Listeria ivanovii to the actin-based cytoskeleton of mammalian cells. *EMBO J* 14(7):1314–1321.

34. Niebuhr K, et al. (1997) A novel proline-rich motif present in ActA of Listeria monocytogenes and cytoskeletal proteins is the ligand for the EVH1 domain, a protein module present in the Ena/VASP family. *EMBO J* 16(17):5433–5444.

35. Geese M, et al. (2002) Contribution of Ena/VASP Proteins to Intracellular Motility of Listeria Requires Phosphorylation and Proline-rich Core but Not F-Actin Binding or Multimerization. *Mol Biol Cell*:1–14.

36. Smith GA, Theriot JA, Portnoy DA (1996) The tandem repeat domain in the Listeria monocytogenes ActA protein controls the rate of actin-based motility, the percentage of moving bacteria, and the localization of vasodilator-stimulated phosphoprotein and profilin. *J Cell Biol* 135(3):647–660.

37. Auerbuch V, Loureiro JJ, Gertler FB, Theriot JA, Portnoy DA (2003) Ena/VASP proteins contribute to Listeria monocytogenes pathogenesis by controlling temporal and spatial persistence of bacterial actin-based motility. *Mol Microbiol* 49(5):1361–1375.

38. Theriot JA, Mitchison TJ, Tilney LG, Portnoy DA (1992) The rate of actin-based motility of intracellular Listeria monocytogenes equals the rate of actin polymerization. *Nature* 357(6375):257–260.

39. Welch MD, Rosenblatt J, Skoble J, Portnoy DA, J MT (1998) Interaction of Human Arp2/3 Complex and the Listeria monocytogenes ActA Protein in Actin Filament Nucleation. *Science (80-)* 281(5373):105–108.

40. Chan AY, Bailly M, Zebda N, Segall JE, Condeelis JS (2000) Role of cofilin in epidermal growth factor-stimulated actin polymerization and lamellipod protrusion. *J Cell Biol* 148(3):531–542.

41. Segall JE, et al. (1996) EGF stimulates lamellipod extension in metastatic mammary adenocarcinoma cells by an actin-dependent mechanism. *Clin Exp Metastasis* 14(1):61–72.

42. Bailly M, et al. (2001) The F-actin side binding activity of the Arp2/3 complex is essential for actin nucleation and lamellipod extension. *Curr Biol* 11(8):620–625.

43. Chan AY, et al. (1998) EGF stimulates an increase in actin nucleation and filament number at the leading edge of the lamellipod in mammary adenocarcinoma cells. *J Cell Sci* 111 (Pt 2:199–211.

44. Mouneimne G, et al. (2004) Phospholipase C and cofilin are required for carcinoma cell directionality in response to EGF stimulation. *J Cell Biol* 166(5):697–708.

45. Riquelme DN, Meyer AS, Barzik M, Keating A, Gertler FB (2015) Selectivity in subunit composition of Ena/VASP tetramers. *Biosci Rep* 35(5).

46. Chen EY, et al. (2013) Enrichr: interactive and collaborative HTML5 gene list enrichment analysis tool. *BMC Bioinformatics* 14(1):128.

47. Subramanian A, et al. (2005) Gene set enrichment analysis: A knowledge-based approach for interpreting genome-wide expression profiles. *Proc Natl Acad Sci*

102 (43):15545–15550.

48. Lanier LM, et al. (1999) Mena is required for neurulation and commissure formation. *Neuron* 22(2):313–325.

49. Leerberg JM, et al. (2014) Tension-Sensitive Actin Assembly Supports Contractility at the Epithelial Zonula Adherens. *Curr Biol*:1–11.

50. Svitkina TM, Verkhovsky AB, Borisy GG (1995) Improved procedures for electron microscopic visualization of the cytoskeleton of cultured cells. *J Struct Biol* (115):290–303.

51. Furman C, et al. (2007) Ena/VASP is required for endothelial barrier function in vivo. *J Cell Biol* 179(4):761–775.

52. Cai L, Marshall TW, Uetrecht AC, Schafer DA, Bear JE (2007) Coronin 1B Coordinates Arp2/3 Complex and Cofilin Activities at the Leading Edge. *Cell* 128(5):915–929.

Chapter 4: Regulation of Mena11a function

Figure 4.6 was contributed by Dr. Michele Balsamo. Figures 4.3, 4.4, and 4.6 contributed to the following manuscript: Balsamo and Mondal, et al. "Mena-dependent regulation of actin cytoskeleton organization and cell behavior is regulated by the alternatively-included 11a sequence." Manuscript submitted. Figure 4.3 was completed in collaboration with the Taplin Mass Spectrometry Facility and Amanda Del Rosario.

TABLE OF CONTENTS

4.1 Abstract

Previous work has shown that Mena11a is phosphorylated in human epithelial-like breast cancer cells upon long-term EGF stimulation (1). We mapped the phosphorylation sites of the 11a sequence using an IP/tandem MS approach and determined that the sequence harbors a unique serine phosphorylation site (hereafter S3). We find that S3 phosphorylation regulates Mena11a-driven effects on membrane protrusion, barbed end formation and Arp2/3 recruitment to the leading edge. Based on reduced Arp2/3 at the leading edge and decreased density of the actin network in Mena11a expressing cells, we examined whether Mena11a is involved in the mechanism of actin debranching. Pharmacological inhibition of Arp2/3 demonstrated that Mena11a has no apparent effect on debranching.

4.2 Introduction

Mena function is regulated by post-translational modifications, including serine / threonine phosphorylation (2) and tyrosine phosphorylation (3). Mena harbors two cAMP/cGMP-dependent PKA/PKG phosphorylation sites, including S236 after the LERER repeat region, and S376 in the EVH2 domain (Figure 1.6). In terms of localization and function, the two PKA/PKG sites do not affect Mena subcellular targeting, and S236 affects Mena function (conversion of S236 to an alanine restores the hypermotility phenotype (2) that Ena/VASP deficient fibroblasts demonstrate (4, 5)). While the S376 site does not affect random fibroblast motility, pseudophosphorylation of this site impairs F-actin levels (6). Interestingly, phosphorylation of the S236 equivalent site in VASP (S157) affects VASP subcellular localization, and the S376 equivalent site in VASP (S239) impairs actin polymerization (6).

During cancer progression, Mena is alternatively spliced to produce protein isoforms with distinct functions. The epithelial-enriched splice isoform, Mena11a, is phosphorylated in human epithelial-like breast cancer cells. Using two-dimensional gel electrophoresis, DiModugno et al. determined that stimulation of T47D cells with EGF for 24 hours shifted the Mena11a gel band towards a more acidic pH (1), suggesting a post-translational modification adding negative charge to the protein occurred; therefore, we reasoned that Mena11a-specific phosphorylation might contribute to its ability to regulate actin polymerization (Balsamo and Mondal, submitted).

4.3 Results

4.3.1 The 11a sequence contains a unique phosphorylation site, S3.

Using the bioinformatics tool NetPhos2.0, we find that the 21 amino acid 11a sequence has three putative phosphorylation sites: S3, Y16, and S18 (Figure 4.1) (7). To map post-translational modifications of Mena11a, we used a rabbit anti-GFP antibody to immunoprecipitate GFP-Mena11a from GFP-Mena11a expressing MTLn3 cells that were starved and then stimulated for 60 seconds with 5nM EGF. We confirmed the immunoprecipitation by staining a 1D PAGE gel with Coomassie Brilliant Blue and by western blotting with the anti-rabbit Mena11a antibody (Figure 4.2 A-B, respectively). Control immunoprecipitations were performed in parallel with a rabbit IgG (Figure 4.2 A-B). Using a Lys-C and Trypsin digest (Figure 4.3 A), we were able to map the phosphorylation sites of the entire 11a sequence. Mass spectrometry analysis identified a unique serine phosphorylation site, S3, within the 21 amino acid 11a sequence (demarcated in blue, Figure 4.3 B-C). Interestingly, alignment of the Mena11a

protein sequence from different vertebrate species showed 100% conservation of this serine and the surrounding residues (Figure 4.4) (Balsamo and Mondal, submitted).

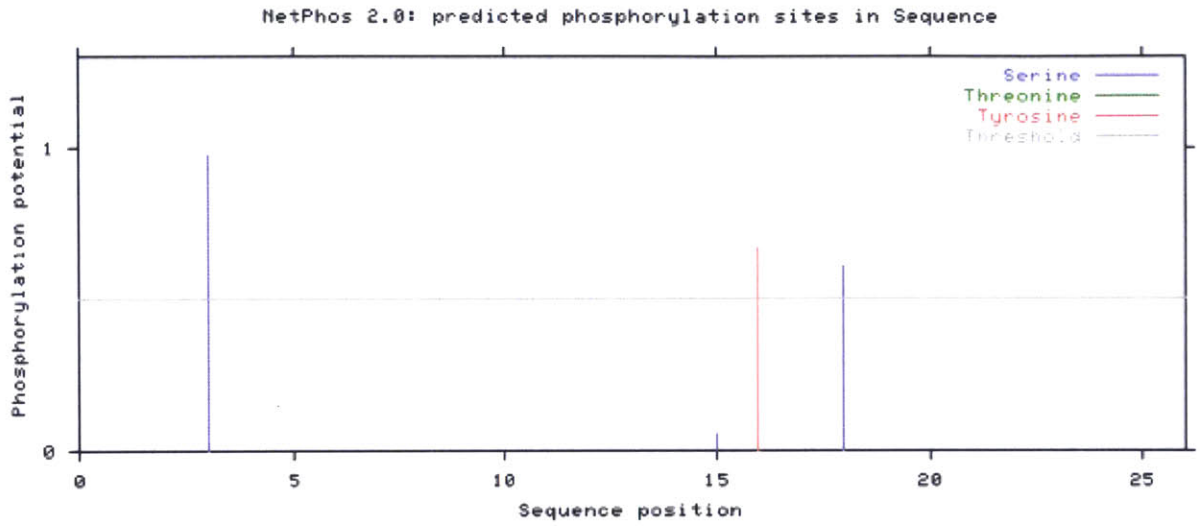

Sequence Position

1	2	3	4	5	6	7	8	9	10	11	12	13	14	15	16	17	18	19	20	21
R	D	**S**	P	R	K	N	Q	I	V	F	D	N	R	S	Y	D	S	L	H	R

11a sequence

Figure 4.1: The 11a sequence has 3 putative phosphorylation sites. NetPhos2.0 server was used to predict serine, threonine, and tyrosine phosphorylation sites. Shown is the prediction for the 11a inclusion; predicted serine = blue, predicted tyrosine = red, bold = phosphorylation site discovered in Gertler laboratory (Balsamo and Mondal, submitted). Human Mena11a protein sequence was accessed from NCBI (NP_001008493.1).

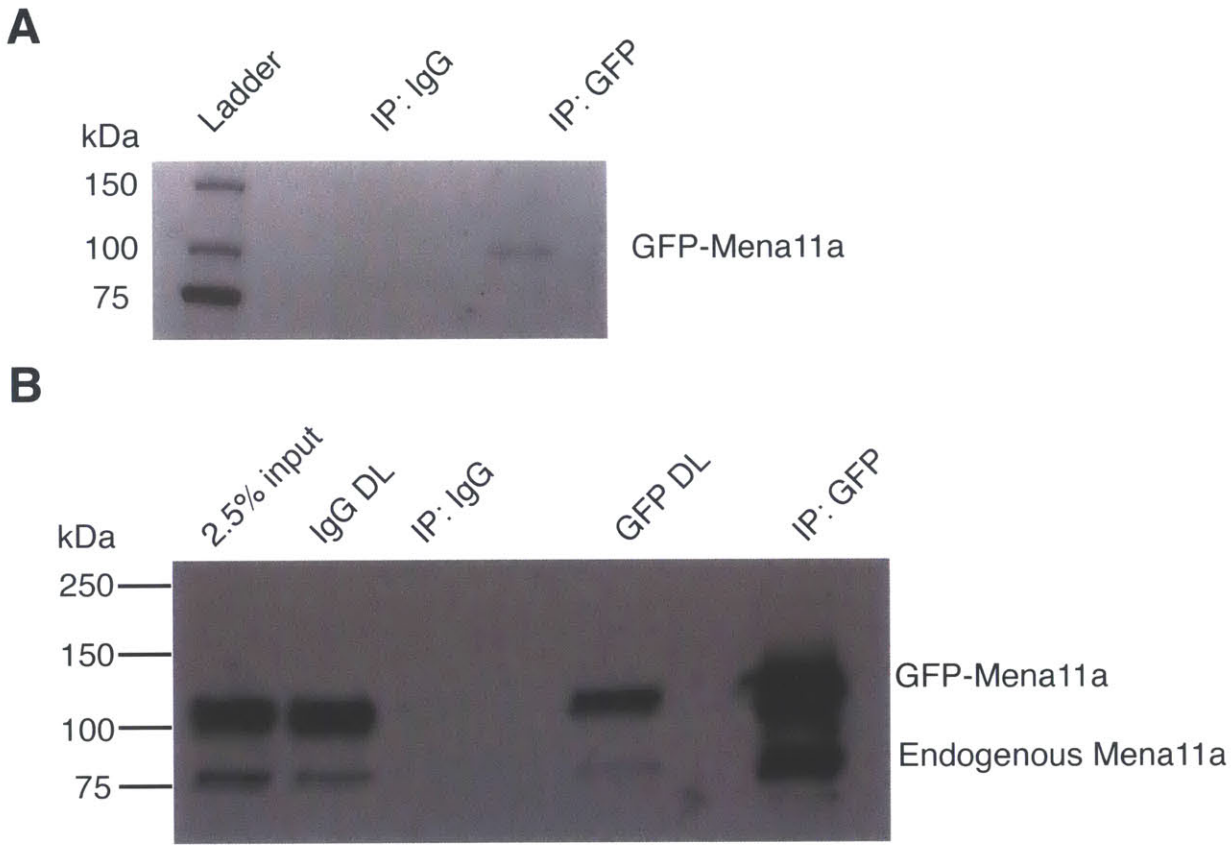

Figure 4.2: Immunoprecipitation (IP) of Mena11a from MTLn3 rat mammary adenocarcinoma cells. (A)-(B): MTLn3 cells stably expressing GFP-tagged Mena11a. (A) Coomassie stain of IP of GFP-Mena11a with α-GFP (Rb) antibody. Control IP was done in parallel using rabbit IgG. (B) Western blot of immunoprecipitation of GFP-Mena11a with α-Mena11a antibody. Control IP was done in parallel using rabbit IgG. DL = depletion of target protein from lysate after immunoprecipitation.

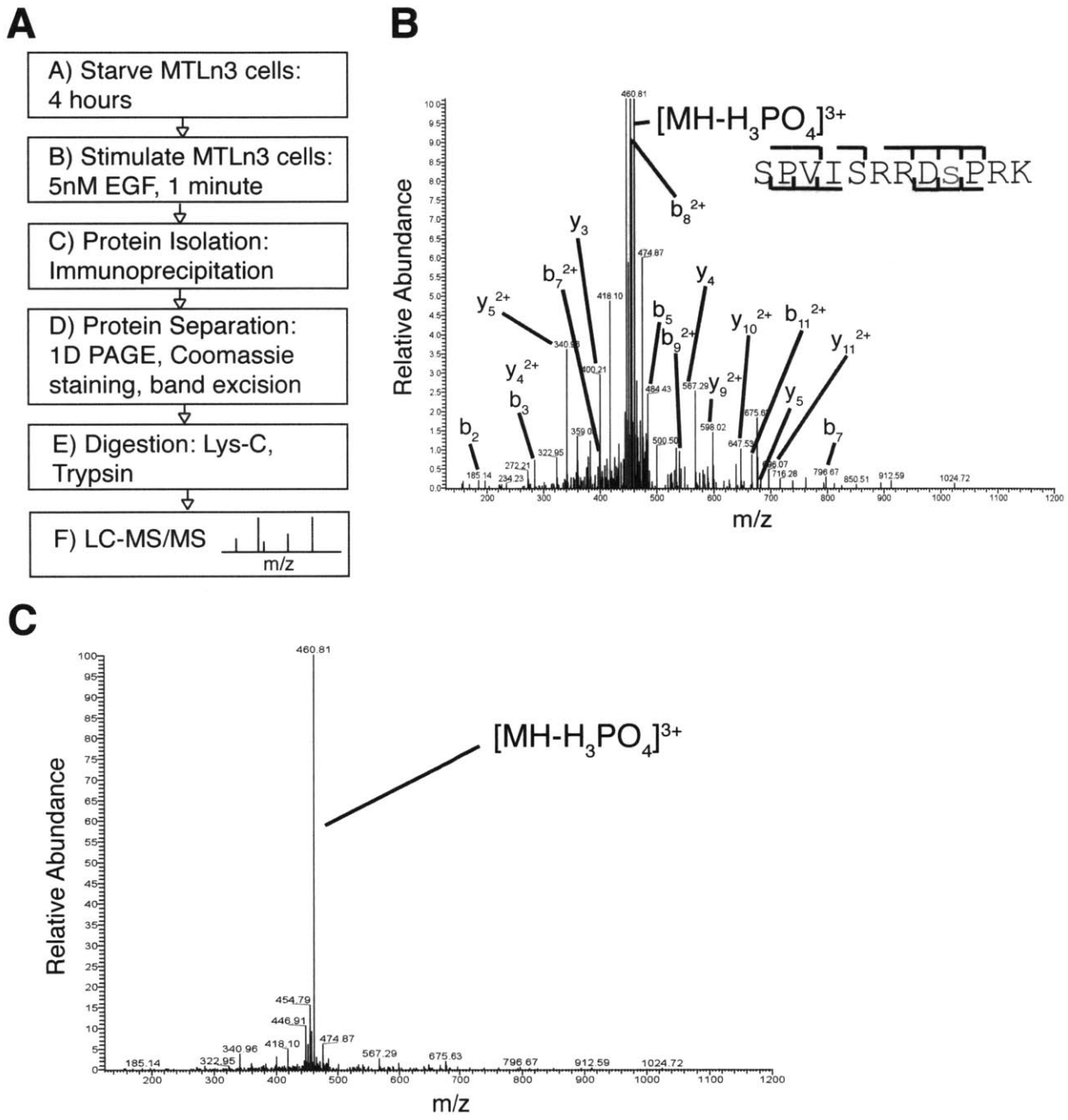

Figure 4.3: Tandem MS approach. (A) Strategy for immunoprecipitation (IP)/tandem-mass spectrometry (MS/MS) of GFP-Mena11a from MTLn3 cell lysates after 5nM EGF stimulation for 60 seconds. (B) MS/MS spectrum of phospho-peptide SPVISRRDsPRK (zoomed in for peak detail). Ions labeled with $-H_3PO_4$ indicate a neutral loss of phosphoric acid. "b" and "y" ion series represent fragment ions containing the N- and C-termini of the peptide, respectively. (C) MS/MS spectrum of phospho-peptide. Ion labeled with $-H_3PO_4$ indicates a neutral loss of phosphoric acid.

	11a insertion sequence
Homo sapiens	*SPVISR***RDSPRKNQIVFDNRSYDSLHR***PKSTPL*
Mus musculus	*SPVISR***RDSPRRNQIVFDNRAYDSLHR***PKSTPS*
Rattus norvegicus	*SPVISR***RDSPRKNQIVFDNRSYDSLHR***PKSTPS*
Heterocephalus glaber	*SPVISR***RDSSRKNQIVFDNRFYDLLHR***PISRPS*
Gallus gallus	*SPVISR***RESPWKN-LVSENRFYDSLNR***TKSTTT*

Figure 4.4: Sequence alignment of 11a sequence.
Alignment of Mena11a protein sequences across species. Blue: conserved serine 3 in the 11a insertion sequence.

4.3.2 Mena11a function is phospho-regulated.

To study the contribution of phosphorylation to Mena11a function, we generated a non-phosphorylatable mutant and a phosphomimetic mutant at serine 3 (Mena11aS>A and Mena11aS>D, respectively) using site-directed mutagenesis. We expressed mutants at similar levels in MTLn3 rat mammary carcinoma cells (Figure 4.5 A), stimulated the cells with 5 nM EGF, and investigated lamellipodial behavior with time-lapse microscopy. After acute stimulation with 5 nM EGF, Mena11aS>D expressing cells have the same dampened protrusion phenotype that Mena11a expressing cells do (Figure 4.5 B). The Mena11aS>A expressing cells ablate the dampening effect of Mena11a on membrane protrusion (Figure 4.5 B).

To determine whether Mena11a phosphorylation regulates the dynamics of actin polymerization that drive membrane protrusion, we examined whether Mena11aS>A expressing cells affected G-actin incorporation to barbed ends and Arp2/3 complex recruitment. Previously, we found that, compared to controls, the expression of Mena11a, but not Mena, reduced the number of free barbed ends present in lamellipodia 60 seconds after stimulation with 5 nM EGF (Figure 3.11). In contrast, we

find no differences in barbed end accumulation between cells expressing Mena and Mena11aS>A 60 seconds after treatment (Figure 4.6 A). Therefore, the presence of phosphorylatable S3 is required for Mena11a to dampen protrusion and reduce barbed end accumulation in cells treated with 5 nM EGF. After 180 seconds of stimulation with 5 nM EGF, Mena11a cells had reduced Arp2/3 complex at the lamellipodial leading edge compared to Mena and control cells (Figure 3.10). Cells expressing Mena11aS>A had similar levels of Arp2/3 at the lamellipodial leading edge as Mena did (Figure 4.6 B). Thus, phosphorylation is required for Mena11a-specific functions (Balsamo and Mondal, submitted).

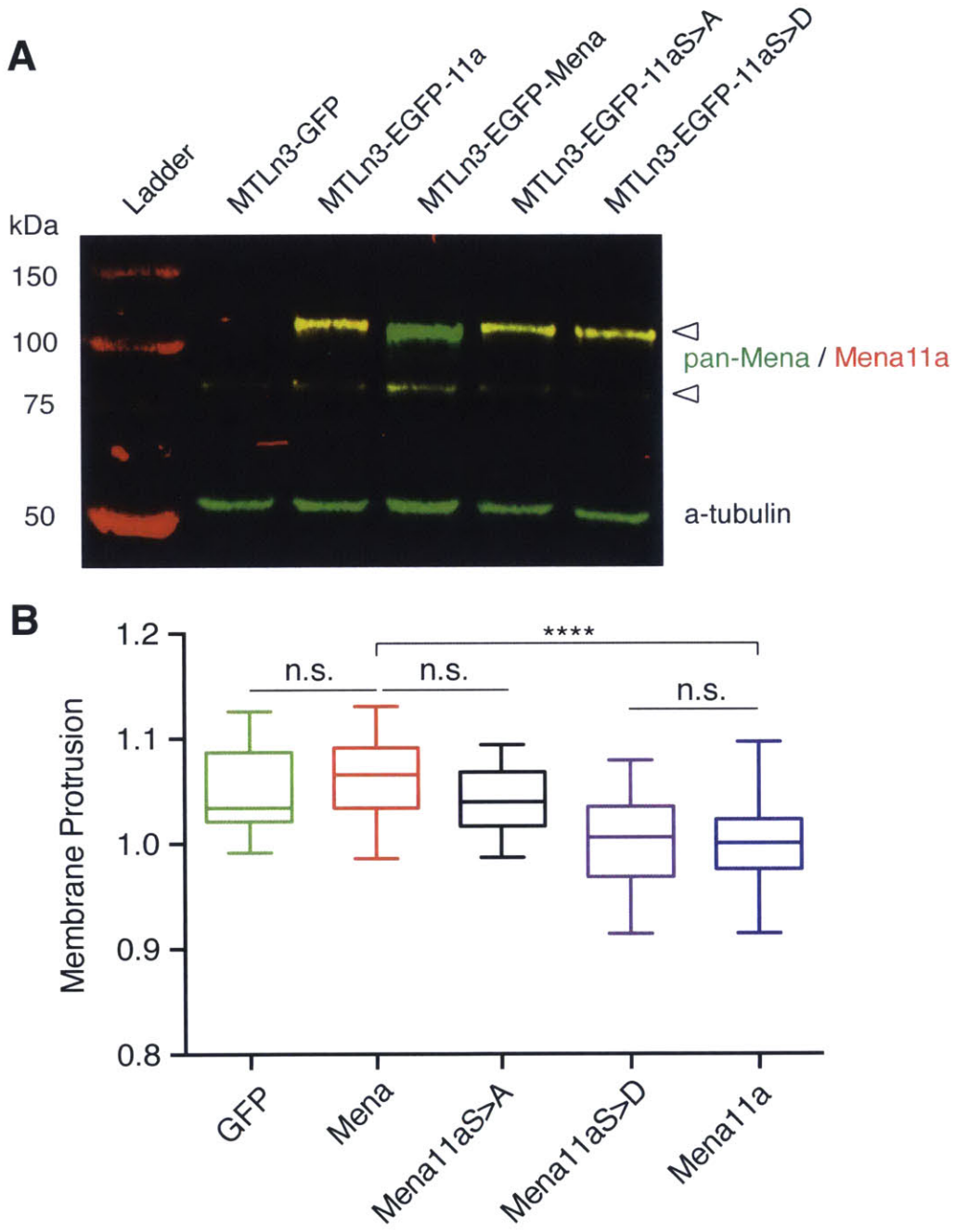

Figure 4.5. Mena11a phosphomimetic dampens membrane protrusion. (A) Western blot showing GFP-tagged Mena, Mena11a, Mena11a S>A, and Mena11a S>D stable expression in MTLn3 cells. Blot probed with α-Mena11a (Rb) and α-pan-Mena (Ms), and α-tubulin as a loading control. Upper arrowhead = ectopic expression of GFP-tagged protein. Lower arrowhead = endogenous expression of protein. (B) Membrane protrusion of MTLn3 cells stably expressing GFP, Mena, Mena11a, Mena11a S>A, and Mena11a S>D after stimulation with 5 nM EGF for 60 seconds.

Error bars: SEM. Results represent five experiments, >20 cells analyzed for each condition. One-way ANOVA ****p<0.0001.

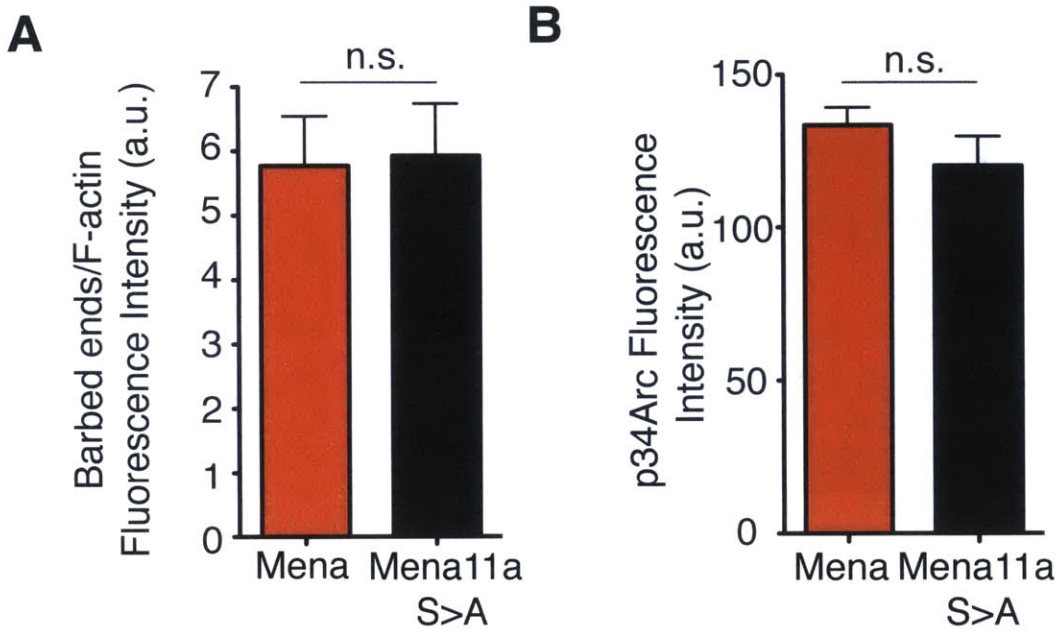

Figure 4.6 Mena11a phosphorylation site regulates barbed end formation and Arp2/3 recruitment to the leading edge.
(A) Quantification of relative number of barbed ends at leading edge after stimulation with 5 nM EGF for 60 seconds in >20 cells. Unpaired t-test, n.s. not significant. (B) Quantification of p34Arc fluorescence intensity sum of the initial 0.65 µm from the leading edge of >40 cells after stimulation with 5nM EGF for 180 seconds. a.u. = arbitrary units.

4.3.3 Mena11a does not affect debranching activity.

When compared to control cells, MV^{D7} cells expressing Mena11a have a decrease in density of the actin network and a reduction of Arp2/3 complex at the edge of lamellipodia (Figure 3.8). In addition, MTLn3 cells expressing Mena11a have reduced Arp2/3 recruitment to the leading edge in a phospho-S3 (11a)-dependent manner (Figure 3.10 F and 4.6 B). The phenotype of reduced branched actin and decreased Arp2/3 could be due to the destabilization of existing actin branches. To determine if Mena11a affects destabilization of actin branches, we used a pharmacological inhibitor

CK666 which binds directly to free Arp2/3 (8) and inhibits new branch formation. Because CK666 does not affect existing branches, any decrease of Arp2/3 at the edge of the cell after addition of the inhibitor represents the disassembly of branched actin. Using MV^{D7} cells (Ena/VASP-deficient fibroblasts) that stably express GFP, Mena11a, and Mena, we treated the cells with CK666 inhibitor for 60 seconds and subsequently measured Arp2/3 intensity levels from the edge of the cell inward. We find that wash-in of CK666 at 60 seconds decreases Arp2/3 levels for GFP, Mena11a, and Mena (Figures 4.7 A-C) below that of the control cells treated with DMSO only. However, there was no significant difference in Arp2/3 levels in the CK666-treated GFP, Mena11a, and Mena cells (Figure 4.7 D), suggesting that Mena11a does not affect the extent of debranching (e.g. decrease the final amount of Arp2/3 signal retained in lamellipodia following 60 seconds of Arp2/3 inhibition) beyond that of GFP and Mena cells.

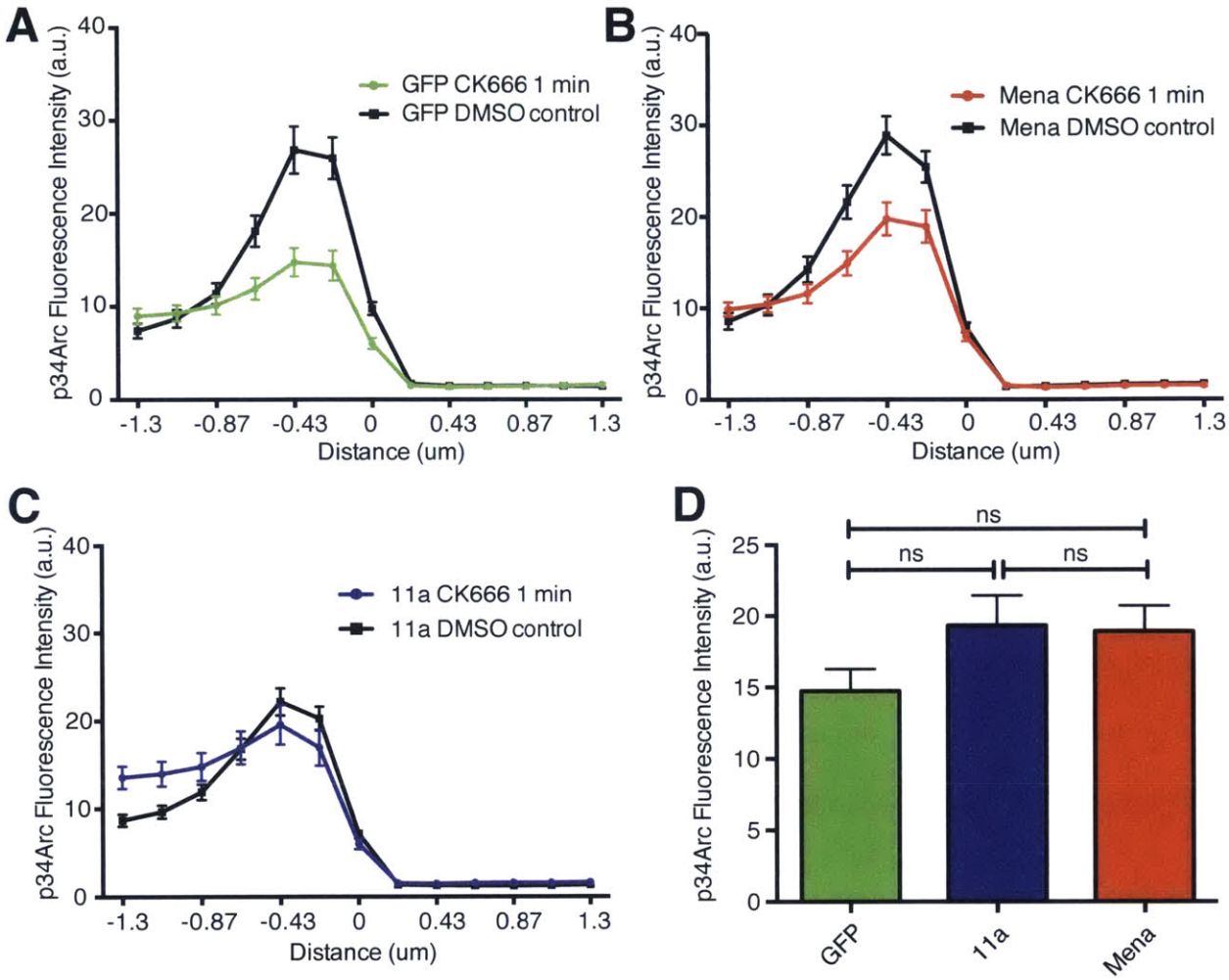

Figure 4.7. Mena11a has no effect on debranching. (A-C) Normalized pixel intensities of p34Arc, plotted as a function of distance from the cell edge (mean ± SEM). Negative values represent the inside of the cell, positive values represent outside of cell. Results represent triplicates, >30 cells analyzed. (A) GFP, (B) GFP-Mena11a, and (C) GFP-Mena MV^{D7} cells were treated with DMSO (control) or with CK666 inhibitor for 60 seconds and fixed. (D) Quantification of p34Arc fluorescence intensity sum of initial 0.43 µm from the leading edge 60 seconds after application of CK666. a.u.= arbitrary units. >30 cells analyzed. Error bars: SEM. Results represent triplicates. One-way ANOVA, n.s., not significant.

4.4 Conclusion

We demonstrate that Mena11a contains a phosphorylation site within the 21 amino acid 11a insertion that regulates its function. We find that the Mena11a phosphomimetic Mena11a S>D dampens membrane protrusion like Mena11a, and that the non-phosphorylatable form, Mena11a S>A, does not retain the ability of Mena11a to dampen protrusion, and reduce barbed ends and Arp2/3 complex at the lamellipodial edge.

We also examined whether the Mena11a-dependent phenotypes of decreased actin network density and Arp2/3 recruitment in lamellipodia were due to an increase in actin debranching, and find that there is no apparent difference in Arp2/3 levels in CK666-treated cells expressing GFP, Mena, or Mena11a. Visualization of Mena11a effects on Arp2/3 branching *in vitro* using total internal reflection microscopy (TIRFM) can further elucidate how Mena11a directly regulates actin polymerization.

4.5 Materials and Methods

Cell Lines:

MTLn3 cells were maintained in alpha-MEM media supplemented with 5% heat-inactivated fetal bovine serum (HyClone), L-glutamine, and antibiotics (penicillin/streptomycin; Invitrogen). MV^{D7}, Ena/VASP-deficient mouse embryonic fibroblastic cells were isolated as described (4), and cultured at 32°C in DMEM with 15% FBS, penicillin/streptomycin, L-glutamine, and 50 U/mL recombinant mouse IFN-γ (Invitrogen). Adherent cultures were incubated at 37°C in 5% CO_2. Cell lines were tested routinely for Mycoplasma contamination (Universal Mycoplasma Detection Kit, ATCC).

Antibodies and Growth Factors

The rabbit polyclonal anti-Mena11a (9) and mouse monoclonal anti pan-Mena (10) antibodies were generated in our laboratory. Commercially available antibodies are: mouse monoclonal anti-Tubulin (BD Biosciences, dilution 1:5000), rabbit polyclonal anti-p34Arc (Millipore, dilution 1:100), chicken IgY anti-GFP (Aves labs, dilution 1:500), rabbit polyclonal anti-GFP (Invitrogen). Control rabbit IgG was purchased from Jackson ImmunoResearch. CF405-Phalloidin was purchased (Biotium) and diluted 1:50. Mouse recombinant Epidermal Growth Factor (EGF) was from Invitrogen. Concentrations of growth factors are indicated in text.

Molecular Cloning

EGFP-Mena splice isoforms were subcloned into the pMSCV retroviral vector using standard techniques. The EGFP-Mena11aS>A and EGFP-Mena11aS>D point mutations were created with the QuikChange Site-directed Mutagenesis Kit (Stratagene) and confirmed by Sanger sequencing.

Retroviral packaging, infection and fluorescence-activated cell sorting

Retroviral packaging, infection, and fluorescence-activated cell sorting were performed as previously described (4). Retroviral plasmids and plasmids containing VSV-g and GAG-Pol cDNA were transiently transfected with X-tremeGENE 9 DNA transfection reagent (Roche) into HEK 293T cells to package virus. Virus was packaged at 32°C and supernatant was collected after 48 hours. MTLn3 cells were infected with virus for 24 hours in the presence of 1 mg/ml polybrene (Invitrogen) and cultured to 80% confluence. Cells were then trypsinized, filtered with 40 µm cell strainers, and fluorescence-activated cell sorting (FACS) in PBS + 5% Fetal Bovine Serum (FBS). MTLn3 cells expressing EGFP-Mena isoforms were sorted to expression levels as described (11).

Immunoprecipitation

MTLn3 cells were cultured in 15 cm dishes and starved for 4 hours in L15 media (Gibco) supplemented with 0.35% BSA. Cells were stimulated with 5 nM recombinant mouse EGF (Gibco) for 1 minute, and solubilized immediately after in 400 µl ice cold RIPA buffer per dish (0.1% SDS, 1% NP40, 150 mM NaCl, 50 mM Tris (pH 8.0), 0.5%

Na-deoxycholate, phosphatase inhibitors (PhosStop, Roche), and Complete mini protease inhibitor cocktail tablet (Roche)). Solubilized and insolubilized material was centrifuged at 10,000 rpm for 15 min at 4°C. Supernatants were removed and pre-cleared with Protein Plus A Agarose beads (Pierce) for 2 hours. Pre-cleared lysates were immunoprecipitated with a rabbit polyclonal antibody to GFP (BD biosciences) and a rabbit IgG control antibody (1 µg of antibody was used / mg of protein). The antibody-antigen mixture was combined with Protein Plus A Agarose beads (Pierce) and rotated overnight at 4°C. The beads-antibody-antigen mixture was spun down and washed extensively in RIPA buffer. Bound protein was solubilized by boiling for 10 min at 95°C in 1X Laemlli sample buffer.

Western Blotting
The 2.5% input, depleted lysates, and corresponding immunoprecipitations were run on an 8% SDS-PAGE gel, transferred for 1.5 hours at 80V to a PVDF membrane (Millipore), blocked for 1 hour at room temperature in 5% nonfat milk in 1x TBSxT, and probed with a polyclonal rabbit anti-Mena11a antibody (diluted 1:1000) overnight at 4°C. The membrane was washed with 1x TBSxT, and a rabbit affinity purified HRP-conjugated secondary (diluted 1:5000) from Jackson Immunoresearch was added for 1 hour at room temperature. The membrane was subsequently washed in 1x TBSxT, and developed with a BM Chemiluminescence Western Blotting Kit (Roche) on film.

For the Western blot in Figure 4.5, protein lysates were run on an 8% SDS-PAGE gel, transferred onto a nitrocellulose membrane (Biorad), blocked in Licor blocking buffer for 1 hour at room temperature, and probed with antibodies as indicated in PBSxT. Mouse and rabbit 680 and 800 fluorescently conjugated-secondary antibodies were diluted 1:10000 (Licor) and added for 45 min at room temperature, and membranes were scanned with the Licor Odyssey Infrared Imaging System.

Tandem mass spectrometry
Immunoprecipitated protein (see above) was run on a 4-15% gradient polyacrylamide gel (BioRad) prior to Coomassie Brilliant Blue G-250 staining. Bands were cut out of the gel and sent to the Taplin Biological Mass Spectrometry Facility (Harvard Medical School) to identify post-translational modifications. Protein was subjected to a LysC and trypsin digest followed by HPLC-MS/MS. MS analysis was conducted by the Swanson Biotechnology Proteomics Core (Koch Institute for Integrative Cancer Research, MIT).

Membrane Protrusion Assays
MTLn3 cells were plated overnight on acid-treated MatTek glass bottom dishes coated with 100 µg/ml rat-tail collagen I (BD Biosciences) in 0.02 N acetic acid. Cells were starved for 4 hours at 37°C in L15 media supplemented with 0.35% bovine serum albumin (BSA), and subsequently stimulated with a bath application of 5 nM mouse recombinant EGF (Gibco). Time-lapse live cell imaging was done in a Solent Incubator Chamber (Solent Inc) at 37°C fitted for a Nikon TE300 Eclipse inverted microscope with an ORCA-ER camera (Hammamatsu). Differential interference microscopy (DIC) was used with the above system to take 10 minute movies (1 frame every 3 seconds) with a 20x DIC objective, and images were collected and compiled with the Metamorph

imaging software (Molecular Devices). In ImageJ, cell area was measured through manual cell tracing twice, averaged, and normalized to area at time = 0 minutes.

Barbed Ends Assay

Barbed ends assay was performed as described (12) with some modifications. MTLn3 cells were starved for 4 hours in L15 medium supplemented with 0.35% BSA. For stimulation, cells were treated with bath application of 0.5 nM or 5 nM EGF at 37°C, and 60 or 180 seconds later were permeabilized with 0.125 mg/ml saponin (Sigma) in the presence of 0.5 mM rhodamine–conjugated G-actin. After 1 minute of labeling, samples were fixed in 0.5% glutaraldehyde in cytoskeleton buffer, permeabilized with 0.5% Triton X-100 in cytoskeleton buffer, quenched in 100mM Na-Borohydride in PBS, and blocked in the presence of CF405–phalloidin (Biotium). Images were taken with a deconvolution microscope. The ratio of barbed end intensity to phalloidin intensity along the edge was quantified. Signal intensities from rhodamine-labeled barbed ends along the cell edge were quantified with a published contour-based ImageJ macro (13). We measured the distribution of signal along the membrane plotted as a function of distance from the cell edge (mean ± SEM) and the sum of the intensities in the first 0.65 µm from the cell edge.

Immunofluorescence

Cells were plated on glass coverslips coated with 100 µg/ml rat-tail Collagen type I (BD Bioscience), fixed in 4% paraformaldehyde in cytoskeleton buffer (10 mM MES, pH 8.0, 3 mM $MgCl_2$, 138 mM KCl, 2 mM EGTA, pH 6.1, 0.32 M sucrose) for 20 minutes at room temperature, permeabilized in 0.2% Triton X-100 in 1X PBS, blocked in 10% BSA in PBS for 1 hour, incubated with antibodies (indicated in figures and legends) for 1 hour at 37°C, washed 3 times in 1X PBS and incubated with fluorescently labeled secondary antibodies (AlexaFluor, Molecular Probes) and phalloidin to visualize F-actin. Coverslips were imaged as described below.

CK666 Assay

CK666 wash-in was performed as in (14) with slight modifications. GFP, GFP-Mena11a, and GFP-Mena MV^{D7} cells were plated overnight on coverslips coated with 10 µg/ml fibronectin. An equal volume of 300 µM CK666-containing media was washed into the existing media in the well to achieve a final concentration of 150 µM for 1 min and then fixed immediately in Krebs-S buffer (145 mM NaCl, 5 mM KCL, 1.2 mM CaCl2, 1.3 mM MgCl2, 1.2 mM NaH2PO4, 20 mM HEPES pH 7.4, 0.4 M sucrose) for 30 min on ice. Cells were permeabilized in 0.1% Triton X-100 for 5 min, blocked in 5% BSA/NGS mixture for 1 hr at room temperature. Primary antibody was added at 4°C overnight, secondary antibody was added for 1.5 hours at room temperature, and coverslips were washed extensively between steps with 1X PBS and mounted using Fluoromount-G (Southern Biotech). DMSO controls were done simultaneously under the same conditions. Coverslips were imaged as below, and signal intensities along the cell edge were quantified with a published contour-based ImageJ macro (13). We measured the distribution of signal along the membrane plotted as a function of distance from the cell edge (mean ± SEM) and the sum of the intensities in the first 0.43 µm from the cell edge.

Microscopy
z-series of cells and tissues were imaged using a Deltavision microscope using SoftWoRx acquisition software (Applied Precision), 40X and 60X 1.4 NA Plan-Apochromat objective lens (Olympus), and a camera (CoolSNAP HQ; Photometrics). Images taken with the Deltavision microscope were deconvolved using Deltavision SoftWoRx software and objective-specific point spread function.

BioInformatics analysis

The NetPhos2.0 server was used to predict serine, threonine, and tyrosine phosphorylation sites in eukaryotic proteins (7).

Statistical Analysis
Statistical differences between two conditions were determined using a student's unpaired t-test. For multiple conditions, means were compared by analysis of variance (ANOVA). All data found to be significant ($p < 0.05$) by ANOVA were compared with Tukey's honestly significant difference *post hoc* test. For box and whiskers plots, center line of box indicates the median, top indicates 75^{th} quartile, bottom indicates 25^{th} quartile; whiskers represent 90^{th} and 10^{th} percentiles.

4.6 References

1. Di Modugno F, et al. (2007) Molecular cloning of hMena (ENAH) and its splice variant hMena+11a: epidermal growth factor increases their expression and stimulates hMena+11a phosphorylation in breast cancer cell lines. *Cancer Res* 67(6):2657–65.
2. Loureiro JJ, et al. (2002) Critical roles of phosphorylation and actin binding motifs, but not the central proline-rich region, for Ena/vasodilator-stimulated phosphoprotein (VASP) function during cell migration. *Mol Biol Cell* 13(7):2533–2546.
3. Tani K, et al. (2003) Abl interactor 1 promotes tyrosine 296 phosphorylation of mammalian enabled (Mena) by c-Abl kinase. *J Biol Chem* 278(24):21685–21692.
4. Bear JE, et al. (2000) Negative regulation of fibroblast motility by Ena/VASP proteins. *Cell* 101(7):717–728.
5. Bear JE, et al. (2002) Antagonism between Ena/VASP proteins and actin filament capping regulates fibroblast motility. *Cell* 109(4):509–521.
6. Benz PM, et al. (2009) Differential VASP phosphorylation controls remodeling of the actin cytoskeleton. *J Cell Sci* 122(Pt 21):3954–3965.
7. Blom N, Gammeltoft S, Brunak S (1999) Sequence and structure-based prediction of eukaryotic protein phosphorylation sites. *J Mol Biol* 294(5):1351–1362.
8. Hetrick B, Han MS, Helgeson LA, Nolen BJ (2013) Small Molecules CK-666 and CK-869 Inhibit Actin-Related Protein 2/3 Complex by Blocking an Activating Conformational Change. *Chem Biol* 20(5):701–712.
9. Pino MS, et al. (2008) Human Mena+11a isoform serves as a marker of epithelial phenotype and sensitivity to epidermal growth factor receptor inhibition in human pancreatic cancer cell lines. *Clin Cancer Res* 14(15):4943–50.
10. Lanier LM, et al. (1999) Mena is required for neurulation and commissure formation. *Neuron* 22(2):313–325.
11. Philippar U, et al. (2008) A Mena invasion isoform potentiates EGF-induced carcinoma cell invasion and metastasis. *Dev Cell* 15(6):813–828.
12. Furman C, et al. (2007) Ena/VASP is required for endothelial barrier function in vivo. *J Cell Biol* 179(4):761–775.
13. Cai L, Marshall TW, Uetrecht AC, Schafer DA, Bear JE (2007) Coronin 1B

Coordinates Arp2/3 Complex and Cofilin Activities at the Leading Edge. *Cell* 128(5):915–929.

14. Haynes EM, et al. (2015) GMFbeta controls branched actin content and lamellipodial retraction in fibroblasts. *J Cell Biol* 209(6):803–812.

Chapter 5: Conclusion and Future Directions

TABLE OF CONTENTS

5.1 Mena11a reduces lamellipodial protrusion at the leading edge and elongation of *Listeria* tails

Mena and other Ena/VASP proteins, in coordination with a multitude of actin regulatory proteins, drive the dynamics and geometry of assembling F-actin networks underlying cell motility, cell-cell and cell-matrix adhesion (1–6). This is the first study directly comparing Mena to Mena11a function in the absence of other Mena isoforms and Ena/VASP proteins. We find that Mena11a is not simply an attenuated or less active form of Mena, but is endowed with unique and distinct functions; Mena11a decreases the abundance of free barbed ends, the accumulation of Arp2/3 complex, and the F-actin network density in lamellipodia when expressed in MV^{D7} cells, which are otherwise Ena/VASP-deficient. We assayed the ability of Mena and Mena11a to stimulate *Listeria monocytogenes* actin tail assembly in MV^{D7} cells. Like Mena, Mena11a is recruited to the bacterial surface and increases the frequency of actin tail formation; however, it does not promote tail elongation. Previously, we found that Ena/VASP proteins lacking the F-actin binding FAB motif can support actin tail elongation (7). Thus, the inability of Mena11a to promote *Listeria* F-actin tail elongation may not simply be a consequence of reduced F-actin binding activity (Balsamo and Mondal, submitted).

Ena/VASP proteins have “anti-capping activity”; they bind to barbed ends and promote elongation of actin filaments in the presence of capping protein (1). Visualization of actin polymerization assays *in vitro* using total internal reflection microscopy (TIRFM) will illustrate better the effects of Mena11a on actin filament

elongation and branching. Interestingly, Ena/VASP proteins also have "anti-branching" activity (reviewed in (1)), which may or may not regulate actin polymerization *in vivo* synergistically with "anti-capping" activity. Compared to control MV^{D7} cells and independent of Mena expression, we find that Mena11a has a less dense actin network than that of Mena. Thus, we examined if the reduction of Arp2/3 complex at the edge of the lamellipodia was due to destabilization of branched actin by Mena11a. We find that control MV^{D7} cells and those expressing Mena11a and Mena have similar levels of Arp2/3 after treating with the CK666 inhibitor. We have demonstrated that Mena11a affects early protrusion events; thus, examining the formation of nascent, synchronized lamellipodia using a washout of CK666 inhibitor (8) will give more insight into how Mena11a affects the rate of actin branch formation.

A recent study from Rotty et al. analyzed Arp2/3-mediated assembly of F-actin networks in fibroblasts (9); in *Arpc2* $^{-/-}$ fibroblasts, actin assembly and maintenance was dependent on profilin-1 and Ena/VASP function (but not formins), and in the wild type fibroblasts, profilin-1 inhibited Arp2/3 complex-mediated actin nucleation. Since Ena/VASP proteins can directly bind both profilin-actin and G-actin monomers, the "anti-branching" activity observed could be due to local fluctuations in monomer concentration or a preferential usage of profilin-actin for elongation of actin filaments, rather than branching. Further studies directly analyzing Mena11a effects on elongation and branching (in the presence or absence of Arp2/3 and profilin) will be necessary to clarify the complex relationship between these proteins.

In addition to its unique functions, Mena11a also acts antagonistically to Mena in cells with both isoforms. While it has been demonstrated that Mena and Mena11a are capable of forming mixed tetramers in MV^{D7} cells cotransfected with tagged versions of both isoforms (10), further analyses must be done to analyze the extent of mixed oligomer formation in cells with endogenous Mena and Mena11a. Endogenous or ectopic Mena11a co-expression with Mena causes reduction in the levels of F-actin barbed ends at the leading edge of lamellipodia and dampens lamellipodial protrusion and stability. Other Mena isoforms, particularly the invasion-specific $Mena^{INV}$ isoform, enhance growth factor elicited lamellipodial protrusion (11, 12). $Mena^{INV}$ also potentiates carcinoma cell responses to EGF, allowing them to protrude and invade when treated with concentrations below those normally required to evoke such response (11). The dampening of growth factor elicited lamellipodial protrusion by Mena11a likely arises as a consequence of reduced actin assembly rather than dysregulated signal transduction, as acute EGF-elicited EGFR activation and downstream signaling were unaffected in Mena11a-expressing cells. (Balsamo and Mondal, submitted).

In HER2 overexpressing breast cancer cells recent work demonstrates that sustained, long-term activation of Her2 signaling results in Mena11a upregulation and phosphorylation (13), and downregulation of Mena11a reduces both Her2 and Her3 phosphorylation at this longer time scale (13, 14). However, the mechanism by which Mena11a maintains Her3 and subsequent Akt activation, resulting in pro-survival signaling, has not been elucidated (14). Mena11a has been proposed to be required for cell proliferation *in vitro* (14, 15); however, *in vivo* studies examining Mena11a function in mammary tumor formation demonstrate that Mena11a expression has no effect on

tumor growth (16) and both xenograft and transgenic mouse models of breast cancer verify that Mena expression does not affect primary tumor growth (11, 17) (Balsamo and Mondal, submitted).

5.2 Mena11a function is phospho-regulated.

While the mechanism by which Mena11a reduces actin polymerization and Arp2/3 accumulation has yet to be elucidated, we find that a phosphorylation site within the 21 amino acid 11a insertion regulates Mena11a function. We speculate that phosphorylation within 11a is important for unique Mena11a functions, such as dampened membrane protrusion, decreased abundance of free barbed ends and reduced accumulation of Arp2/3 complex. The phosphorylation is also likely to attenuate Mena-dependent effects on actin polymerization by adding negative charge to a residue in proximity to the actin binding sites in the EVH2 domain.

The presence of a key phosphorylation site within the 11a sequence allows for isoform-specific modulation of Mena11a. The sequence R-R-D-S-P-R-K matches consensus phosphorylation sequences of the cAMP-dependent kinase PKA (R-R-X-S/T-ϕ, where X is any residue and ϕ is a hydrophobic residue) (18, 19) and CDK5 (S/T-P-X-K) (20), as predicted by Scansite and other phosphoproteomic databases (21, 22). Both PKA and CDK5 have roles in regulating actin dynamics (23, 24) and cancer progression; PKA is demonstrated to regulate cell growth and proliferation in breast cancer (25), and CDK5 plays a role in invadopodia formation (26) and regulation of the tumor suppressor protein DLC1 in lung adenocarcinoma (27). The role of these and other kinases in regulating Mena11a function is a subject for further investigation;

however, the presence of two additional PKA phosphorylation sites (28) and one additional CDK5 phosphorylation site (not shown) in Mena11a complicates the identification of specific kinases. In addition, the generation of a phospho-specific antibody will be integral in understanding the phosphoregulation of the Ser3 site of 11a *in vivo* at different sites of actin remodeling. Interestingly, a Mena paralog, EVL, is also alternatively spliced to include a 21 amino acid insertion at an equivalent site between the F-actin binding and tetramerization sites (Figure 1.6). Although they lack sequence similarity, both inserted sequences are phosphorylated, raising the intriguing possibility that alternative splicing produces discrete pools of Ena/VASP proteins that are differentially regulated by different kinases (Balsamo and Mondal, submitted).

5.3 Mena11a is expressed in normal epithelia and muscle

We have demonstrated that Mena11a is enriched in embryonic and adult muscle and epithelia. During development, the inclusion of 11a in epidermis is regulated by the ESRP family of splicing factors; a double knockout of ESRP1 and ESRP2 in E18.5 epidermis resulted in a dramatic decrease in the 11a percent spliced in (29). However, ESRP1 and ESRP2 are not expressed in muscle, suggesting that an alternate splicing program must regulate 11a inclusion in muscle. Analysis of 11a inclusion, function, and regulation in various types of muscle will be intriguing, as Mena has a physiologically relevant role in normal cardiac muscle function and contributes to heart failure pathophysiology (30, 31).

5.4 Mena11a regulates behavior of epithelial-like breast cancer cells

Mena11a contributes to the phenotype of epithelial-like breast cancer cells. In these cells, Mena11a localizes to both tight- and adherens- junctions. Mena11a-specific knockdown perturbs E-cadherin distribution at cell:cell junctions, and increases migration of T47D cells. These data suggest a role for Mena11a in regulating the architecture and behavior of epithelial-like breast cancer cells by supporting organized cell-cell contacts and a low migratory phenotype.

During EMT, Mena11a is down regulated by the actions of gene expression and alternative splicing programs that execute this complex phenotypic transition (32). Multiple factors regulate 11a inclusion during EMT, including the ESRP and the RbFox family of splicing factors (32–38), as well as other proteins, such as CLK2 kinase (39). The epithelial-specific splicing factors ESRP1 and ESRP2 can promote Mena11a expression in epithelial cells and regulate exon inclusion in other genes important in the control of cell migration and expression of EMT phenotypes, including Exo70 and CD44, among others (33–35, 38, 40). The pivotal role of alternative splicing programs during EMT and tumor progression is highlighted by several studies in which either perturbation of both ESRP1 and ESRP2 levels has an effect on EMT-like phenotypes (32, 34, 38, 40, 41).

Interestingly, during EMT, ESRP1/2 regulated alternative splicing gives rise to epithelial isoforms of both Mena and Exo70 that differ in their ability to influence Arp2/3-dependent actin polymerization compared to their mesenchymal isoforms (40); the Exo70-M isoform stimulates Arp2/3 activity and lacks a 23-residue sequence present in the epithelial-specific Exo70-E that suppresses its ability to regulate Arp2/3. Thus Mena

and Exo70 both harbor epithelial enriched exons that reduce Arp2/3 abundance in lamellipodia. It will be interesting to determine whether additional genes encode ESRP1/ESRP2 regulated epithelial-specific isoforms with altered effects on Arp2/3 function compared to mesenchymal isoforms (Balsamo and Mondal, submitted).

To extend our analysis of Mena11a function beyond the molecular and cellular level to human cancer, we utilized transcriptome data from multiple cancer cohorts in the Cancer Genome Atlas and found that while neither Mena nor Mena11a expression alone had correlation with clinicopathological features of patients, a $MenaCalc^{RNA}$ metric examining the difference between Mena and Mena11a expression levels had much greater predictive power. Patients with high levels of Mena and low levels of Mena11a (a high $MenaCalc^{RNA}$) in the colorectal adenocarcinoma cohort (regardless of follow-up time) had increased metastasis formation. Although transcriptomic data is not a surrogate for protein expression, independent studies demonstrate that low protein levels of Mena11a in tumors with high protein levels of pan-Mena are associated with poor clinical outcome in breast cancer patients (42, 43).

In conclusion, our findings help explain why Mena11a expression promotes an epithelial phenotype and drives formation of tumors with a highly cohesive, well-differentiated appearance (44), and we propose that Mena11a expression diminishes the capacity of cancer cells to acquire aggressive, invasive phenotypes needed for metastatic progression (Balsamo and Mondal, submitted).

5.5 References

1. Bear J, Gertler F (2009) Ena/VASP: towards resolving a pointed controversy at the barbed end. *J Cell Sci* 122(12):1947–1953.
2. Breitsprecher D, et al. (2011) Molecular mechanism of Ena/VASP-mediated actin-filament elongation. *EMBO J* 30(3):456–467.
3. Hansen S, Mullins R (2010) VASP is a processive actin polymerase that requires monomeric actin for barbed end association. *J Cell Biol* 191(3):571–584.
4. Bisi S, et al. (2013) Membrane and actin dynamics interplay at lamellipodia leading edge. *Curr Opin Cell Biol* 25(5):565–573.
5. Bear JE, Haugh JM (2014) Directed migration of mesenchymal cells: where signaling and the cytoskeleton meet. *Curr Opin Cell Biol* 30C(Figure 1):74–82.
6. Bravo-Cordero JJ, Magalhaes MA, Eddy RJ, Hodgson L, Condeelis J (2013) Functions of cofilin in cell locomotion and invasion. *Nat Rev Mol Cell Biol* 14(7):405–15.
7. Geese M, et al. (2002) Contribution of Ena/VASP Proteins to Intracellular Motility of Listeria Requires Phosphorylation and Proline-rich Core but Not F-Actin Binding or Multimerization. *Mol Biol Cell*:1–14.
8. Haynes EM, et al. (2015) GMFbeta controls branched actin content and lamellipodial retraction in fibroblasts. *J Cell Biol* 209(6):803–812.
9. Rotty JD, et al. (2015) Profilin-1 Serves as a Gatekeeper for Actin Assembly by Arp2/3-Dependent and -Independent Pathways. *Dev Cell* 32(1):54–67.
10. Riquelme DN, Meyer AS, Barzik M, Keating A, Gertler FB (2015) Selectivity in subunit composition of Ena/VASP tetramers. *Biosci Rep* 35(5).
11. Philippar U, et al. (2008) A Mena invasion isoform potentiates EGF-induced carcinoma cell invasion and metastasis. *Dev Cell* 15(6):813–828.
12. Hughes SK, et al. (2015) PTP1B-dependent regulation of receptor tyrosine kinase signaling by the actin-binding protein Mena. *Mol Biol Cell* .
13. Di Modugno F, et al. (2010) The cooperation between hMena overexpression and HER2 signalling in breast cancer. *PLoS One* 5(12):e15852.
14. Trono P, et al. (2015) hMENA11a contributes to HER3-mediated resistance to PI3K inhibitors in HER2-overexpressing breast cancer cells. *Oncogene*.

15. Di Modugno F, et al. (2007) Molecular cloning of hMena (ENAH) and its splice variant hMena+11a: epidermal growth factor increases their expression and stimulates hMena+11a phosphorylation in breast cancer cell lines. *Cancer Res* 67(6):2657–65.

16. Roussos ET, et al. (2011) Mena invasive (MenaINV) promotes multicellular streaming motility and transendothelial migration in a mouse model of breast cancer. *J Cell Sci* 124(Pt 13):2120–2131.

17. Roussos ET, et al. (2010) Mena deficiency delays tumor progression and decreases metastasis in polyoma middle-T transgenic mouse mammary tumors. *Breast Cancer Res* 12(6):R101.

18. Adams JA, Taylor SS (1993) Phosphorylation of peptide substrates for the catalytic subunit of cAMP-dependent protein kinase. *J Biol Chem* 268(11):7747–7752.

19. Kemp BE, Graves DJ, Benjamini E, Krebs EG (1977) Role of multiple basic residues in determining the substrate specificity of cyclic AMP-dependent protein kinase. *J Biol Chem* 252(14):4888–4894.

20. Sharma P, et al. (2002) Phosphorylation of MEK1 by cdk5/p35 down-regulates the mitogen-activated protein kinase pathway. *J Biol Chem* 277(1):528–534.

21. Amanchy R, et al. (2007) A curated compendium of phosphorylation motifs. *Nat Biotech* 25(3):285–286.

22. Obenauer JC, Cantley LC, Yaffe MB (2003) Scansite 2.0: proteome-wide prediction of cell signaling interactions using short sequence motifs. *Nucleic Acids Res* 31 (13):3635–3641.

23. Howe AK (2004) Regulation of actin-based cell migration by cAMP/PKA. *Biochim Biophys Acta - Mol Cell Res* 1692(2–3):159–174.

24. Xu J, et al. (2011) Actin interaction and regulation of cyclin-dependent kinase 5/p35 complex activity. *J Neurochem* 116(2):192–204.

25. Caretta A, Mucignat-Caretta C (2011) Protein kinase a in cancer. *Cancers (Basel)* 3:913–926.

26. Quintavalle M, Elia L, Price JH, Heynen-Genel S, Courtneidge SA (2011) A cell-based high-content screening assay reveals activators and inhibitors of cancer cell invasion. *Sci Signal* 4:ra49.

27. Tripathi BK, et al. (2014) CDK5 is a major regulator of the tumor suppressor DLC1. *J Cell Biol* 207 (5):627–642.

28. Loureiro JJ, et al. (2002) Critical roles of phosphorylation and actin binding motifs, but not the central proline-rich region, for Ena/vasodilator-stimulated phosphoprotein (VASP) function during cell migration. *Mol Biol Cell* 13(7):2533–2546.

29. Bebee TW, et al. (2015) The splicing regulators Esrp1 and Esrp2 direct an epithelial splicing program essential for mammalian development. *Elife* 4.

30. Belmonte SL, Ram R, Mickelsen DM, Gertler FB, Blaxall BC (2013) Cardiac overexpression of Mammalian enabled (Mena) exacerbates heart failure in mice. *Am J Physiol - Hear Circ Physiol* 305(6):H875–H884.

31. Aguilar F, et al. (2011) Mammalian enabled (Mena) is a critical regulator of cardiac function. *Am J Physiol Heart Circ Physiol* 300(5):H1841–52.

32. Shapiro IM, et al. (2011) An EMT–Driven Alternative Splicing Program Occurs in Human Breast Cancer and Modulates Cellular Phenotype. *PLoS Genet* 7(8):21.

33. Warzecha CC, Sato TK, Nabet B, Hogenesch JB, Carstens RP (2010) ESRP1 and ESRP2 Are Epithelial Cell-Type-Specific Regulators of FGFR2 Splicing. *Mol Cell* 33(5):591–601.

34. Warzecha CC, et al. (2010) An ESRP-regulated splicing programme is abrogated during the epithelial-mesenchymal transition. *EMBO J* 29(19):3286–300.

35. Dittmar KA, et al. (2012) Genome-Wide Determination of a Broad ESRP-Regulated Posttranscriptional Network by High-Throughput Sequencing. *Mol Cell Biol* 32:1468–1482.

36. Lu H, et al. (2013) Exo70 isoform switching upon epithelial-mesenchymal transition mediates cancer cell invasion. *Dev Cell* 27(5):560–73.

37. Braeutigam C, et al. (2014) The RNA-binding protein Rbfox2: an essential regulator of EMT-driven alternative splicing and a mediator of cellular invasion. *Oncogene* 33(9):1082–1092.

38. Brown RL, et al. (2011) CD44 splice isoform switching in human and mouse epithelium is essential for epithelial-mesenchymal transition and breast cancer progression. *J Clin Invest* 121:1064–1074.

39. Yoshida T, et al. (2015) CLK2 Is an Oncogenic Kinase and Splicing Regulator in Breast Cancer. *Cancer Res* 75(7):1516–1526.

40. Lu H, et al. (2013) Exo70 isoform switching upon epithelial-mesenchymal transition mediates cancer cell invasion. *Dev Cell* 27(5):560–573.

41. Di Modugno F, et al. (2012) Splicing program of human MENA produces a previously undescribed isoform associated with invasive, mesenchymal-like breast tumors. *Proc Natl Acad Sci* 109(47):19280–5.

42. Agarwal S, et al. (2012) Quantitative assessment of invasive mena isoforms (Menacalc) as an independent prognostic marker in breast cancer. *Breast Cancer Res* 14(5):R124.

43. Forse C, et al. (2015) Mena calc , a quantitative method of metastasis assessment, as a prognostic marker for axillary node-negative breast cancer. *BMC Cancer* 15(1):483.

44. Roussos ET, et al. (2011) Mena invasive (Mena(INV)) and Mena11a isoforms play distinct roles in breast cancer cell cohesion and association with TMEM. *Clin Exp Metastasis* 28(6):515–527.